Different toughening strategies for UV-cured epoxy resins

# POLITECNICO DI TORINO

Applied Science & Technology Department



PhD dissertation

Materials Science and Technology

XXVI Cycle

# Different toughening strategies for UV-cured epoxy resins


Mohamed Naguib Ibrahim

Tutor: Prof. Marco Sangermano


2014

*To my beloved family*

# Acknowledgement

Foremost, I would like to express my sincere gratitude to my supervisor Prof. Marco Sangermano for his continuous support in all stages of my PhD research. His guidance helped me in all the time of research. I would also like to thank him for being an open person to ideas, and for encouraging and helping me to shape my interest and ideas.

My sincere thanks also go to Prof. Brigitte Voit and Dr. Doris Pospiech at Leibniz-Institut für Polymerforschung Dresden, Germany for offering me a special opportunity in their respective institute and for their help and guidance.

I would like to express my deep gratitude and respect to Prof. A. Abd El Hakim and Prof. Magdy Elnashar at National Research Center of Egypt for all they have made to build my scientific career. Also, many thanks for prof. Nadia A. Rizk and prof. Nader Ismail for their kind help and support.

Last but not least, I thank my lab colleagues in Applied Science and Technology Department for their friendly contribution and stimulating discussions.

# Contents

## *Aim of the work*

Owing to their outstanding properties, epoxy resins are widely used in different industries and recently used in novel applications such as semiconductors and lithographic inks. Due to their low fracture toughness, Toughening of epoxy is widely discussed in literature during last decades. Many toughening agents including organic and inorganic materials are used to accomplish this purpose.

The objectives of this research are to synthesize and use different toughening agents and study the influence of these modifiers on the mechanical and thermal properties in general and the fracture toughness in particular of the UV-cured cycloaliphatic epoxy resins. Particularly, we desired to improve the fracture toughness of modified epoxies cured via UV light without sacrificing their thermal and other mechanical properties.

Polymeric molecules or ceramic nanoparticles have been introduced; (1) Hyperstar polymers based on hyperbranched polyester core with or without hydroxyl reactive groups in their arms (2) reactive core/shell polymeric nanoparticles prepared by seeded emulsion polymerization (3) reactive or nonreactive diblock copolymer prepared via ATRP and based on polyethylene oxide and (4) commercial alumina nanoparticles as inorganic particles.

The effect of the addition of these toughening agents on the rate of UV-curing process and glass transition temperature, $T_g$, have been investigated. Subsequently, the morphology of the facture surfaces has been studied carefully using FE-SEM. The stress intensity factor, $K_{IC}$, measurements which is an indicator for fracture toughness was evaluated in terms of single-edge-notch three-point-bending (SENB).

Cationic UV-curing technique was utilized for the preparation of the modified epoxy composites. Specifically, the cationic photopolymerization of cycloaliphatic epoxy is known to proceed through nucleophilic attack of neutral monomer to oxonium cation, which is active chain end of the polymerization. The UV induced polymerization technique is a solvent free method occurring at room temperature which is eco-friendly. It is indeed a polymerization process used for industrial applications because of the high production rate and the low energy consumption compared to thermal processes. The

rapid UV-curing process helps to maintain good dispersion of modified particles avoiding further aggregation that could occur during longer thermal treatment.

# 1

# Introduction and literature survey

## 1.1. Epoxy polymers

Epoxy resins were first introduced into markets in 1940s and gradually entered in many industrial applications. While protective coatings are the main area of application, they are also involved important applications in many sectors such as printed circuit board (PCB), semiconductor encapsulants, and adhesives. Recently, epoxy resins have new growing applications include lithographic ink and photoresists for the electronics industry.

Some of the characteristics of epoxy resins are high chemical and corrosion resistance, good mechanical and thermal properties, outstanding adhesion to various substrates, low shrinkage upon cure, good electrical insulating properties, and the ability to be processed under a variety of conditions.[1]

## 1.2. Polymerization of epoxy

Epoxy polymer is an important class of polymeric materials, characterized by the presence of at least one oxirane ring. Linear or crosslinked epoxy polymers can be obtained by the reaction of the epoxy monomers or oligomers with hardners and/or initiators. Epoxy polymers can be produced by step or chain polymerizations or a combination of both mechanisms.

Step-growth polymerization proceeds via step by step mechanism. Each step includes the disappearance of two co-reacting sites and generation of a new covalent bond between a pair of functional groups. The chain-growth polymerization is characterized by the presence of initiation, propagation, chain transfer and termination steps. In case of epoxies, an ion is generated as result of chemical or irradiation initiation. Once these active centers (ions) are generated they start to produce chains by consecutive addition of monomers through propagation step. The main parameters that affect the polymer structure are the functionality of monomer, the molar ratio between the initiator and monomers, the amount of chain transfer species and temperature that affects the relative rates of different steps.[1,2]

## 1.3. Transformations during epoxy network formation

During curing of the epoxy resins into networks some transformations occur. They will be discussed here concisely[1]:

**Gelation**, it is a critical transition that takes place during the formation of the polymer network and corresponds to the generation of a giant macromolecular structure which is characterized by the change from a liquid to solid. In the post - gel stage there is an increase in crosslinking density with a corresponding increase in the elastic modulus of the solid.

**Virtification**, during polymerization of an epoxy formulation vitrification may occur if the glass transition temperature of the system, $T_g$, equals or higher than the reaction temperature, T. The condition $T_g \geq T$, can be achieved for both isothermal or non-isothermal processing and before or after gelation (gelation and vitrification are independent transitions). When the system gets into the glassy state the polymerization kinetics is strictly retarded. Unreacted epoxy formulations may be safely stored in the

glassy state provided that ($T_g$ − T) is high enough to avoid any significant advance in the polymerization reaction.

**Reaction induced phase separation,** Many epoxy formulations include a particular modifier, such as rubber, thermoplastic …etc, that is miscible before reaction but becomes phase separated in the course of polymerization (reaction induced phase separation). Reaction induced phase separation is employed to produce different morphologies in the final products that are appropriate to increase toughness.

For example, block copolymers are used as modifiers of epoxy formulations to obtain nanostructured materials with specific properties. In this case both blocks are initially miscible and the less miscible block becomes phase separated in the course of polymerization.

## 1.4. Thermoplastic epoxy

Despite epoxy resins are well known as thermosetting polymers, thermoplastic epoxies that can be processed as thermoplastic polymers are commercially available. The "epoxy thermoplastics" term refers to a group of high molecular weight, hydroxyl functionalized macromolecules, derived from conventional epoxy containing building blocks, which can be thermally fabricated by such conventional processes as injection molding and blow molding. Researchers developed many of thus thermoplastics epoxy resins such as Poly(hydroxy ethers), poly(hydroxy ether sulfides) and poly(hydroxy amino ethers).[1]
The high cohesive energy density of these resins gives them excellent gas-barrier properties against oxygen and carbon dioxide. They also possess excellent adhesion to many substrates, optical clarity, excellent melt strength, and good mechanical properties.[3]

## 1.5. Epoxy acrylate

Although conventional epoxy resins have excellent properties, the presence of ether linkages and aromatic structures in most of them leads to poor UV and oxidative stability and hence to poor outdoor weather stability. Epoxy functional acrylic polymers "epoxy acrylates" succeeded to combine the good properties of epoxy resins with excellent outdoor weatherability.[1]

## 1.6. Epoxy toughening

Thermosetting polymers, in general, and epoxy resins, in particular, are identified as rigid and brittle polymeric materials. While rigidity and strength are desired for many engineering applications, brittleness or lack of crack growth resistance hinders wider usage of epoxies. Fracture toughness is considered as the indicator for this internal brittleness and the crack propagation resistance of the material. Many research efforts try to develop toughening agents which do not affect the thermo-mechanical properties of the epoxy polymeric matrices. Therefore, toughening of epoxies has become a necessity to ensure the feasibility of these materials for practical applications.[4,5]

A variety of toughening agents have been used to modify epoxy polymers to improve the fracture toughness without significantly sacrificing other important characteristics.
Organic toughening agents as well as inorganic agents are commonly used for this purpose.

Generally, some factors affect the efficacy of these toughening agents on the fracture toughness. Among these parameters are the chemical structure, concentration inside matrix, their particle size and dispersion as well as particle size distribution. Some of these famous toughening agents will be described briefly in the following items.

### 1.6.1. Reactive liquid rubber

Reactive rubbery oligomers have been in use since 1970 for toughness modification for epoxy resins. The reactive oligomer used in this technique, is dissolved in the epoxy first. As the epoxy resin begins to cure and the molecular weight starts to rise, the rubbery phase begins to precipitate out to form the second phase particles. The volume fraction and the size of the rubbery domains are influenced by the degree of compatibility of the two phases and also the kinetics of gelation.
Butadiene-acrylonitrile based rubbers are the principle liquid elastomers used for the toughening of epoxies[3]. Among them, carboxyl-terminated butadiene-acrylonitrile (CTBN) rubbers have been extensively used. Other elastomers from this family include ATBN (amino-terminated), ETBN (epoxy-terminated), and VTBN (vinyl- terminated).[6]

### 1.6.2. Hyperbranched polymers

Hyperbranched polymers (HBP) have a high potential as additives and modifiers in engineering materials, thus these HBP have been recently proposed as a very interesting

new class of additives in epoxy resins[7,8]. Hyperbranched polymers have peculiar and often unique properties due to their highly branched dendritic structure[9]. Their structure gives them excellent flow and processing properties, and they are characterized by lower viscosity than that of linear polymers of comparable molecular weight. These properties make HBP good candidates to be used as additives in coating technology since they will not significantly affect the viscosity of the formulation, which is important during surface coating. Besides, the highly branched structures give further access to a large number of reactive end groups and thus, HBPs have been successfully used in various applications in order to improve some of their properties such as fracture toughness.[7-11]

### 1.6.3. Core/shell polymeric particles

A quite attractive and well known strategy to enhance toughness of epoxy material is the use of core/shell nanoparticles.[12,13] They consist of the core (soft) encapsulated with the shell (rigid). These particles, when used in place of liquid rubbers, provide better thermo-mechanical properties.[14] The rigid shell is introduced to the rubbery core to make handling and working with particles possible. In the absence of the rigid shell, rubber particles can easily stick together and lose their size and shape. Additionally, the core/shell morphology allows varying the chemistry of the rubbery core and the rigid shell independently.[15]

### 1.6.4. Block copolymers

The incorporation of nanostructured amphiphilic block copolymers into epoxy thermosets was firstly reported in 1997. It is well known that epoxy resins can be greatly toughened by the formation of nanostructures in the matrix. It is critical to understand the formation of nanostructures to establish the correlation of the morphology with the properties of nanostructured reinforced epoxy.[16,17] The formation of nanostructures in thermosets by the use of block copolymers (BCP) could follow two different mechanisms: i) self-assembly and ii) reaction-induced microphase separation.

For self-assembly approach, the precursors of epoxy act as the selective solvents of one block copolymers and various self-assembly nanostructures such as lamellar, cylindrical, and spherical structures are formed in the mixtures depending on the blend composition before the curing reaction. These nanostructures can be further fixed via subsequent suitable curing process.[18]

Recently, reaction-induced microphase separation mechanism was reported. In this approach, it is not required that the amphiphilic block copolymers are self-organized into

microphases before curing reaction; i.e., all the subchains of block copolymers are miscible with precursors of epoxy resin and only a part of subchains of block copolymers are microphase-separated out upon curing.[19]

### 1.6.5. Inorganic particles

Different inorganic toughening agents are also reported in literature. In order to gain improvements of multiple properties, it is suggested that low or high aspect ratio fillers are incorporated into epoxy. These fillers should possess (1) a higher rigidity than the polymer to increase its stiffness, (2) a high specific surface, (3) a sufficient filler-matrix bonding to improve strength and to allow a controlled stress transfer from the matrix to the fillers, and (3) preferably small dimensions to reduce local stress concentrations and to generate high toughness and impact resistance.

Akbari et al.[20] used clay as nanofiller to modify epoxy resin. Silica nanoparticles were synthesized by sol gel technique and used to enhance the fracture toughness and elastic modulus of epoxy resins.[21] Alumina nanoparticles are interestingly used by other researchers to modify the properties of the epoxy resins including toughness. Zhao et al. studied the effect of alumina nanoparticles on the fracture toughness and fatigue crack propagation of epoxy nanocomposites.[22] Recently, treated and untreated alumina nanoparticles are used to improve the mechanical performances of epoxy structural adhesives.[23]

Generally, rigid fillers with good adhesion to the matrix interfere with crack propagation via various toughening mechanisms such as pining, bridging and/or deflection leading to a higher toughness and rougher fracture surface.[24] Conversely, weakly bonded rigid particles debond easily to activate the plastic void growth, thus dissipating more energy.[25,26]

## 1.7. Toughness mechanisms

Generally, toughening agents are working for dissipating energy and hence increase the fracture energy. Various toughening mechanisms have been proposed to explain the complicated toughening phenomena in epoxy polymers. They can be categorized in two main types, on-plane mechanisms (such as crack pining and crack deflection) or off-plane mechanisms (such as debonding and plastic void growth). Some of these mechanisms are discussed in more details in the following sections.

### 1.7.1. Crack pining

The crack pining theory was first proposed by Lange[27], who identified pining by the bowed shape of the crack front, and further extended by Evans[28] and Green.[29] The authors describe the interaction of a propagating crack front with impenetrable obstacles in brittle composites, and crack-particle interactions are believed to result in higher toughness. Where a crack propagating through the matrix will encounter the particles as obstacles and may be pinned. The crack front between the obstacles moves on and extends by bowing so that the crack length increases. This particularly leads to a higher dissipating which is suggested to enhance the crack resistance. Besides, secondary cracks and new fracture surface may be generated. An example[5] for crack pinning in fracture surface of epoxy/$TiO_2$ is shown in figure 1.1.

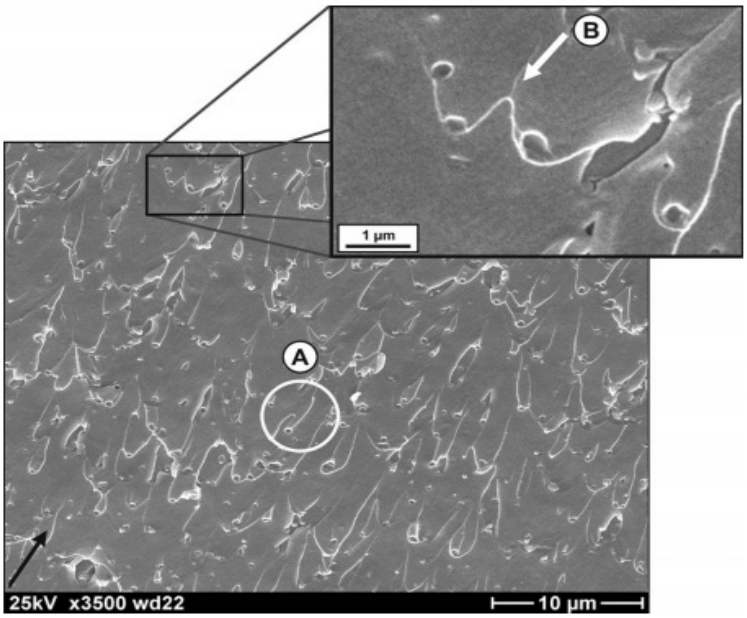


**Figure 1.1:** Crack pinning (item A) and crack front bowing (item B) in epoxy/$TiO_2$ nanocomposites.

### 1.7.2. Crack deflection

The toughening effect could be as a result of crack deflection occurring, where the crack front tilts or twists when it encounters the particles and hence passes around them The theory was described by Faber and Evans.[30,31] It is assumed that the deflected crack is forced to move out of the initial propagation plane by tilting and twisting. Such deflection causes a change in the stress state from mode I to mixed-mode, e.g. mode I/II (tensile/in-plane shear) in the case that the crack tilts, and mode I/III tensile/anti-plane shear) if the crack twists. To propagate crack under mixed mode conditions requires a higher driving force than in pure mode I, which results in a higher fracture toughness of the material.

Compared to the fracture surface area generated by an undeflected crack, the deflection processes increase the total fracture surface area. An indication for the change in fracture surface can be gained by measuring the average surface roughness, Ra, of a fracture surface, which should increase if deflection processes are present. An illustration of crack deflection mechanism is shown in figure 1.2.

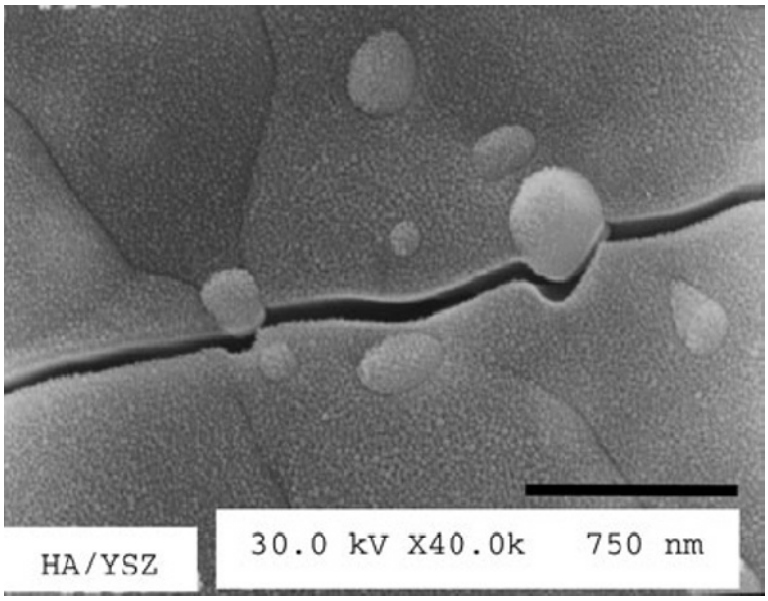


**Figure 1.2:** Crack deflection mechanism in Hydroxyapatite reinforced with 3 mol% of $Y_2O_3$ partially stabilized $ZrO_2$[32]

### 1.7.3. Plastic void growth

In this mechanism weakly bonded particles debond easily to activate the plastic void growth, thus dissipating more energy. The debonding process (cavitation) is generally considered to absorb little energy compared to the plastic deformation of the matrix. However, debonding is essential because this reduces the constraint at the crack tip and hence allows the matrix to deform plastically via a void growth mechanism.[33] Figure 1.3 gives an example for the presence of voids around several of the silica nanoparticles.[34]

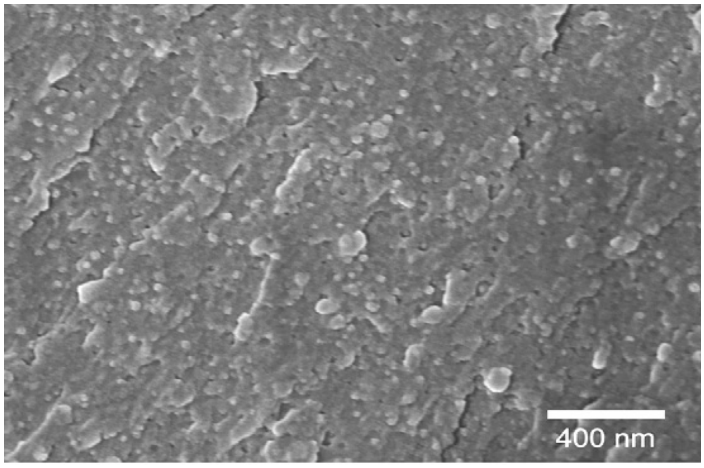


**Figure 1.3:** SEM of the fracture surface of the epoxy polymer containing 9.6 vol% nanosilica**.**

## 1.8. Photoinitiated polymerization

Photoinitiated polymerization is a process in which the monomer is transformed into polymer by a chain reaction initiated by reactive species (free radical or ions), which are generated from photosensitive compounds (photoinitiators/photosensitizers) under the effect of UV light irradiation (figure 1.4).

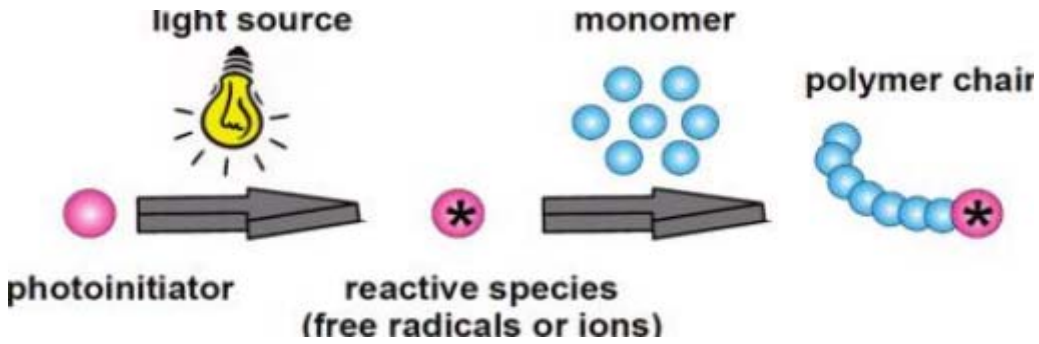


**Figure 1.4:** schematic representation of photoinitiated polymerization

Recently, photopolymerization has become powerful industrial process widely used in various applications including coatings, inks, adhesives, electronics, and photolithography because of its excellent advantages. It offers high rate of polymerization at ambient temperature, lower energy cost, and solvent free formulations. Free radical and cationic photopolymerization mechanisms are well known.[35,36]

### 1.8.1. Photoinitiators

The role of photoinitiator is to convert the physical energy of incident light into chemical energy in the form of reactive intermediates that are capable of initiating the

polymerization process. In spite of its lowest volume in the formulation, a photoinitiator plays a major role in the polymerization. In photocurable systems, photoinitiators affect mainly cure speed, yellowing, and cost.[2] However, other factors such as commercial availability (or easy preparation), solubility particularly in a wide range of monomers, storage stability, and low migration, low odor, and nonyellowing properties in the cured films should also be taken into consideration. In addition, the light absorption properties of the selected photoinitiator need to match the emission wavelength of the light source. Each photoinitiator has advantages and disadvantages, and the selection of photoinitiator very much depends on the requirements of a particular application.[37,38]

In case of cationic photoinitiators, the solubility can be improved by introducing these photoinitiators as mixtures of various compounds. Mostly they are handled as solutions in polar propylene carbonate at 30 to 50% by weight of initiator. These solutions can be easily incorporated into organic materials. The propylene carbonate solvent copolymerizes with the reactive monomers,

The compatibility of the photoinitiator with its environment is a critical factor in determining the efficiency of acid production. For example the quantum yield for acid generation of triphenylsulphonium hexafluoroantimonate (polar salt) in a relatively polar polymethyl methacrylate matrix was found to be in the range of 0.8 to 1.0 (irradiation at 254 nm), whilst the same quantum yield, measured in a less polar polystyrene matrix, was only 0.1-0.2.[39]

### 1.8.2. Free radical photopolymerization

The generation of free radicals from the absorption of UV light by the photoinitiator follows two distinct mechanisms, type I (cleavage) and type II (H-abstraction).[39-41] The majority of type I photoinitiators are aromatic carbonyl compounds with appropriate substitution. An example of type I photoinitiator is given in figure 1.5.

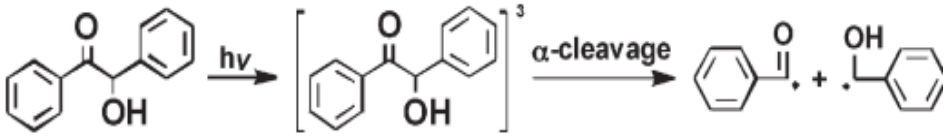


**Figure 1.5:** Photolytic α-cleavage of benzoin

In type II, the initiation is based on a bimolecular reaction, the generation of free radicals and curing rates are generally slower than the generation of free radicals from type I photoinitiators, which are based on unimolecular formation of radicals.

Photolysis of aromatic ketones, such as benzophenone, thioxanthones, and benzil, in the presence of hydrogen donors leads to the formation of a ketyl radical produced from the carbonyl compound and another radical derived from the hydrogen donor.

The overall mechanism of the photoinitiation on the example of benzophenone is represented in figure1.6. The photopolymerization of vinyl monomers is usually initiated by the radical produced from the hydrogen donor where the ketyl radical are relatively stable radicals towards vinyl monomers due to steric hindrance and to the delocalization of unpaired electron.

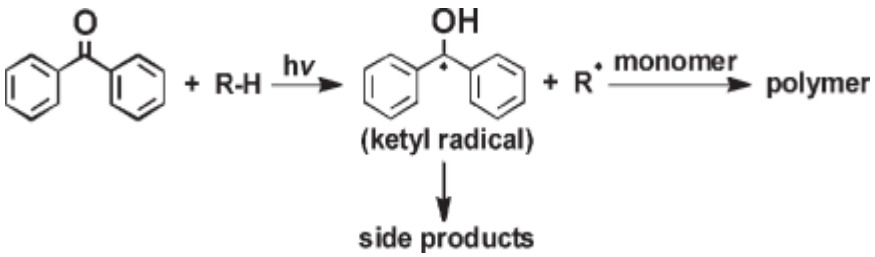


**Figure 1.6:** Type II photoinitiation mechanism with benzophenone and hydrogen donors

One of the major drawbacks of photoinitiated free radical polymerization is related to the well-known oxygen inhibition. Various reactive species playing a role in the polymerization, such excited states as well as initiating and propagating radicals are quenched by $O_2$. Influence of oxygen on the photoinitiated free radical polymerization is schematically represented in figure 1.7. Many strategies have been developed to combat $O_2$ inhibition including use of high-intensity lamps/high cure dosage, high concentration of photoinitiator, inert atmospheres, and additives such as amines and thiols.[36,42]

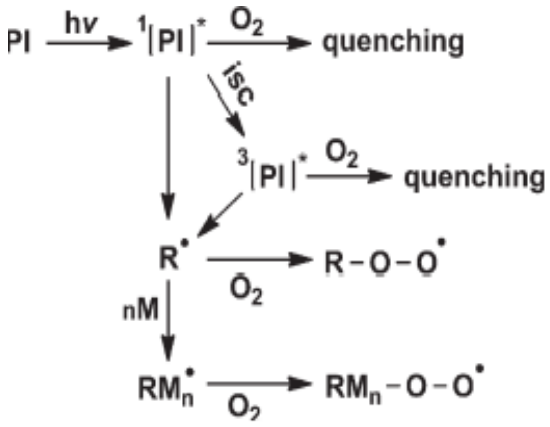


**Figure 1.7:** A scheme of inhibition of photoinitiation and polymerization reactions by oxygen

### 1.8.3. Cationic photopolymerization

Cationic photopolymerization is defined as a polymerization process initiated by the light in which initiating species, Brønsted or Lewis acids, are generated from a photoinitiators. Various types of cationically polymerizable monomers are known:[39,43]

a. Heterocyclic compounds like cyclic ethers, epoxy, cyclic suphides.
b. Vinyl compounds such as vinyl ethers.

Figure 1.8 illustrates how the initiating species attack the vinyl or heterocyclic compounds.

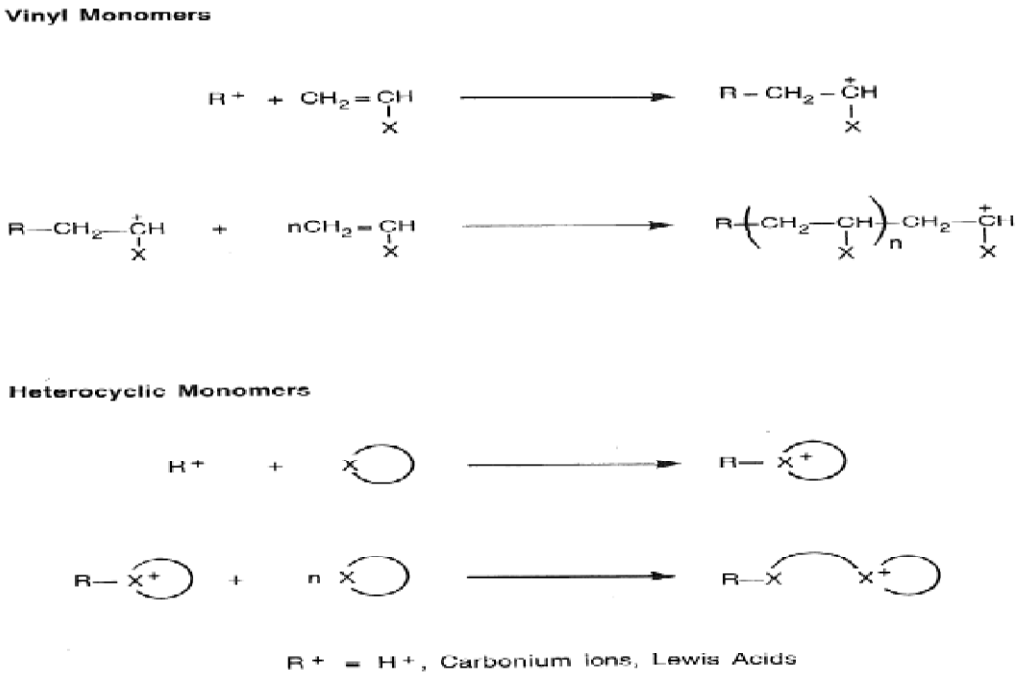


**Figure 1.8**: Cationic photopolymerization of vinyl and heterocylic monomers.

Primarily cationic photopolymerization differs from free radical photopolymerization in the following ways:

- Unlike to free radicals, the initiating species Brønsted or Lewis acids) is usually chemically stable for long time.
- The polymerization, once initiated, continue for a long time even in the absence of light (dark cure).
- Cationic processes are not inhibited by oxygen like free radical ones.

However there are some disadvantages of cationic photopolymerization including inhibition by bases and water which act as chain transfer agent.

Different classes of cationic photoinitiators such as diazonium salts, diaryliodonium salts, triarylsulphonium salts, and ferrocenium salts are already used.

As a result of exposure to UV radiation or visible light, the cationic photoinitiator form a cation. This cation has the ablilty to initiate the polymerization process. The cationic photoinitiator can form a cation directly upon iiradiation or the generation of a cation can depend on the interaction of a sensistizer and a photoinitiator. The mechanism of photoinduced cationic photopolymerization can be summarized as shown in the figure 1.9. triarylsulphonium salt photoinitiator is used as an example.

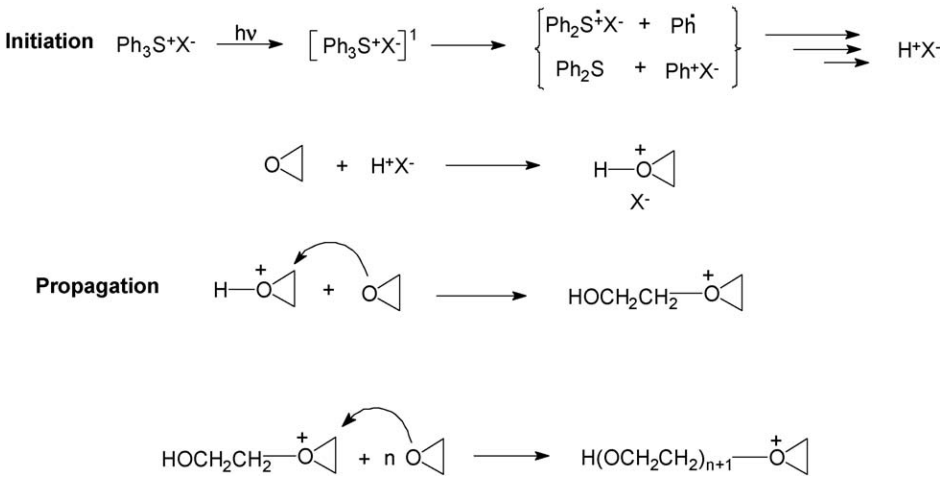


**Figure 1.9:** Mechanism of cationic photopolymerization.

Termination usually is controlled by diffusion mechanism. The reaction stops when the molecular weight is high enough to prevent the diffusion of the unreacted species in the polymeric network.

In presence of OH groups (e.g. water or alcohols) chain transfer mechanism can occurs. The mechanism (see figure 1.10) includes termination of a growing chain and release of another acid species that could start another chain. Hence rate of the reaction is not affected (excepted in the case that the new acid species is less reactive than the growing chain) and, at the same time, groups conversion could increase because the released species possesses a higher mobility than the growing chains. On the other side, if this mechanism becomes predominant low molecular weight chains are obtained. For this reason cationic photopolymerization is strongly affected by presence of humidity and it's not applicable for waterborne formulations.

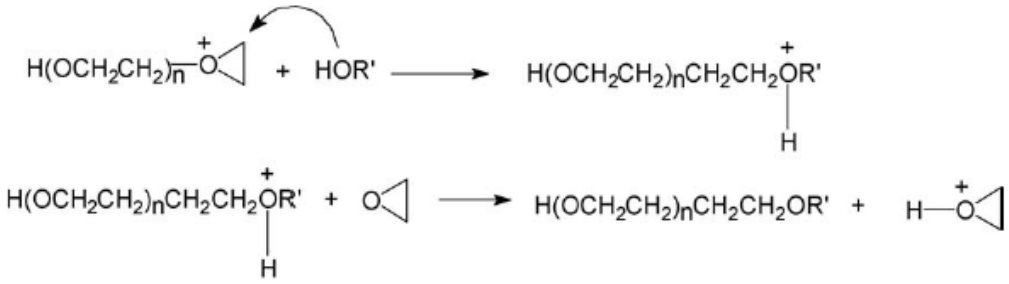

**Figure 1.10**: Chain transfer mechanism in cationic photopolymerization

Cationic photopolymerization historically had a slower development if compared with free radical because this reaction mechanism is strongly controlled by chain transfer mechanism and termination at room temperature. With the synthesis of novel photoinitiators able to generate very stable counterions (e.g.$PF_6^-$ and $SbF_6^-$), and so achieving the possibility of reach high molecular weight, this technique had a great impulse both in scientific and industrial world.

The most widely used category of cationic photoinititors are –onium salts. Different types of onium salts photoinitiators are shown in figure 1.11. diaryliodonium or triarylsulfonium salts are the most important representatives of this class and they are commercially available.

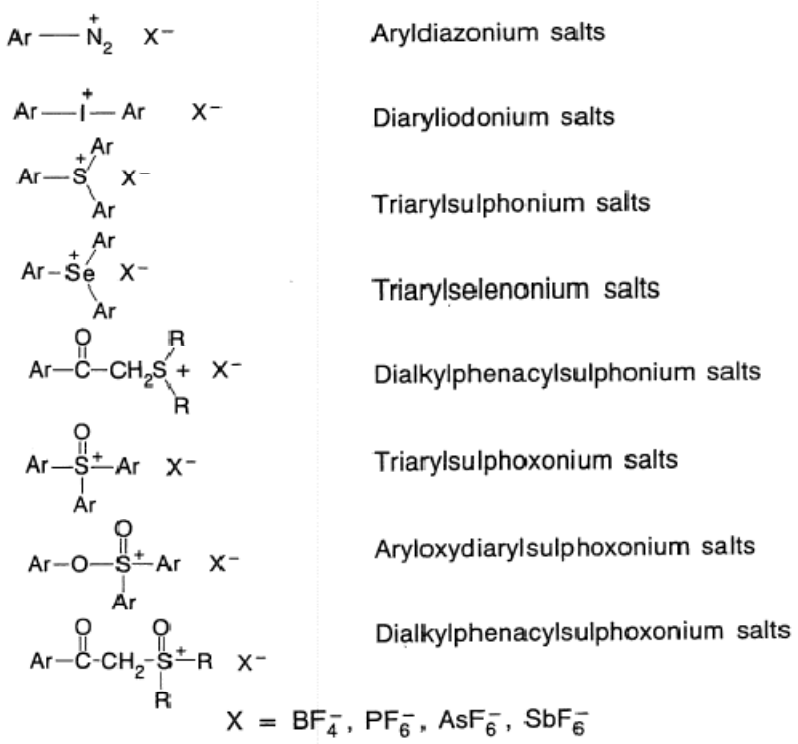


**Figure 1.11:** types of onium salts photoinitiators

## 1.9. Literature survey

Modification of thermosetting epoxy as well as fracture toughness enhancement was discussed in many contributions. Some of these authors' contributions will be briefly presented in the following lines.

Four different generations of hyperbranched polymer (HBPs) (HBP-G1 to HBP-G4) were synthesized via Dhevi et al.[44] using Dipentaerythritol, DIPE, as a core and dimethylol propionic acid, DMPA, as AB2 monomer, and were characterized by spectral, thermal and physical methods. The newly synthesized HBPs were confirmed to exhibit a highly branched structure but the thermal stability decreased with increasing HBP generations. The toughening of epoxy resin was accomplished by reacting each generation of the HBP with hexamethylene diisocyanate, HMDI, and epoxy resin leading to the formation of HBP-Polyurethane/Epoxy-g-Interpenetrating Polymer Networks (HBP-PU/EP-g-IPNs). Compared to neat epoxy and linear PU/EP samples, the HBP modified epoxy samples exhibit greater toughness as observed from the higher impact strength values, which is attributed to the two-phase morphology and tearing of rubber particles which reduces the rate of crack propagation as confirmed from the SEM micrographs. Flexural, thermal stability as well as $T_g$ properties of the modified epoxy samples are lower than that of neat epoxy sample owing to the incorporation of flexible PU linkages into the epoxy resulting in reduced crosslink density of the thermoset epoxy matrix.

Zhang and JiaInc[45] reported the use of low viscosity liquid thermosetting hyperbranched poly(trimellitic anhydride-diethylene glycol) ester epoxy resin (HTDE) as an additive to an epoxy amine resin system. Four kinds of variety molecular weight and epoxy equivalent weight HTDE as modifiers in the diglycidyl ether of bisphenol-A (DGEBA) amine systems are discussed in detail. It has been shown that the content and molecular weight of HTDE have important effect on the performance of the cured system, and the performance of the HTDE/DGEBA blends has been maximum with the increase of content and molecular weight or generation of HTDE. The impact strength and fracture toughness of the cured systems with 9 wt % second generation of HTDE are 58.2 kJ/m$^2$ and 3.20 MPa m$^{1/2}$, which are almost three and two times, respectively, of DGEBA performance. Furthermore, the tensile and flexural strength can be enhanced about 20%. The glass transition temperature, however, was found to decrease to some extent. The

fracture surfaces are evaluated by using scanning electron microscopy, which showed that the homogeneous phase structure of the HTDE blends facilitates an enhanced interaction with the polymer matrix to achieve excellent toughness and strength enhancement of the cured systems, and the "protonema" phenomenon in SEM has been explained by in situ reinforcing and toughening mechanism and molecular simulation.

Varley and Tian[46] reported the use of an epoxidized hyperbranched polymer (HBP) as an additive to an epoxy anhydride resin system. The hyperbranched polymer used was aliphatic polyester with a molecular weight of around 10500 $gmol^{-1}$. The epoxy resin mixture used was a combination of a difunctional diglycidyl ether of bisphenol A (DGEBA) epoxy and an epoxy novolac, and was cured with a catalysed anhydride curing agent. It has been shown that, at a concentration range of 0 to 20wt% addition, the HBP is able to almost double the fracture toughness, with little evidence of any deleterious effects upon processing and the durability of the cured resin system. The flexural modulus and stress, however, were decreased by about 30% as a result of HBP addition while the $T_g$ was found to decrease by about 10%. The processability of the uncured resin systems has been investigated by using rheological and calorimetric techniques and it was found that the processability window, as determined by the gel time and viscosity changes, was relatively unaffected by HBP addition. The fracture surfaces were evaluated by using scanning electron microscopy which showed that the unique structure of the HBP facilitates an enhanced interaction with the polymer matrix to achieve excellent toughness enhancement of the polymer matrix. The durability of the epoxy network has been investigated via thermogravimetric analysis and solvent uptake, and the HBP has been shown to have little systematic deleterious effect upon the degradation temperatures and the total amount of solvent absorbed.

Mixtures of a typical commercial epoxy resin (3,4-epoxy-cyclohexylmethyl -3', 4'epoxycyclohexyl carboxylate, CE) in the presence of hydroxyl hyperbranched polymers (Boltorn H20, H30 and H40) were investigated in the cationic UV curing process.[47] The kinetics of photopolymerization of the systems was studied and compared with that of the pure CE resin. It was found that the epoxy group conversion increased by increasing the amount of HBP. These results were interpreted on the basis of a chain-transfer reaction involving the hydroxyl groups on the surface of the HBP molecule; this determines the flexibility of the network and increases the curing rate. The thermal and mechanical properties of the photocured products were investigated and correlated to the composition

of the UV-curable mixtures and to the structure of the HBP employed. For all the systems investigated, the introduction of the HBP products determined the decrease of the glass transition temperature of the epoxy matrix, since HBPs act as plasticizers. Moreover, the tensile strength was found to decrease with increasing HBP content in the CE resin. In all samples investigated, a clear increase of the impact resistance was observed and attributed to the plasticization effect induced by the presence of the HBPs.

A well-defined multiarm star copolymer, hyperbranched poly(glycidol)-b-poly(ε-caprolactone), with an average of 100-110 arms per molecule and a molecular weight of arms of 1000 g/mol (s-PCL) and a linear PCL analog (l-PCL) were used as modifiers in the curing of diglycidylether of bisphenol A (DGEBA) using ytterbium triflate as cationic initiator.[48] The effect of the polymer topology on the curing and gelation was studied by dynamic scanning calorimetry (DSC) and rheometry. The addition of s-PCL to the resin left the complex viscosity practically unaltered. In contrast the addition of l-PCL incremented substantially the viscosity. The addition of star-shaped modifiers decreased the shrinkage after gelation in a higher extent than the linear analog. The homogeneity of pure DGEBA and modified thermosets was proved by dynamic thermomechanical analysis (DMTA) and electronic microscopy (SEM). The addition of star-like structures led to a higher impact energy fracture in comparison to pure DGEBA and l-PCL modified thermosets and to a lower effect on the microhardness than the linear analog.

The effects of organically modified layered double hydroxide (O-LDH) and epoxy functionalized hyperbranched aliphatic polyester (E1), on the mechanical strength, thermal property and toughness of diglycidyl ether of bisphenol A (DGEBA) epoxy resin were studied in detail by Lv et al.[49] The crystalline structure and morphology of the nanocomposites composed of DGEBA/O-LDH and DGEBA/E1/O-LDH were investigated by wide angle X-ray diffraction analysis and transmission electron microscopy observation. Both results showed that the LDH nanosheets were sufficiently exfoliated and randomly dispersed in the epoxy matrix. The thermal and mechanical properties were compared with the corresponding neat polymer matrix. The enhancement in strength and toughness was achieved by the addition of O-LDH and E1, respectively, and confirmed in terms of fracture surface analysis by scanning electron microscopy.

The properties and morphologies of UV-cured epoxy acrylate (EB600) blend films containing hyperbranched polyurethane acrylate (HUA)/hyperbranched polyester

(HPE) were investigated.[50] A small amount of HUA added to EB600 improved both the tensile strength and elongation at break without damaging its storage modulus (E'). The highest tensile strength of 31.9 MPa and an elongation at break around two times that of cured pure EB600 were obtained for the EB600-based film blended with 10% HUA. Its log E' (MPa) value was measured to be 9.48, that is, about 98% of that of the cured EB600 film. The impact strength and critical stress intensity factor ($K_{Ic}$) of the blends were investigated. A 10 wt % HUA content led to a $K_{Ic}$ value 1.75 times that of the neat EB600 resin, and the impact strength of the EB600/HPE blends increased from 0.84 to 0.95 kJ $m^{-1}$ with only 5 wt% of HPE. The toughening effects of HUA and HPE on EB600 were demonstrated by scanning electron microscopy photographs of the fracture surfaces of films. Moreover, for the toughening mechanism of HPE to EB600, it was suggested that the HPE particles, as a second phase in the cured EB600 film, were deformed in a cold drawing, which was caused by the difference between the elastic moduli of HPE and EB600.

Novel epoxy nanocomposites based on a diglycidyl ether of bisphenol A (DGEBA) epoxy, an epoxy functionalized hyperbranched polymer (HTTE) and nano-$Al_2O_3$ were synthesized with the aim of determining the effect of the nano-$Al_2O_3$ particles and HTTE on the structure and properties of epoxy nanocomposites.[51] The mechanical properties, thermal conductivity, bulk resistivity, and thermal stability of the nano-$Al_2O_3$/HTTE/DGEBA ternary composites were evaluated and compared with the corresponding matrix. The improvement in impact properties of these nanocomposites was explained in terms of fracture surface analysis by SEM. The results indicate that the incorporation of nanoparticles and hyperbranched epoxy effectively improved the toughness of epoxy composites without sacrificing thermal conductivity and bulk resistivity compared to the neat epoxy and $Al_2O_3$/DGEBA, obtaining a well dispersion of nanoparticles in epoxy matrix and solving the drawbacks for single filers filled epoxy nanocomposite.

Novel HBPs with different ratio of hydroxyl and undecenoyl end groups were synthesized starting from Boltorn H30, of which the terminal hydroxyl groups were partially replaced with undecenoyl chains.[52] These novel HBPs have been used as polymeric modifiers for diglycidyl ether of bisphenol A/Methylhexahydrophthalic anhydride(DGEBA/MHHPA) formulations. In that work, the curing kinetics of neat and modified DGEBA/MHHPA formulations has been studied with DSC and FTIR. While

DSC gives limited insight into the curing mechanism, a more detailed picture of the process can be obtained using FTIR. The curing mechanism is complex and involves a series of competing reactions, as determined with FTIR. The effect of the HBPs on the curing kinetics is complex and depends on the amount of reactive hydroxyl groups and the changes in viscosity and mobility that arise from the different degree of modification. The participation of hydroxyl groups from the HBP in the curing may enhance the reaction rate but the lower mobility of the HBP may slow down the process. Incorporation of the HBP into the matrix is assured by the formation of carboxylic acid and subsequent esterification with epoxy groups.

An epoxy resin cured with an anhydride was modified by the addition of commercial core–shell rubber (CSR) particles.[53] These particles were well dispersed through the epoxy matrix, with no agglomeration being observed using atomic force microscopy. The glass transition temperature of the epoxy was 145 $^{o}$C. The addition of CSR particles did not alter the measured value of $T_g$, but the Young's modulus of the epoxy was reduced. Fracture energy of 77 J/m$^2$ was measured for the unmodified epoxy polymer. Addition of the CSR particles increased the fracture energy, a maximum value of 840 J/m$^2$ was measured for the epoxy with the 15 wt% of 115 nm diameter CSR particles. Scanning electron microscopy of the fracture surfaces showed that core to shell debonding followed by plastic void growth of the epoxy, plus shear yielding, were the toughening mechanisms. The measured fracture energies were compared to those using a similar amount, 9 wt%, of a carboxyl-terminated butadieneacrylonitrile (CTBN) rubber. The CTBN particles gave greater fracture energy than using the CSR particles, with a $G_C$ of 671 J/m$^2$ being measured compared to fracture energies of 480–600 J/m$^2$ for the CSR formulations. However, for equal volume fractions of rubber the fracture energies for the CSR and CTBN-modified epoxies are very similar. The operative toughening mechanisms of (i) shear band yielding and (ii) core to shell debonding and plastic void growth were modelled. Excellent agreement was seen between the experimental and the predicted fracture energies. No effect of particle size on the predicted fracture energy was identified for the 100 and the 300 nm diameter particles employed.

Becu et al.[54] used two sets of core-shell (CS) the first CS1 were based on a poly(butadiene co styrene) core and a poly(methyl methacrylate) shell. The second CS2 were based on a poly(butyl acrylate) core and a poly(methyl methacrylate) shell. Dispersion of core shell particles (CS) in an epoxy network was analyzed by manual and

automatic image processing methods yielding quantitative morphological indexes. These indexes were mainly based on the classical coefficient of variation, used for the statistics of the particles counted in a grid, or for the neighbor distances. The rubbery CS were either commercial or homemade having different core nature, shell thickness and functionalization (carboxy or epoxy). Two dispersion methods were used: a laboratory high speed mixer ("Ultraturrax"), or a co-rotating twin screw extruder with different screw profiles and temperature. The shell functionalization was to be a key factor leading to high dispersion. Samples were taken along the extruder screws and analyzed. Multiple kneading blocs followed by reverse screw element were necessary for the obtention of a dispersion equivalent to the one obtained using the "Ultraturrax". The presence of particles (9.5 to 24% in volume) slightly decreased the quasi-static mechanical properties, which are Young's modulus and yield strength. On the contrary, toughness is enhanced, as expected, especially with functionalized particles. In addition, the scatter on the fracture properties was directly related to the morphological heterogeneity index.

The effect of composition and concentration of polystyrene-block-polybutadiene-block-poly- (methyl methacrylate) (SBM) copolymer triblock on final morphologies and properties of modified epoxy networks has been investigated.[55] The DGEBA-MCDEA(4,4′-methylenebis(3chloro-2,6-diethylaniline)) epoxy system, which ensures the miscibility of most of the PMMA blocks until the end of the reaction and thus the generation of a nanostructurated material, has been chosen. For low copolymer concentration (10 wt %), the network structure is found to be independent of the composition and micelles of PS and PB blocks can be indifferently observed. However, increasing copolymer amounts from 10 to 50 wt % induces a morphology change to either "spheres on spheres" or "core-shell" structure depending on the PB content in the triblock. For copolymer concentration higher than 50 wt %, the morphology strongly depends on the processing technique used, and only films prepared by solvent casting show an organization with long-range order similar to the neat block copolymer. The toughness of nanostructured epoxy networks has been evaluated. For low SBM concentration the toughness was observed to linearly vary with the PB concentration. For higher SBM concentrations (30 and 50 wt %) the "spheres on spheres" morphology is found to be more efficient than the "core-shell" one to improve the toughness of the epoxy network. But in all cases a higher toughness is obtained when the nanostructure is preserved; when a macrophase separation occurs, the toughness increase is lower.

The effects of novel core−shell (dendrimer) (CSD) particles on the mechanical properties of epoxy are further studied with the focus on addressing associated processing challenges and hot−wet performance.[56] The particles are produced in a novel grafting reaction between vinyl-containing groups of a monomer of interest (e.g., styrene) and amine-containing polymer (e.g., polyethyleneimine, PEi) in the presence of t-butyl hydroperoxide (TBHP) initiator and with mild heating. Strong interactions between PEi and epoxy occur when the concentrated particle dispersion is mixed with the epoxy/curing agent system, causing a significant increase in the viscosity of the mixture with attendant difficulties in processing. Furthermore, the additional amine groups in the modified epoxy are expected to attract more water molecules, leading to a possible increase in water absorption and subsequent decrease in mechanical properties. Both problems are addressed with the addition of a small amount of styrene monomer to the mixture. First, the viscosity of the curing mixture is reduced dramatically, but not at the expense of subsequent mechanical properties, and SEM micrographs suggest that there are no notable changes in the particle-epoxy interactions. Secondly, while the modulus of the CSD reinforced system obtained under hot-wet conditions is reduced by approximately 20% from values obtained under dry conditions, this reduction shrinks to less than 10% with the addition of styrene monomer.

Epoxy/core-shell particle blends were prepared using a diglycidylether of bisphenol A epoxy and acrylics-type core-shell particles.[57] The core-shell particles (EXL-2330) were commercially available from Rohm and Haas, which consisted of crosslinked poly (butylacrylate) core and grafted poly (methylmehthacrylate) shell. The impact strength of the blends was tested, and the result showed that the epoxy was greatly toughened with optimum core-shell particle content. Meanwhile, the dielectric properties of both epoxy and its blends were investigated using a broadband dielectric analyzer. It was found that the dielectric constant of the epoxy blends with lower core-shell particle content were less than that of the epoxy in the investigated frequency range, while the dielectric loss was less than that of the neat epoxy over a low frequency range, even for the epoxy blends with the optimum core-shell particle content. The dielectric breakdown strength of the epoxy blends at room and cryogenic temperature were also investigated. To identify the primary relationship of the above properties and structure of the epoxy blends, the microstructure of the core-shell particle and the morphology of the samples were observed by transmission electron microscopy and scanning electron microscopy. It

was considered that these epoxy/core-shell particle blends with improved toughness and desirable dielectric properties could have a potential application in the insulation of electronic packaging system.

Liu et al.[17] blended an amphiphilic poly(ethylene-alt-propylene)-b-poly(ethylene oxide) (PEP-PEO) block copolymer (BCP) with a bisphenol A-based epoxy resin formulation and self-assembled into a wormlike micelle structure. With an incorporation of 5 wt % of the BCP material, the fracture toughness was improved by >100% over the neat epoxy. The morphology and mechanical properties of this BCP-modified epoxy were investigated using transmission electron microscopy, dynamic mechanical analysis, tensile tests, and fracture toughness measurements. Toughening mechanisms from the wormlike micelle-modified material were investigated using the double-notch four-point-bending technique(DN-4NPB), and the results are compared with data obtained from the same epoxy thermoset formulation containing a BCP that self assembled into spherical micelles. Elongated cylindrical micelles produce improved toughness, which is interpreted on the basis of a combination of mechanisms including crack tip blunting, cavitation, particle debonding, limited shear yielding, and crack bridging.

Yi et al.[16] synthesized Poly(2,2,2-trifluoroethyl acrylate)-block-poly(glycidyl methacrylate) (PTFEA-b-PGMA) amphiphilic diblock copolymer via sequential RAFT polymerization with 2-phenylpropyldithiobenzoate as a starting chain transfer agent. The reactive amphiphilic diblock copolymer was incorporated into epoxy to obtain the nanostructured thermosets. The results of small-angle X-ray scattering (SAXS) and atomic force microscopy (AFM) showed that the PTFEA-b-PGMA diblock copolymer can be self-assembled in its mixtures with the precursors of epoxy and the microphases of PTFEA were formed before curing reaction. The nanostructures can be fixed via curing reaction at elevated temperature. It is found that the demixing of the reactive block (viz. PGMA) out of epoxy matrix occurred in the process of curing reaction, which exerted a profound impact on the glass transition temperatures of the nanostructured thermosets. The measurements of static contact angles indicate that the nanostructured thermosets containing PTFEA-b-PGMA diblock copolymer displayed a significant enhancement in surface hydrophobicity as well as a reduction in surface free energy. The improvement in surface properties was ascribed to the enrichment of the fluorine containing subchain (i.e., PTFEA) of amphiphilic diblock copolymer on the surface of the nanostructured thermosets, which was evidenced by surface atomic force microscopy. The measurement

of critical stress intensity factor ($K_{IC}$) showed that the fracture toughness of the materials was significantly enhanced by the inclusion of 10 % of PTFEA-b-PGMA diblock copolymer.

A PEP-PEO diblock copolymer at 5 wt % loading was utilized to toughen bisphenol A type of epoxy. The BCP self-assembled into ca. 15 nm spherical micelles that were well dispersed in the matrix. Mechanical characterization indicates that the PEP-PEO diblock block copolymer can greatly improve the fracture toughness of epoxy without compromising its modulus. The DN-4PB test and TEM observation suggest that the major toughening mechanisms in BCP-toughened epoxy include copolymer micelle cavitation followed by matrix shear banding. The fundamental cause(s) for such a small-scale cavitation process is yet to be determined. The likely contributing factors for the observed nanoscale cavitation phenomenon may include the unique BCP micelle structural characteristics and a possible influence of the surrounding epoxy network, which is significantly modified by the PEO block.[58]

Ritzenthaler et al.[59] achieved transparent nanostructurated thermosets by blending and reacting an epoxy system with polystyrene-block-polybutadiene-block-poly(methyl methacrylate) triblock copolymers (SBM triblock), synthesized anionically at an industrial scale. The only requirement is the solubility of the corresponding PMMA homopolymer with the growing thermoset polymer during the whole reaction obtained when MCDEA is used as hardener. Otherwise, using DDS instead of MCDEA, macrophase separation takes place similarly to classical thermoset/thermoplastic blend. The strongly immiscible PB mid block significantly affects the solubility with epoxy, of the chemically linked PS blocks compared to its homopolymer. Indeed, whereas homo PS is initially miscible with epoxy monomers and phase separates during the reaction process, PS blocks were found to be microphase separated even before reaction. The structure of PS and PB blocks is therefore not affected by the reaction. Even if a local segregation of PMMA units at the vicinity of PB microdomains was revealed by viscoelastic measurements, the efficient intermixing of the main PMMA fraction with epoxy, up to the end of the reaction, ensures the structuration of the blend at a nanometer scale.

Because of the synthesis process, fractions of SB diblock copolymer are inherently present in the initial SBM. When blended with epoxy, the triblock used in this

study was shown to have the ability to fully incorporate SB "impurities", through the absence of isolated macrophase-separated region and the only increase of the size of the triblock segregated microdomains. This constitutes their main advantage over similarly synthesized BM diblocks. The generation of nanostructurated thermosets from such industrial SBM does not require any purification step.

Polystyrene-block-poly(methyl methacrylate) (PS-b-PMMA) block copolymers with linear and tetra-armed star-shaped topological structures were synthesized via sequential atomic transfer radical polymerization (ATRP).[60] By controlling the direct connection of the subchains to core, the star-shaped block copolymers with two sequential structures (i.e., s-PMMA-b-PS and s-PS-b-PMMA) were prepared. The arm lengths of the star-shaped block copolymers were controlled to be comparable with the molecular weight of the linear PS-b-PMMA diblock copolymers and the compositions of the star-shaped block copolymers are identical with their linear homologue (i.e., l-PMMA-b-PS). The design of the block copolymers allows one to investigate the effect of topological structures of block copolymers on the morphological structures. It is found that the nanostructures were formed in the thermosets containing l-PMMA-b-PS and s-PS-b-PMMA block copolymers. Considering the difference in miscibility of epoxy with PMMA and/ or PS, it is judged that the reaction-induced microphase separation occurred in the systems. Nonetheless, there is morphological difference between the two blending systems. It is noted that the long-range order of the nanostructures in the epoxy thermosets containing l-PMMA-b-PS is obviously higher than that in the system containing s-PS-b-PMMA. The formation of the morphological difference has been interpreted on the basis of the effects of topological structure of the miscible subchains (i.e., PMMA) on the surface free energy of PS nanodomains. However, the phase separation at the scale of micrometer occurred in the thermosetting blends of epoxy resin with the s-PMMA-b-PS block copolymer. This observation could be responsible for the insufficient suppression of the PMMA chains of macroscopic phase separation of the tetra-armed PS at shell in the block copolymer.

Polystyrene-block-polybutadiene-block-poly[(methylmethacrylate)-stat-methacrylic acid)] (SB(MA)) block copolymers incorporating acid-reactive functionalities in the last block have been synthesized and studied as modifiers for epoxy thermosets based on the diglycidyl ether of bisphenol A (DGEBA). Different techniques including differential scanning calorimetry (DSC), Fourier transform infrared spectroscopy (FT-IR),

and transmission electron microscopy (TEM) have been used to demonstrate the effectiveness of the reaction-induced modification compared to that with the nonreactive or slowly reacting polystyrene-block-polybutadiene-block-poly[(methyl methacrylate)-stat-(tert-butyl methacrylate)] SB(MT) triblock copolymer. Morphological characteristics revealed by TEM indicate that SB(MT) and SB(MA) are both miscible with the epoxy prepolymer. The kinetics of grafting, network formation, and possibly phase separation were quantified from FT-IR, DSC, and cloud point investigations of DGEBA/ DDS (4,4′-diaminodiphenyl sulfone) as an epoxy-thermoset model system in the presence of poly[(methyl methacrylate)-stat-(methacrylic acid)] (HT121) or the block copolymers. The cure of the thermoset/block copolymer system has been explored using six different curing processes: 2-phenylimidazole (2-PI), alone or in the presence of methyltetrahydrophthalic anhydride (MTHPA) as comonomer, accelerated dicyandiamide (DICY), and three different diamines as comonomers without accelerator: 4,4′-methylenebis(3chloro-2,6-diethylaniline) (MCDEA), 4,4′-methylenedianiline (MDA), and DDS. The use of reactive block copolymers instead of nonreactive ones permits a better control of morphology. The materials' performances are analyzed in terms of transparency, glass transition temperature, $T_g$, and linear elastic mechanics at break, $K_{IC}$, as a function of the hardener type.[61]

Höfflin et al.[62] used thermoplastic elastomers based on polyetheresters with polyoxytetramethylene soft segments and poly(hexamethyleneterephthalate) hard segments to toughen anhydride-cured epoxy resins. The ratio between hard and soft segments and the crystallinity of the hard segments prepared by incorporating poly(hexamethyleneisophthalate) in the block copolymer were varied in order to examine the effect of the modifier's molecular architecture on morphology and mechanical properties of the resin, such as toughness, strength, and stiffness. The experimental data show that segmented polyetheresters are suitable toughening agents for epoxies. The compatibility between resin and toughener and also the mechanical properties of the modified resin depend on the ratio between the hard and soft segments. Epoxy resins blended with 10 wt % of the polyetherester exhibit an increase in toughness by 50–150%, while strength and modulus decrease by 20% or less. An optimal phase adhesion at levels between 70 and 85 wt % of soft segments in the modifier results in a maximum of toughness enhancement (by about 150%) of the resin accompanied with only a slight drop

in strength and stiffness (by about 15%). The glass transition temperature is only slightly affected.

Ma et al.[63] investigated the effect of silica nanoparticles on the mechanical property and fracture toughness of two epoxy systems cured by Jeffamine D230 (denoted J230) and 4,40-diaminodiphenyl sulfone (denoted DDS), respectively. Toughening mechanisms were identified by a tailor-loaded compact tension method which quantitatively recorded the deformation of a damage zone in the vicinity of a sub-critically propagated sharp crack tip. 20 wt% silica nanoparticles' fraction provided 40% improvement in Young's modulus for both systems; it improved the toughness of J230-cured epoxy from 0.73 to 1.68 $MPam^{1/2}$, and for the other system improved from 0.51 to 0.82 $MPam^{1/2}$. The nanoparticles not only stiffen, strengthen and toughen epoxy, but reduce the effect of flaws on mechanical performance as well. In both systems, nanosilica particle deformation, internal cavitation and interface debonding were not found, different to previous reports. This could be due to the various hardeners used or different identification techniques employed. The toughening mechanisms of the J230-cured nanocomposite were attributed to the formation and development of a thin dilatation zone and nanovoids, both of which were induced, constrained and thwarted by the stress fields of the silica nanoparticles. Regarding 10 wt% silica-toughen epoxy cured by J230, a thicker and shorter dilatation zone was found, where neither nanoparticles nor nanovoids were observed. With regard to the DDS-cured system, much less dilatation and voids were found due to the hardener used, leading to moderately improved toughness.

Hybrid materials have been formed using an epoxy polymeric matrix and a range of inorganic particles[64], including mica and organically-modified montmorillonites (organoclays), with various concentrations of the silicate modifier up to about 30 wt.% depending upon the viscosity increase induced by the presence of the silicate. Wide-angle and small-angle X-ray scattering plus transmission electron microscopy were used to identify the morphologies produced, which included particulate, intercalated and ordered exfoliated. The modulus of these composites increased with the weight fraction of silicate. The morphology had a small effect on the measured modulus; the nano-composites with the ordered exfoliated microstructure showing the highest values of the modulus for a given volume fraction of silicate. The fracture toughness, $K_c$, and the fracture energy, $G_c$, initially increased as the weight fraction of the silicate was increased, but then decreased at relatively high concentrations. The measured moduli and

toughnesses were compared to theoretical predictions. The measured moduli values showed very good agreement with the predicted values, whilst the agreement for values of the measured fracture energy, $G_c$, with the predicted values, based upon a crack deflection toughening mechanism, were less convincing. Indeed, analysis of the fracture surfaces using scanning electron microscopy showed that the main toughening effect of the silicate particles is due to plastic deformation of the epoxy matrix around the particles.

In a study reported by Rafiee et al.[65], the mechanical properties of epoxy nanocomposites with graphene platelets, single-walled carbon nanotubes, and multi-walled carbon nanotube additives were compared at a nanofiller weight fraction of 0.1±0.002%. The mechanical properties measured were the Young's modulus, ultimate tensile strength, fracture toughness, fracture energy, and the material's resistance to fatigue crack propagation. The results indicate that graphene platelets significantly out-perform carbon nanotube additives. The Young's modulus of the graphene nanocomposite was~31% greater than the pristine epoxy as compared to~3% increase for single-walled carbon nanotubes. The tensile strength of the baseline epoxy was enhanced by~40% with graphene platelets compared to~14% improvement for multi-walled carbon nanotubes. The mode I fracture toughness of the nanocomposite with graphene platelets showed~53% increase over the epoxy compared to ~20% improvement for multi-walled carbon nanotubes. The fatigue resistance results also showed significantly different trends. While the fatigue suppression response of nanotube/epoxy composites degrades dramatically as the stress intensity factor amplitude is increased, the reverse effect is seen for graphene-based nanocomposites. The superiority of graphene platelets over carbon nanotubes in terms of mechanical properties enhancement may be related to their high specific surface area, enhanced nanofiller-matrix adhesion/interlocking arising from their wrinkled (rough) surface, as well as the two-dimensional (planar) geometry of graphene platelets.

Mixed mode fracture resistance of epoxy-based nanocomposites reinforced with carbon nanoparticles of three different shapes is studied.[66] The nanodiamond (ND) of spherical shape, the carbon nanofiber (CNF) of cylindrical shape and the graphene oxide (GO) nanoplatelets are used to prepare the nanocomposites. The semi-circular bending specimen (SCB) is employed to perform a total number of 36 mixed mode fracture tests on the prepared nanocomposites. Fracture toughness of nanocomposites having high aspect ratio fillers (i.e. CNF and GO) is found to be higher than that of ND

nanocomposites. The fracture mechanisms of nanocomposites and the effect of filler shape on these mechanisms are discussed. In addition, the dispersion state of reinforcements and the fracture surface characteristics are investigated using the photographs taken by transmission electron microscopy (TEM) and scanning electron microscopy (SEM).

The three different sized chemical functionalized graphene (GO) sheets, namely GO-1 (D50 = 10.79 μm), GO-2 (D50 = 1.72 μm) and GO-3 (D50 = 0.70 μm), were used to fabricate a series of epoxy/GO nanocomposites.[67] Fracture toughness of these materials was assessed. The results indicate that GO sheets were dramatically effective for improving the fracture toughness of the epoxy at a very significant low loading. The enhancement of the epoxy toughness was strongly dependent on the size of GO sheets incorporated. GO-3 with smaller sheet size gave the maximum reinforcement effect compared with GO-1 and GO-2. The incorporation of only 0.1 wt% GO-3 was observed to increase the fracture toughness of pristine epoxy by ~75%. The toughening mechanism was well understood by fractography analysis of the tested samples. Massive cracks in the fracture surfaces of the epoxy/GO nanocomposites were observed. The GO sheets effectively disturbed and deflected the crack propagation due to its two dimensional structure. GO-3 sheets with smaller size were highly effective in resisting crack propagation, and a large area of whitening zone was observed. The incorporation of GO also enhanced the stiffness and thermal stability of the epoxy.

## 1.10. References:


1. J. Pascault, R. Williams, Epoxy polymers - New materials and Innovations. Weinheim, Germany: Wiley-VCH; 2011.
2. W. Green, Industrial Photoinitiators -A Technical Guide,. CRC Press Taylor & Francis Group; 2010.
3. H. Pham , M. Marks, Epoxy resins , in The Encyclopedia of Polymer Science and Technology (online edition), John Wiley & Sons, Inc. , New York , pp. 678-804; 2004.
4. R. Bagheri, B. Marouf, R. Pearson, Polym Rev 2009; 49: 201.
5. B. Wetzel, P. Rosso, F. Haupert, K. Friedrich. Eng Fract Mech 2006; 73: 2375.
6. A. Collyer, ''Rubber Toughened Engineering Plastics,'', Chapman & Hall, London; 1994.
7. M. Sangermano, E. Amerio, A. Di Gianna, A. Priola, D. Pospiech, B. Voit, Macromol Symp 2007; 254:9.
8. M. Sangermano, H. El Sayed, B. Voit, Polymer 2011; 52:2103.
9. I. Blanco, G. Cicala, C. Lo Faro, O. Motta, G. Recca. Polym Eng Sci 2006; 46: 1502.
10. D. Ratna, G. Simon, Polymer 2001; 42:8833.
11. D. Foix, M. Erber, B. Voit, A. Lederer, X. Ramis, A. Mantecón, A. serra, Polym Degrad Stab 2010; 95:445.
12. H. J. Sue, Polym. Eng. Sci. 1991; 3: 275.
13. H. J. Sue, E. I. Garcia-Meitin, N. A. Orchard, J. Polym. Sci: Polym. Phys. 1993; 31:595.
14. C. K. Riew, A. R. Siebert, R. W. Smith, M. Fernando, A. J. Kinloch, Polym. Mater. Sci. Eng. 1994; 207:5.
15. Z. Zhong, Y. Jian, G. Zhaoxia, L. Ying, Front. Chem. Chin. 2006; 1: 459.
16. F. Yi, R. Yu, S. Zheng, X. Li, Polymer 2011; 52:5669.
17. J. Liu, Z. Thompson, H. Sue, F. Bates, M. Hillmyer, M. Dettloff , G. Jacob, N. Verghese , H. Pham, Macromolecules, 2010; 43:7238.
18. M. Hillmyer, P. Lipic, D. Hajduk, K. Almdal, F. Bates, J Am Chem Soc 1997; 119:2749.
19. F. Meng, S. Zheng, W. Zhang, H. Li, Q. Liang, Macromolecules 2006;39:711.
20. B. Akbari, R. Bagheri, Eur. Polym. J. 2007; 43:782.
21. C. Basara, U. Yilmazer, G. Bayram, J Appl. Polym. Sci. 2005; 98:1081.
22. S. Zhao, L. S. Schadler, H. Hillborg, T. Auletta, Compos. Sci. Technol. 2008; 68:2976.
23. A. Omrani, L. C. Simon, A. A. Rostami, Mater. Chem. Phys. 2009; 114:145.
24. A. Dorigato, A. Pegoretti, J. Nanopart. Res. 2011; 13:2429.
25. J. Lee, A. F. Yee, Polymer 2000; 41:8363.
26. A.J. Kinloch, A.C. Taylor, J. Mater. Sci. 2002; 37:433.
27. F. Lange, Phil Mag 1970; 22:983.
28. A. Evans, Phil Mag 1972; 26:1327.
29. D. Green, P. Nicholson, J. Embury, J Mater Sci 1979; 14:1657.
30. K. Faber, A. Evans, Acta Metall 1983; 31(4):565.
31. K. Faber, A. Evans, Acta Metall 1983;31(4):577.

32. H. Vasconcelos and M. Barreto, Nanoscale Res. Lett., 2011, 6:20
33. R. Bagheri, R. Pearson, Polymer 2000; 41:269.
34. B. Johnsen A. Kinloch, R.Mohammed, A. Taylor, S. Sprenger. Polymer 2007; 48:530.
35. J. Fouassier, In Photoinitiation, Photopolymerization, and Photocuring: Fundamentals and Applications; Hanser/Gardner Publications: Munich; 1995.
36. Y. Yagci, S. Jockusch, N. J. Turro, Macromolecules, 2010; 43:6245.
37. Norman S. Allen, Handbook of photochemistry and photophysics of polymer materials, John Wiley & Sons, Inc.; 2010.
38. B. Monroe, G. Weed, Chem. Rev. 1993; 93: 435.
39. K. K. Dietliker, Chemistry and Technology of UV and EB Formulation for Coatings, Inks and Paints, volume III-Photoinitiators for Free radical and Cationic Polymerisation, SITA Technology; 1999.
40. H. Gruber, Prog. Polym. Sci. 1992; 17: 953.
41. H. Hageman, Prog. Org. Coat. 1985; 13:123.
42. J. P. Fouassier, D. Ruhlmann, Y. Takimoto, M. Harada, M. Kawabata, J. Polym. Sci., Part A: Polym. Chem. 1993; 31: 2245.
43. M.Sangermano, G. Malucelli, R. Bongiovanni, A. Priola, U. Annby, N. Rehnberg, Eur. Polym. J. 2002; 38: 655.
44. D. Dhevi, S. Jaisankar, M. Pathak, European Polymer Journal 2013; 49: 3561.
45. D. Zhang, D. JiaInc. J Appl Polym Sci 2006; 101:2504.
46. R. Varley, W. Tian, Polym Int 2004; 53:69.
47. M. Sangermano, G. Malucelli, R. Bongiovanni, A. Priola, A. Harden, Polym Int 2005; 54:917.
48. M. Morell, X. Ramis, F. Ferrando, À. Serra, Polymer 201; 52:4694.
49. S. Lv, Y. Yuan, W. Shi, Progress in Organic Coatings, 2009; 65:425.
50. G. Xu, Y. Zhao, W. Shi, Journal of Polymer Science: Part B: Polymer Physics 2005; 43:3159.
51. J. Fua, L. Shia, Q. Zhonga, Y. Chena, L. Chen, Polym. Adv. Technol. 2011; 22:1032.
52. M. Floresa, X. Francosa, X. Ramis, A. Serra, Thermochimica Acta, 2012; 544:17.
53. G. Giannakopoulos, K. Masania, A. Taylor, J Mater Sci 2011; 46: 327.
54. L. Becu, M. Taha, A. Maazouz, J Mater Sci 2002; 37: 41.
55. S. Ritzenthaler, F. Court, Girard-Reydet, L. Leibler, J. Pascault, Macromolecules 2003; 36:118.
56. F. Nguyen, J. Berg, Composites: Part A 2008; 39:1007.
57. W. Wan, D. Yu, J. He, Y. Xie, L. Huang, X. Guo, Journal of Applied Polymer Science, 2008; 107:1020.
58. J. Liu, H. Sue, M. Hillmyer, Z. Thompson, F. Bates, M. Dettloff, , G. Jacob, N. Verghese, H. Pham, Macromolecules 2008; 41:7616.
59. S. Ritzenthaler, F. Court, L. David, Girard-Reydet, L. Leibler, J. Pascault, Macromolecules 2002; 35: 6245.
60. W. Fan, S. Zheng, Polymer 2008; 49:3157.
61. V. Rebizant, A. Venet, E. Girard-Reydet, F. Tournilhac, C. Navarro, J. Pascault, L. Leibler, Macromolecules 2004; 37:8017.

62. F. Höfflin, L. Könczöl, W. Döll, J. Morawiec, R. Mülhaupt, J Appl Polym Sci 2000; 76:623.
63. J. Ma, M. Mo, X. Du, P. Rosso, K. Friedrich, H. Kuan, Polymer 2008; 49:3510.
64. A. Kinloch, A. Taylor, J Mater Sci 2006; 41: 3271.
65. M. Rafiee, J. Rafiee, Z. Wang, H. Song, Z. Yu, N. Koratkar, ACS Nano, 2009; 3(12): 3884.
66. S. Shadlou, E. Alishahi, M. Ayatollahi, Composite Structures 2013; 95: 577.
67. X. Wang, J. Jin, M. Song, Carbon 2013; 65:324.

# 2

# Experimental & characterization techniques

## 2.1. Materials

Bis-cycloaliphatic diepoxy resin 3,4-epoxy-cyclohexylmethyl- 3,4-epoxycyclohexyl carboxylate (CE), and the cationic photoinitiator triphenylsulfonium hexafluoroantimonate, $Ph_3SSbF_6$ (as a 50% solution in propylene carbonate) were obtained from Aldrich and their chemical structure are given in figure 2.1.

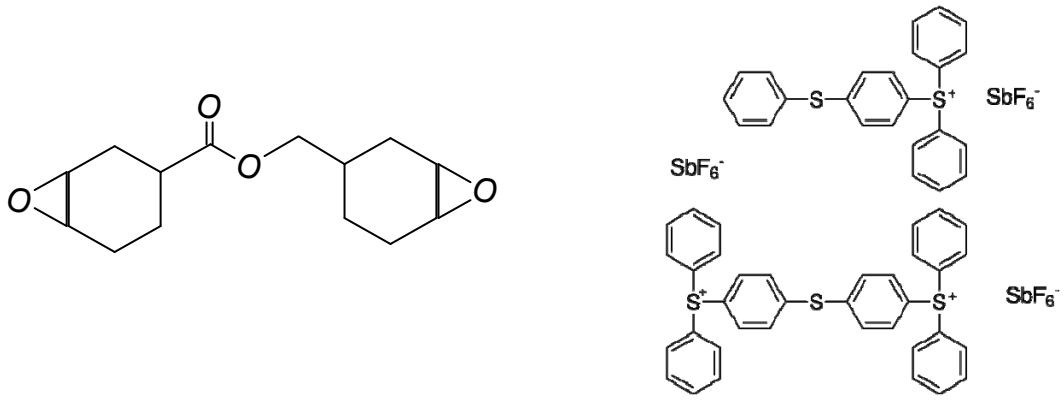


**Figure 2.1:** chemical structures of Cycloaliphatic epoxy(CE) (left) and cationic photoinitiator (right)

The butyl acrylate (BA), methyl methacrylate (MMA), glycidyl methacrylate (GMA), and styrene (St) monomers were purchased from Aldrich and purified by passing through a basic alumina column to remove the inhibitor.

Potassium persulfate, (KPS), crosslinking agent trimethylolpropane trimethacrylate (TMPTMA), sodium dodecyl benzene sulfonate (SDBS), sodium bicarbonate and $AlCl_3$ were used as received.

α- $Al_2O_3$ with 150 nm diameter and 14.5 $m^2.g^{-1}$ specific surface area was purchased from Taimei Chemical Co., Japan

Poly(ethylene glycol) methyl ether (PEG-OH; Mn ca., 2000 and 5000) , N,N,N,N,N pentamethyldiethylenetriamine (PMDETA) (99%, Aldrich), Ethyl 2-bromoisobutyrate (EBrIB) (99%, Aldrich), copper bromide (CuBr) (99.999%, Aldrich), copper chloride (CuCl) (99.99% Aldrich), and diphenyl ether (anhydrous 99.9%, Aldrich) were used as received.

2- bromoisobutyryl bromide, aluminium oxide (neutral, activated) were purchased from Aldrich. Anhydrous tetrahydrofuran, methylene chloride, n-hexane and triethylamine were purchased from Aldrich and the anhydrous solvents were stored over molecular sieves.

## 2.2. Characterization techniques

### 2.2.1. Real Time FT-IR

The kinetics of the photopolymerization was determined by real time FT-IR spectroscopy, using a Thermo-Nicolet 5700 instrument. The liquid formulations were coated onto a silicon wafer by a wire-wound applicator obtaining a 25 μm thick film. The sample was exposed simultaneously to the UV beam, which induces the polymerization, and to the IR beam which analyzes in situ the extent of the reaction. the epoxy group conversion was followed by monitoring the decrease in absorbance of the epoxy groups in the region of 750-780 $cm^{-1}$. A medium pressure mercury lamp (Hamamatsu LC8) equipped with an optical guide was used to start the photopolymerization.

### 2.2.2. Insoluble Fraction

The gel content or insoluble fraction, of the cured films was determined by measuring the weight loss after 24h extraction with chloroform at room temperature, according to ASTM D2765-01 standard test method.

### 2.2.3. Differential Scanning Calorimetry-DSC

DSC measurements were performed with a TA Instruments DSC1 METTLER STAR1/System equipped with a low temperature probe. Different ranges of temperature were utilized for the different samples depending on their $T_g$. In all the experiments the heating rate was 20 °C/min.

### 2.2.4. Field Emission Scanning Electron Microscope-FESEM

The surfaces of the cured coatings were investigated with a FE-SEM Supra 40 Zeiss microscope with the in-lens detector placed above the objective lens, in order to directly detect the beam-path and collect images at very low acceleration voltages (1.5 - 5 kV). In this way the effects due to the accumulation of local charges on the surface of nonconductive materials, that otherwise can significantly deteriorate the imaging quality, were minimized.

### 2.2.5. Dynamic Mechanical Thermal Analysis-DMTA

DMTA on the photocured samples (after additional thermal post-curing for 4 h at 100 $^{o}$C) was performed on a MK III Rheometrics Scientific Instrument at 1 Hz frequency in the tensile configuration with 3 K/min. The storage modulus, E', and the loss factor, tan δ, were measured from low temperature up to the temperature at which the rubbery state was attained. The $T_g$ value was assumed as the maximum of the loss factor curve (tan δ).

### 2.2.6. Dynamic Light Scattering (DLS)

The DLS measurements were done on a Zetasizer Nanoseries ZS90 (Malvern). It was used to determine the particle size and size distribution of core/shell nanoparticles.

### 2.2.7. Impact Resistance

The impact resistance measurements were performed on thick samples under Charpy pendulum according to ASTM D 6110-04. A number of five specimens for each sample were evaluated.

### 2.2.8. Proton Nuclear Magnetic Resonance-$^1$H NMR

$^1$H NMR spectra were recorded using Bruker Avance III 500 spectrometer operating at 500.13 MHz and $CDCl_3$ as solvent at room temperature. Molar masses of the block copolymers, lengths of their block were determined from $^1$H NMR spectra, by comparing the peak integrals of PEG as an internal standard to those of block copolymer.

### 2.2.9. Size Exclusion Chromatography-SEC

SEC was used for determination of molar mass distributions. SEC equipped with HPLC pump Agilent 1200 Series (Agilent, USA) and coupled to a viscosity/differential refractive index (RI) dual detector (ETA-2020, WGE Dr. Bures, Germany) and a multi angle laser light scattering-detector (MALLS) Dawn®EOS (Wyatt Technologies, USA). A PL gel 5 μm Mixed C chromatography column (300 mm x 7,5 mm (Polymer Laboratories, Ltd., UK) was used with THF (Acros, Germany) as a solvent. Flow rate was 1 ml/min. All evaluations were made with the software ASTRA 4.9 (Wyatt Technology Corporation, USA).

### 2.2.10. Scratch Resistance

Scratch test was carried out on a CSM Micro-Combi Tester by using Rockwell C diamond scratch indenter (tip radius R =800 μm) and progressively increasing the load from 0.2 N to 30 N for a scratch length of 3 mm and at a scratch rate of 1 mm.min$^{-1}$.

### 2.2.11. Fracture toughness

Fracture toughness measurements of the prepared epoxy specimens were performed on the basis of the linear elastic fracture mechanics (LEFM) approach. A single-edge-notch three-point-bending (SENB) test was used to obtain the mode I critical stress intensity ($K_{IC}$) and fracture energy ($G_{Ic}$) of the neat epoxy and BCP modified epoxy in accordance with the ISO 13586-2000 method.

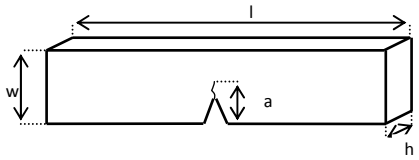


**Figure 2.2:** Notched (SENB) three-point bend specimen

The test was performed on Zwick universal testing machine UPM Z2.5 (max. load 1kN) at a crosshead speed of 3 mm/min. Four specimens were used to determine $K_{IC}$ of the samples. The maximum force prior to fracture (F) is determined from stress-strain graphs then used in the following formula to calculate $K_{IC}$ values.

$$K_Q = f(a/w) \cdot \frac{F}{h\sqrt{w}}$$

Where f(a/w) the fracture geometry factor, a the length of the crack (mm), h the specimen thickness (mm),w is the specimen width (mm) (figure 2.2).

The test was carried out at room temperature (23 ± 1 ° C) and relative humidity (50 ± 3 %.). The specimen dimensions were (*h*=2.5 mm, *w*= 8 mm, *l*= 50 mm) and the span was 32 mm.

# 3

# Epoxy containing hyperstar polymers

## 3.1. Abstract

New hyperstar polymers (HSP) based on a hyperbranched polyester core (HBP-OH) and PMMA or P(MMA-b-HEMA) block copolymer arms have been prepared to use as nanoscale soft particle-like additives in epoxy matrix cured cationically by UV light. The effects of the additive on the epoxy group conversion, gel content, morphology and the thermal and viscoelastic properties of the cured materials were evaluated. It was found that non-reactive hyperstar HBP-PMMA resulted in phase-separated materials with low effect on flexibilization whereas by use of HBP-P(MMA-b-HEMA) the OH groups in the HEMA units allowed chemical bonding of the HSP to the epoxy network and hindered phase separation.

## 3.2. Materials and hyperstar polymers preparation

bis-cycloaliphatic diepoxy resin 3,4-epoxy-cyclohexylmethyl- 3,4-epoxycyclohexyl carboxylate (CE), triphenylsulfonium hexafluoroantimonate, $Ph_3SSbF_6$ (as a 50% solution in propylene carbonate).

The hyperstar polymers were supplied by another group at Leibniz Institute of Polymer Research Dresden, Germany. They synthesized HSPs according to the following reaction reported in figure 3.1.

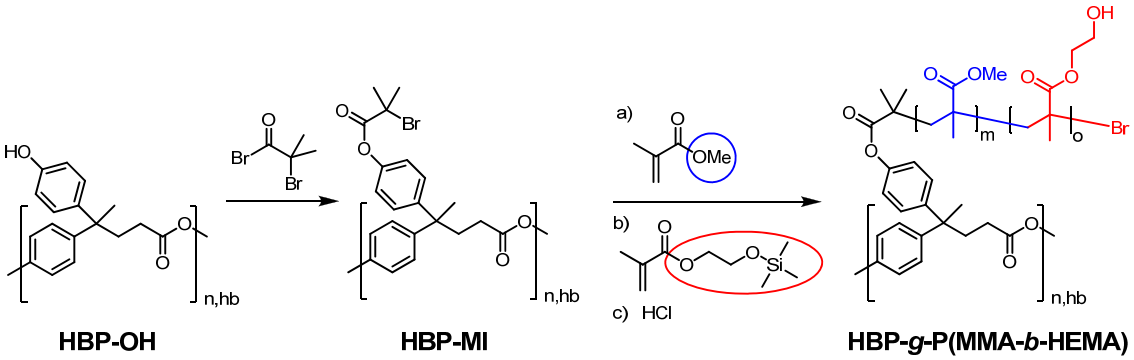


**Figure 3.1**: Scheme of hyperstar polymers synthesis

Briefly, the hyperbranched core HBP-OH, synthesized through polycondensation of 4,4-bis(4-hydroxyphenyl)valeric acid[1], was modified with 2-bromoisobutyryl bromide to yield a Hyperbranched macroinitiator (HBP-MI) for ATRP polymerization similar as described in references[2-4]. HBP-MI was then further used for the controlled radical "grafting from" of MMA followed by addition of respective amount of HEMA leading to short PHEMA blocks at the PMMA chains.

The hyperstar polymers were named as HBP-PMMA/ 0%HEMA, HBP-PMMA/12%HEMA and HBP-PMMA/26%HEMA, respectively. They contain a hyperbranched polyester core named (HBP-OH) and linear arms consisting of either 100% PMMA units (HBP-PMMA/0%HEMA) or block copolymer arms consisting of P(MMA-b-HEMA) with aliphatic OH groups (HBP-PMMA/12%HEMA and HBP-PMMA/26%HEMA) at the end of the hyperstar arms. A schematic representation of the synthesized HSPs is reported in Figure 3.2, which shows the HBP-core, the hyperstar without the HEMA-block (HBP-PMMA/0%HEMA) and the hyperstar with the P(MMA-b-HEMA) star arms (HBP-PMMA/12%HEMA and HBPPMMA/ 26%HEMA).

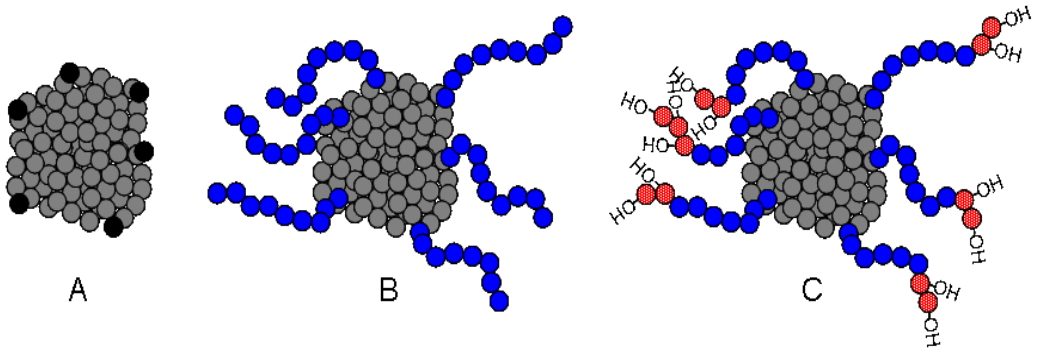


**Figure 3.2:** Schematic representation of the synthesized HBP: the core polyester-HBP (A), the hyperstar polymer with PMMA-arms (B) and the hyperstar with the P(MMA-b-HEMA) arms (C).

The characteristics of the prepared HSPs are reported in Table 3.1.

**Table 3.1:** Characteristics of the hyperstar polymers used in the formulations.

| | $P_{n,th}$[a] (o - p) | $P_{n,NMR}$[b] (o - p) | $M_{n,SEC}$[c] [g/mol] | PD[c] | $T_{g,DSC}$ [°C] |
|---|---|---|---|---|---|
| hb core: HBP-OH | | | 4 000 | 3.0 | 125 |
| macroinitiator: HBP-MI | | | 13 000 | 1.6 | 138 |
| **HBP-*g*-P(MMA-*b*-HEMA): (HSP)** | | | | | |
| HBP-PMMA/0%HEMA | 29 – 0 | 33 (±5) – 0 | 285 000 | 3.4 | 121 |
| HBP-PMMA/12%HEMA | 25 – 4 | 30 (±5) - 4 (±2) | 384 000 | 3.1 | 120 |
| HBP-PMMA/26%HEMA | 21 - 7 | 26 (±4) - 9 (±2) | 350 000 | 3.1 | 118 |

[a] For MMA (o) and HEMA (p): $P_{n,th}$ ≈ monomer conversion·[monomer]/[initiating groups]
[b] Determined *via* NMR
[c] Determined *via* SEC after linear fit (LS-detector, in DMAc + 3 g/L LiCl)

## 3.3. Sample formulation

For photopolymerizable formulations the hyperstar polymers were added to the epoxy resin in the range between 5 and 20 phr (per hundred resin). Triphenylsulfonium hexafluoroantimonate as photoinitiator was added to all the formulations at 2 wt% with respect to the CE content. The formulations were coated on glass slides by means of a wire-wound applicator and cured with a medium vapour pressure mercury dynamic UV

lamp (Fusion, H bulb) with an intensity on the surface of the sample of 350 mW/cm$^2$ (measured with EIT instrument) and a belt speed of 6 m/min.

The thickness of the photocured films was measured with a Minitest 3000 Instrument (Elektrophysik, Germany); the average value was found to be in the range of 100 ± 10 µm for all the series of samples. For DMTA measurements thicker specimens with longer UV-irradiation time were prepared to get fully cured materials. In general all UV-cured samples were thermally post-cured for 4 h at 100 $^0$C before characterization of any thermal, morphological or mechanical properties.

## 3.4. Results and discussion

In this study the toughening effect of organic"soft" nanoscale particles dispersed into an epoxy matrix will be investigated. The new hyperstar polymers HSPs have been prepared according to scheme shown in figure 3.1 consisting of a hyperbranched polyester core (Mn = 4000 g/mol, PDI = 3.0) and PMMA or P(MMA-b-HEMA) arms. The hyperbranched macroinitiator HBP-MI prepared from the hb core exhibits on average 30 initiating sites (±10) for ATRP polymerization of MMA and HEMA allowing for hyperstars with 20-40 arms. The calculation is based on the $M_{n,SEC}$ and the number of bromide groups derived from the OH number of HBP-OH as determined via NMR. For that, a degree of branching (DB) of about 50% and no change in hb core structure was supposed.

The arm length of the PMMA chains varied from 20 to 30 repeating units. As known from previous studies[5-8], OH groups can act as transfer agents in cationic polymerization allowing e.g. for the covalent bonding of hyperbranched polyesters with OH groups into an epoxy matrix. Thus, we varied the composition of our hyperstars from non-reactive (only PMMA arms) to reactive with varying amount (on average 4 to 7 units) of OH groups (P(MMA-b-HEMA) block copolymer arms). The HEMA units at the chain ends should allow a tight covalent bonding of the hyperstars into the epoxy matrix compared to pure physical interactions of the hyperstars with only PMMA arms.

### 3.4.1. Real-Time FT-IR

Real-time FT-IR analyses were performed on photocurable formulations in order to evaluate the effect of the presence of hyperstar polymers on UV-curing process. The disappearance of the epoxy band (750-790 $cm^{-1}$) was monitored during UV-irradiation by means of real-time FT-IR analysis.

Figure 3.3 shows the plots of epoxy group conversion as a function of irradiation time for the pristine CE resin and for the CE formulation containing 5, 10 and 20 phr of HBP-PMMA/0%HEMA (left), HBP-PMMA/12%HEMA (middle) and HBP-PMMA/26%HEMA (right), respectively. It is worth noting that the pristine epoxy resin did not reach full epoxy group conversion because of a vitrification effect (the ultimate $T_g$ of the materials is far above room temperature). When the different hyperstar polymers were added to the photocurable formulation a decrease on photopolymerization rate and epoxy group conversion was evident with increasing HSP addition, whereas the amount of the HEMA had a small additional effect. Thus, we attributed the decrease in conversion to an increase in the viscosity when HSP is added to the photocurable formulation and to an enhanced vitrification effect. The lowering of epoxy group conversion could thus be attributed to the faster vitrification induced by chain-transfer reactions activated by the HSP that acts as a multifunctional crosslinker. Fast vitrification during polymer network formation reduces the polymer chain mobility with a consequent decrease of epoxy group conversion.

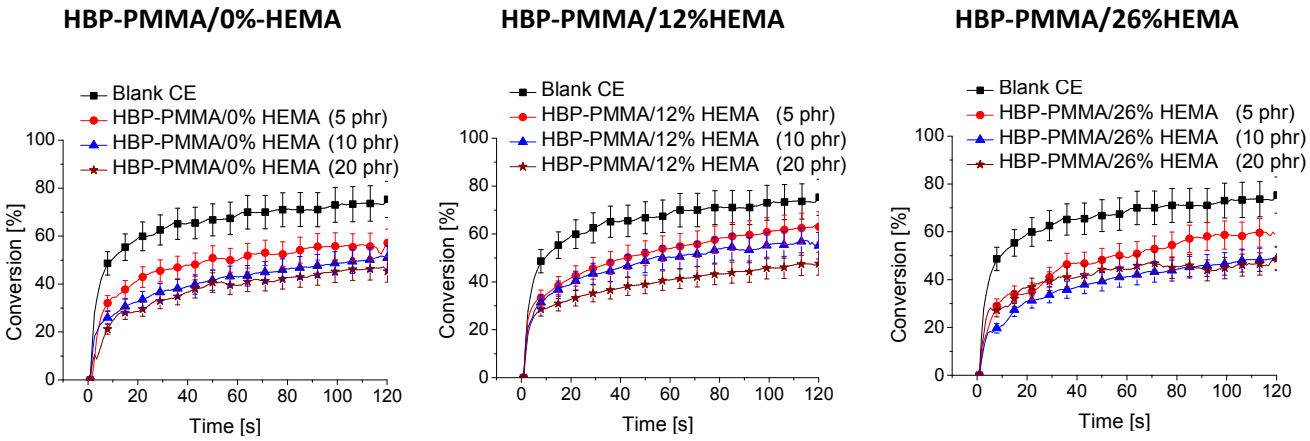


**Figure 3.3:** Epoxy conversion as a function of irradiation time for pure epoxy resin (squares) and containing HBP-PMMA/0%HEMA (left), HBP-PMMA/12%HEMA (middle) and HBP-PMMA/26%HEMA (right) at a content of 5, 10 and 20 phr.

### 3.4.2. Gel content

Notwithstanding the lowering of epoxy group conversion, all the cured films prepared by the HSP with HEMA units showed high gel content values (>98%, see Table 3.2), indicating almost absence of extractable monomer or oligomers. This is a clear indication that these hyperstar polymers can interact with the carbocationic growing chain through a chain transfer mechanism involving the hydroxyl group, so that the additives become chemically linked to the polymer network. This behaviour has already been observed when using hydroxyl terminated HBP[7] and it has been explained on the basis of the activated monomer mechanism described by Kubisa et al.[9]. In contrast to this, the gel content was lowered with increasing content of non-reactive HBP-PMMA/0%HEMA down to 90% indicating non-covalent incorporation of the HSP into the gel structure and thus, it can be at least partially extracted by solvent.

**Table 3.2:** Properties of UV-cured films

| Sample | | Conv [%][a] | Gel content [%][b] | $T_g$ [°C][c] |
|---|---|---|---|---|
| Blank CE | | 75 | 100 | 216 |
| HBP-PMMA/0%HEMA | (5 phr) | 60 | 95 | 210 |
| HBP-PMMA/0%HEMA | (10 phr) | 55 | 90 | 205 |
| HBP-PMMA/0%HEMA | (20 phr) | 50 | 92 | -- |
| HBP-PMMA/12%HEMA | (5 phr) | 63 | 99 | 201 |
| HBP-PMMA/12%HEMA | (10 phr) | 55 | 99 | 186 |
| HBP-PMMA/12%HEMA | (20 phr) | 50 | 98 | 180 |
| HBP-PMMA/26%HEMA | (5 phr) | 60 | 99 | 190 |
| HBP-PMMA/26%HEMA | (10 phr) | 50 | 100 | 194 |
| HBP-PMMA/26%HEMA | (20 phr) | 50 | 100 | 182 |

[a] Determined by Real-Time-FT-IR, after 2 min of irradiation
[b] Determined by extraction with chloroform, ASTM D2765-01
[c] Determined as the maximum of tan δ curves of DMTA analyses

### 3.4.3. Dynamic mechanical thermal analysis (DMTA)

Dynamic mechanical thermal analysis (DMTA) was performed on cured films in order to characterize the thermal and viscoelastic properties of the achieved polymer network. Please note, that all photocured samples had been subjected to a thermal post-curing

process (4 h at 100 $^0$C) to obtain steady epoxy group conversion and therefore reliable and reproducible data for the thermal properties and morphology. Figure 3.4 collects the curves of tan δ versus temperature for the cured pristine crosslinked CE and for the cured system containing 5-20 phr of HBP-PMMA/0%HEMA. In Figures 3.5 and 3.6 the same curves are reported for the cured systems containing respectively HBP-PMMA/12% HEMA and HBP-PMMA/26%HEMA. Table 3.2 shows the values of maximum of tan δ curves (which can be considered as the $T_g$ of the materials).

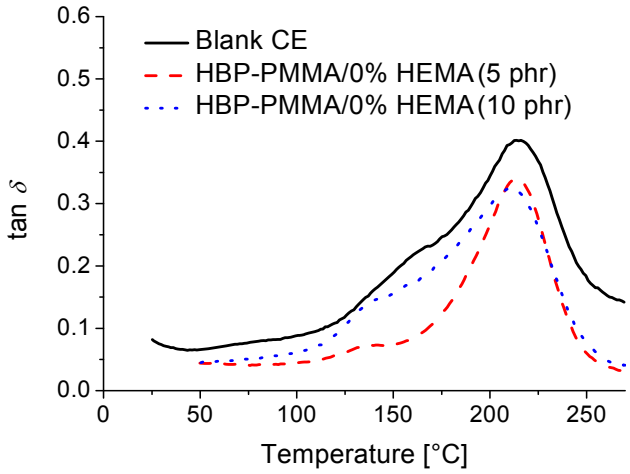


**Figure 3.4:** DMTA: tan *δ vs.* temperature for cured pristine CE and after addition of 5 and 10 phr HBP-PMMA/0%HEMA.

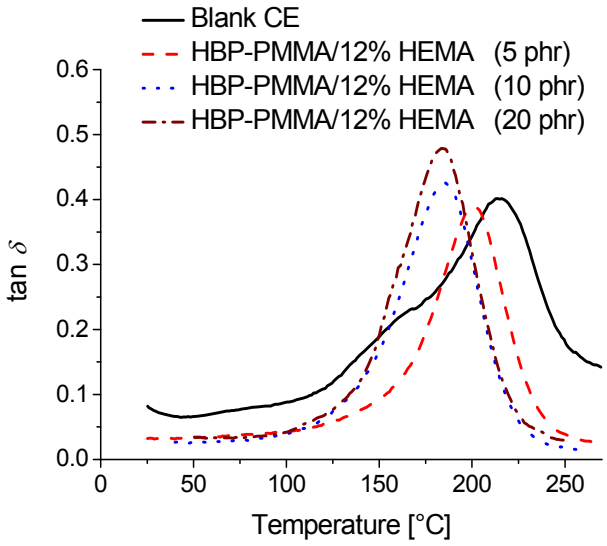


**Figure 3.5:** DMTA: tan δ vs. temperature for cured pristine CE and after addition of 5, 10 and 20 phr HBP-PMMA/12%HEMA.

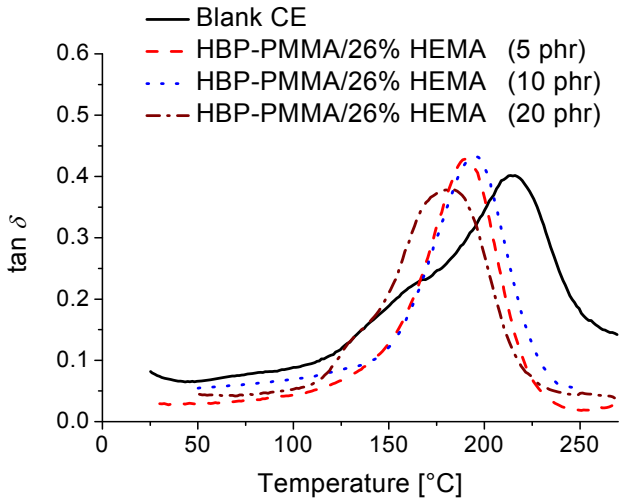


**Figure 3.6:** DMTA: tan *δ vs.* temperature for cured pristine CE and after addition of 5, 10 and 20 phr HBP-PMMA/26%HEMA.

By adding HBP-PMMA/0%HEMA we could observe only a slight decrease of the $T_g$ values of the cured epoxy network; in the presence of HBP-PMMA/12%HEMA and HBP-PMMA/26%HEMA a more evident flexibilization of the network was observed with a more important decrease of $T_g$ down to 180 $^oC$ by increasing the amount of the hyperstar polymers added. The decrease in $T_g$ values could be attributed to both, the decrease in epoxy group conversion as well as to the incorporation of more flexible hyperstar polymers into the UV-cured networks. The HSPs themselves show glass transitions in the range of 120 $^0C$. It should be noted that in the same CE epoxy system pure HBP-OH of similar molar mass as our hb core in the HSP led also to a reduction of Tg by 10 $^oC$ for 10 phr hb additive[10] as observed in this study with HBP-PMMA/ 0%HEMA.

Looking closely at the tan δ curve for the samples with HBPPMMA/ 0%HEMA (Fig. 3.4) one might find indications for a second $T_g$ at lower values which might indicate a phase-separated blend structure fitting to the observation of the extractable HSP phase. Thus, in this case the slight decrease of the $T_g$ values achieved in the presence of HBP-PMMA/0%HEMA can be attributed to the lower epoxy group conversion during UV curing. No indication for two $T_g$'s is given in the case of the reactive HSPs, just a clear shift of tan δ maximum, and this confirms the assumption of chemical bonding of the individual more flexible HSPs with HEMA units into the network structure reducing the phase separation tendency and lowering the overall $T_g$.

### 3.4.4. Morphological characterization

The morphology of the cured materials was investigated by FE-SEM analysis on the fracture surfaces of croslsinked materials. In order to ensure a distinct morphology effect only photocured formulations with a high content of hyperstar polymers (20 phr) were investigated. It is well known that the fracture surface of the pristine cycloaliphatic epoxy is smooth and homogenous as indicated in figure 3.7. By comparing the FE-SEM micrograph for the sample containing 20 phr of HBP-PMMA/0%HEMA (Figure 3.8) with the sample with 20 phr of the reactive HSPs HBP-PMMA/12%HEMA (Figure 3.9) and HBP-PMMA/26%HEMA (Figure 3.10) clear differences in the heterogeneity of the surface for the epoxy matrix are evident. Whereas the material containing the non-reactive HSP appears very heterogeneous like a phase-separated blend, a rather nearly homogenous material is obtained with the reactive HBP-PMMA/26%HEMA. In addition, it can be observed that the higher the content of OH-

groups in the arms the more homogeneous is the fracture surface. These morphological data fully support the above discussed DMTA results and can be explained taking into account that the OH-groups enable the hyperstar polymers to properly link with the polymeric network which hinders phase separation during curing.

Generally, the observation of microphase separation or rougher facture surface in samples might be an indication for enhanced fracture toughness. Where the more roughness exists in the fracture surface, the more dissipated energy consumed during crack propagation. The microphase separation observed in epoxy sample containing HSP with 0% HEMA could be considered as evidence of enhancement of fracture toughness.

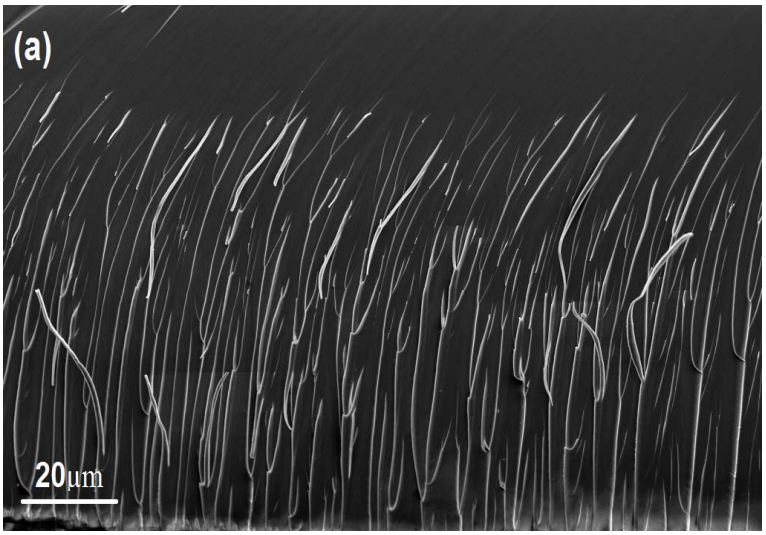


**Figure 3.7:** FE-SEM of the fracture surface of the pristine CE

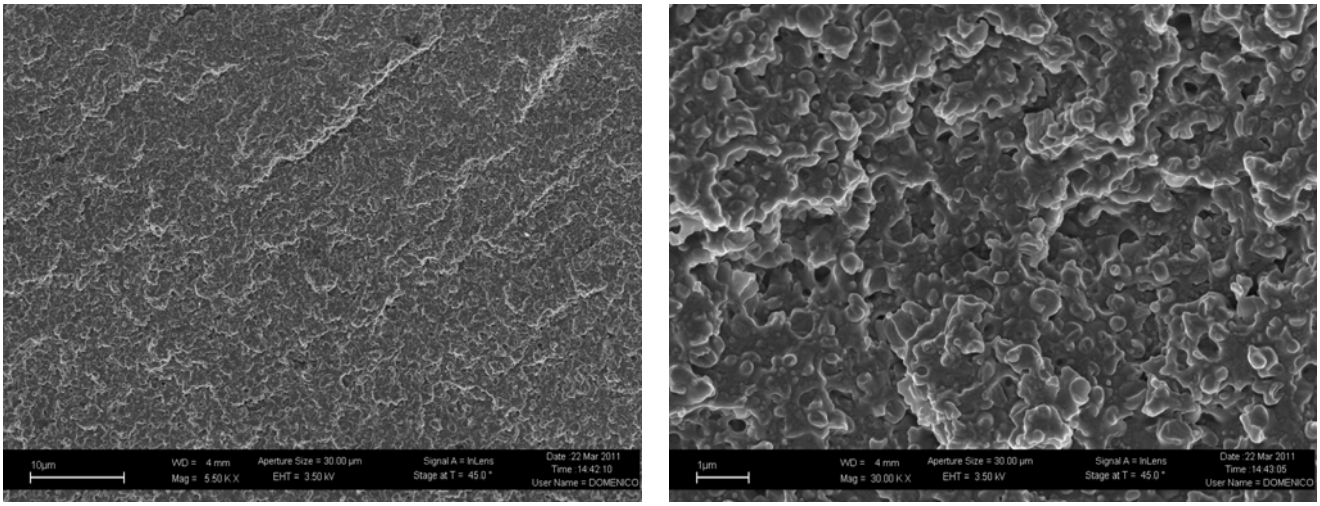

**Figure 3.8:** FE-SEM of the fracture surface of the CE containing 20 phr of HBP-PMMA/ 0%HEMA

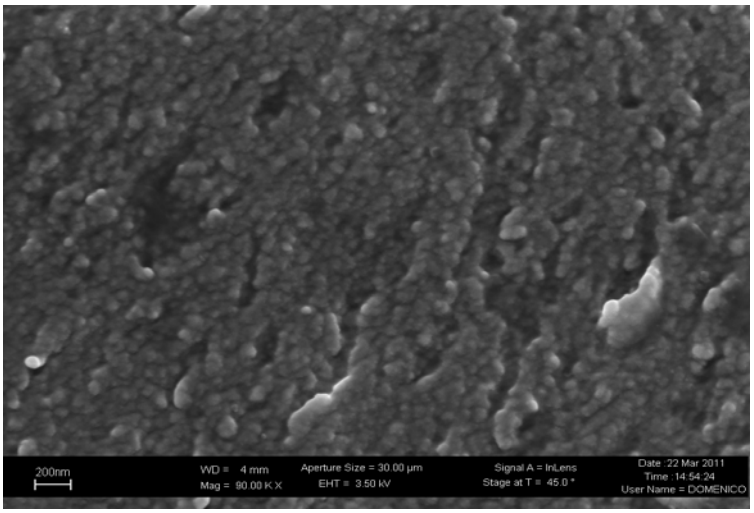


**Figure 3.9**: FE-SEM of the fracture surface of CE containing 20 phr of HBP-PMMA/ 12%HEMA.

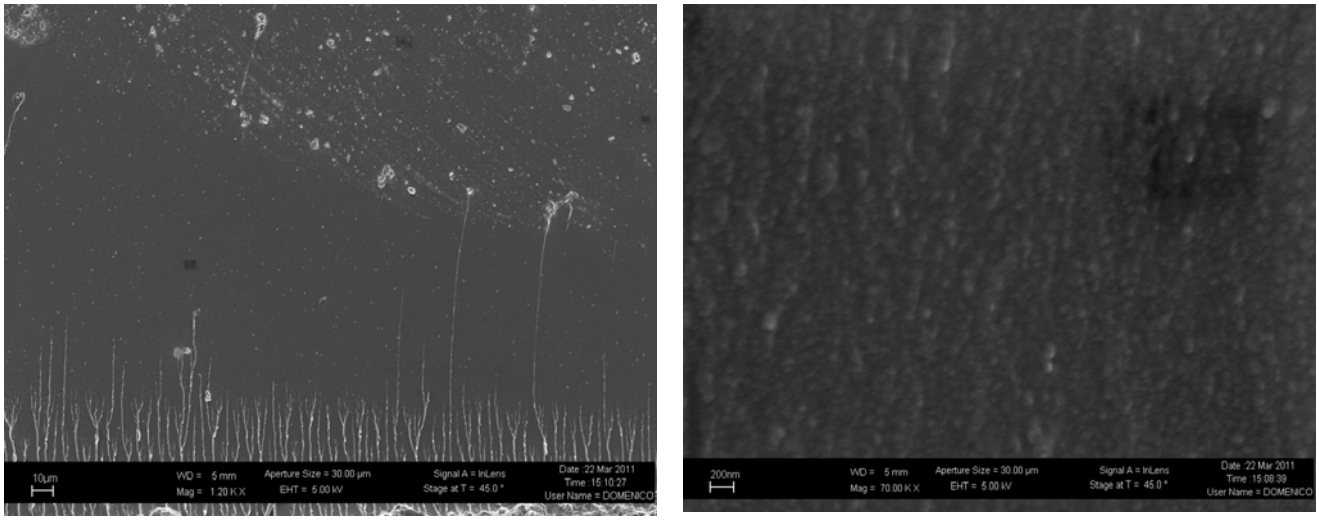


**Figure 3.10**: FE-SEM of the fracture surface of the coating containing 20 phr of HBP-PMMA/26%HEMA.

## 3.5. Conclusion

New hyperstar polymers (HSP) based on a hyperbranched polyester core (HBP-OH) and PMMA or P(MMA-b-HEMA) block copolymer arms have been used as binders in an epoxy matrix, investigating their effect on UV-curing and evaluating the final properties of the cured materials in terms of thermal and viscoelastic properties. These HSPs were prepared up to molar masses of 380,000 g/mol with or without reactive OH groups at the end of the arms and can be considered as polymeric soft nanoparticles. The morphology of the cured materials was investigated in order to understand the phase separation behavior of the hyperstar polymers as a function of their functionality and the curing process

The hyperstar polymers HBP-PMMA/0%HEMA, HBP-PMMA/ 12%HEMA and HBP-PMMA/26% HEMA influenced the epoxy group conversion during UV-curing with a decrease of the final conversion by increasing the binder content in the photocurable formulations. This was explained on the basis of a fast vitrification induced by chain transfer reactions which strongly reduces the mobility of the carbocationic polymer chains.

Thermal and viscoelastic properties of cured materials were investigated by DMTA analyses. In general, through addition of hyperstar into epoxy samples a flexibilization documented in $T_g$ decrease could be observed. This was mainly attributed to the decrease of epoxy group conversion together with the insertion of the HEMA-arm containing hyperstar polymers through a chain transfer reaction.

Morphological investigations were performed on UV-cured materials by FE-SEM analysis. While the addition of HBP-PMMA/0%HEMA results in phase separation during UV-curing of the epoxy formulations, the hyperstar polymers HBP-PMMA/12%HEMA and HBP-PMMA/26%HEMA were tightly incorporated into the network structure through transfer reaction by the OH groups and thus, phase separation during curing was avoided. It offers higher chances to fully exploit the positive effects of our hyperstar polymers as organic soft nanoscale particles and reactive toughening agents in epoxy resins. It might be also more effective to use hyperstar architectures with a lower number of arms or longer arms.

In conclusion, by properly selecting the hyperstar polymer with different functionalities, it is possible to either induce or prevent a phase separation during curing which controls the final properties of the cured epoxy network both in terms of thermal properties and toughness behavior. By direct comparison of the HSP effects on photo- as well as thermally cured epoxy resins[11] it became obvious that the increased temperature during thermal curing enhances the effectiveness of the HSP as multifunctional crosslinker leading to enhanced curing rate and increased crosslinking density of the thermally cured samples, whereas in photocuring the flexibilization effect can be enhanced by having high gel content at lower epoxy group conversion.

## 3.6. References:


1. F. Schallausky, M. Erber, H. Komber, A. Lederer, Macromol Chem Phys 2008;209: 2331.
2. K.E. Tahlawy, S.M. Hudson. J Appl Polym Sci 2003;89:901.
3. Morell M, Voit B, Ramis X, Serra A, Lederer A. J Polym Sci Part A Polym Chem 2011;49:3138.
4. C. Liu, G. Wang, Y. Zhang, J.Huang, J Appl Polym Sci 2008;108:777.
5. M. Sangermano, A. Priola, G. Malucelli, R. Bongiovanni, A. Quaglia, B. Voit, Macromol Mater Eng 2004;289:442.
6. M. Sangermano, A. Di Gianna, G. Malucelli, C. Roncuzzi, A. Priola, B. Voit, J Appl Polym Sci 2004;97:293.
7. M. Sangermano, A. Di Gianni, R. Bongiovanni, A. Priola, B. Voit, D. Pospiech, Macromol Mater Eng 2005;290:721.
8. M. Sangermano, G. Malucelli, R. Bongiovanni, A. Priola, A. Harden, Polym Int 2005;54:917.
9. P. Kubisa, S.Penczek ,Prog Polym Sci 1999;24:1409.
10. M. Sangermano, M. Messori, M.M. Galleco, G. Rizza, B. Voit, Polymer 2009;50: 5647.
11. F. Däbritz , B. Voit, M. Naguib, M. Sangermano, Polymer 2011; 52:5723.

# 4

# Epoxy containing Core/Shell nanoparticles

## 4.1. Abstract

Functionalized crosslinked core/shell particles (CS-GMA) based on polybutyl acrylate(PBA) as core and polymethylmethacrylate-*co*-polyglycidyl methacrylate (PMMA-*co*-PGMA) as shell are prepared by emulsion polymerization and dispersed into a UV-curable cycloaliphatic epoxy resin,CE, in the range between 5 to15 wt %. The presence of the particles did not significantly affect the UV curing process: a slight decrease of final epoxy group conversion is attributed to an increase in the viscosity when CS-GMA is added to the photocurable formulation and to an enhanced vitrification effect. The presence of the particles did not modify the $T_g$ of the cured materials, while an enhancement of impact resistance is observed that does not depend on the particle content. FESEM micrographs for epoxy reinforced with core/shell particles indicate a plastic void growth of the epoxy polymer and shear yielding toughening mechanism.

## 4.2. Preparation of functionalized core/shell particles (CS-GMA)

The experiment is divided into two steps:

***Step 1–Formation of the seed (core):*** In a typical experiment the surfactant sodium dodecyl benzene sulfonate (SDBS), (0.05 g) and sodium bicarbonate (0.1 g) as buffer are introduced into 3-necked flask containing 140 ml of distilled water. The solution is left under magnetic stirring for 30 min. Then a mixture of butyl acrylate (BA), 0.1 mol and 0.22 g trimethylolpropane triacrylate (TMPTA, as crosslinker) was added at 50 $^{o}$C and left under nitrogen atmosphere for 30 min. A solution of potassium persulfate (KPS), (0.16 g) in 12 ml water, was introduced to initiate the polymerization. The temperature was then raised and held at 75 $^{0}$C for 2 h under nitrogen.

The rate of conversion of BA monomer for the core formation was determined gravimetrically over 2 h, according to the equation:

$$\text{Conversion } \% \ = \ \frac{weight\ of\ polymer\ formed\ in\ 1\ ml}{theoretical\ weight\ of\ polymer\ in\ 1ml} * 100$$

***Step 2–Formation of shell:*** 100mL of previous core emulsion is introduced into the shell formation step. Where, an additional portions of sodium bicarbonate (0.05 g) and KPS (0.16 g) in 5ml water were added and was kept under stirring for 15 min. then the mixture of MMA, 0.05 mol, 0.02 mol GMA, (70:30) and TMPTA (0.2 g), was added drop-wise at a rate of 5 ml.h$^{-1}$. After completion of addition of this mixture the reaction system was continuously stirred at 75 $^{0}$C for 2 h. the whole polymerization was under nitrogen. After demulsification with $AlCl_3$ solution, the product was collected by filtration and was washed thoroughly with hot water and then dried.

## 4.3. Epoxy sample formulation

The core/shell particles were added to the epoxy resin in the range between 5 and 15 wt%. The formulations were mixed with Ultra Turrex (30,000 rpm) for 5 min and then the cationic photoinitiator triphenylsulfonium hexafluoroantimonate,$Ph_3SSbF_6$, was added to all the formulations at 2 wt% with respect to the CE content.

The formulations were coated on glass slides and cured with a medium vapor pressure mercury dynamic UV lamp (Fusion, H bulb) with an intensity on the surface of the

sample of 350 mW.cm$^{-2}$ (measuredwith EIT instrument) and a belt speed of 6 m. min$^{-1}$. The thickness of the photocured films was in the range of 100 ±10 µm for all the series of samples.

Samples of 0.25 cm thickness, 5 cm length, and 1.5 cm width were prepared by pouring the photocurable formulations into a transparent plastic mould. The formulations were cured by both sides with a static lamp (light intensity of about 35 mW. Cm$^{-1}$) until fully cured thick samples were achieved.

## 4.4. Results and discussion

Functionalized crosslinked PBA/PMMAPGMA core/shell particles were prepared by seeded emulsion polymerization in a two step synthesis, as described in the previous part. The conversion of core monomer BA is estimated gravimetrically during 2 h of polymerization as shown in figure 4.1. It is obvious that the conversion increase rapidly in the first stage and reaches its maximum (84%) after 2 h.

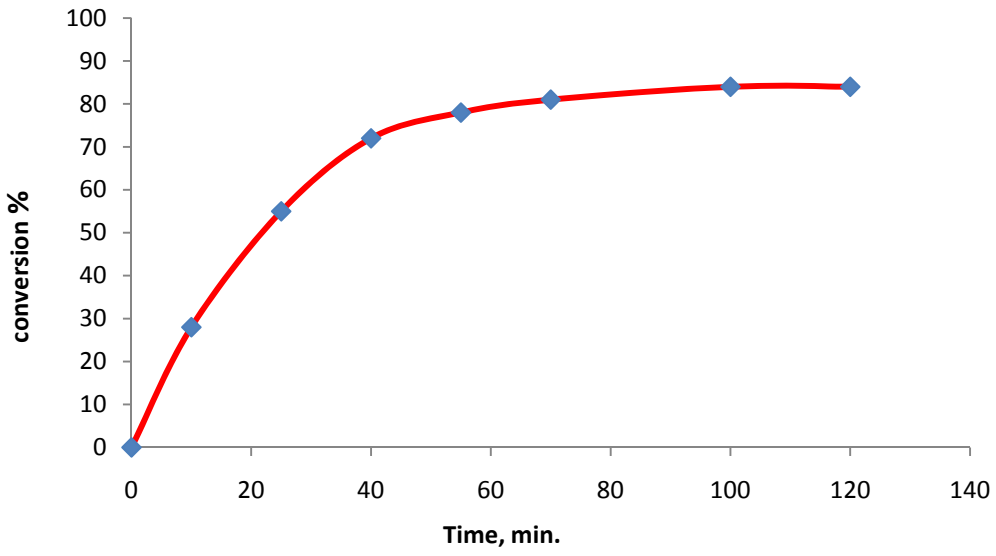


**Figure 4.1:** The conversion of core monomer, BA.

After formation of the core, the shell is formed by a starved process where the mixture of MMA and GMA is fed dropwise to the reaction system. During the polymerization, GMA and MMA came into micelles gradually because the presence of a large amount of GMA will affect the stability of the electric double layers of micelles due to the strong polarity

of GMA molecule. Hence, using this semicontinuous process already reported in literature[1], high conversion and hence yield of the shell is obtained about 70%. By using a MMA-GMA mixture for the shell we could achieve epoxy functionalized particles, which could assure a strong interaction with the epoxy matrix during curing.

The dimension of the core/shell nanoparticles were evaluated by dynamic light scattering analysis (DLS). The DLS curves are shown in Figure 4.2 for the synthesized core and following for the crosslinked core/shell particles. The PBA core has an average particle size of about 102 nm. The size distribution is narrow and monodisperse. After formation of shell, the average particle size becomes 202 nm. The size distribution shows the tendency of broadening that might be due to particle agglomeration which explains the increase of shell size more than theoretical one around 124 nm(calculated using mathematical equations related to the volume of sphere $V=4/3\pi r^3$). This agglomeration could be attributed to the partially water solubility of GMA.

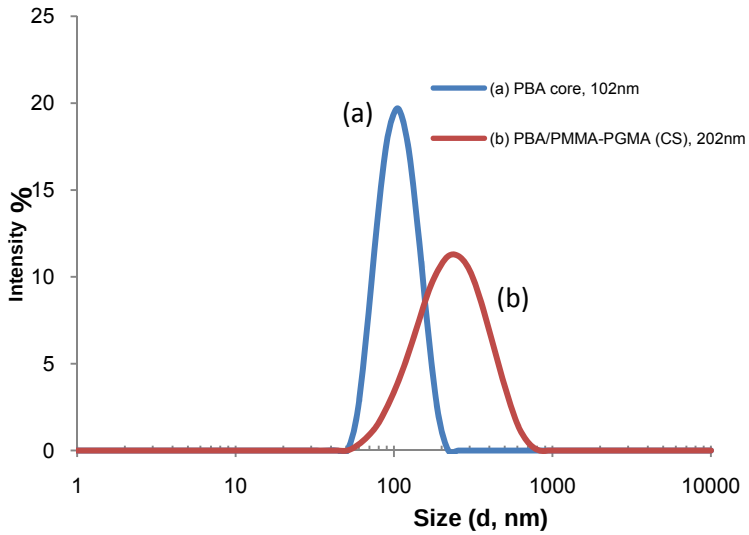


**Figure 4.2:** Particle size distribution of core (curve a) and core/shell (curve b) particles.

Figure 4.3 shows the DSC spectrum of the core/shell particles. It can been seen that the $T_g$ of the PBA core and PMMA-PGMA copolymerized shell are –39 (A) and 131 $^0$C (C), respectively. These $T_g$ values are higher than expected due to the crosslinking introduced by TMPTMA. In addition, another transition appeared at 74 $^o$C (B), which was believed to be the $T_g$ of the core/shell interphase region where core and shell polymers

interpenetrated with each other. This behavior was previously observed in core/shell particles reported in literature.[2]

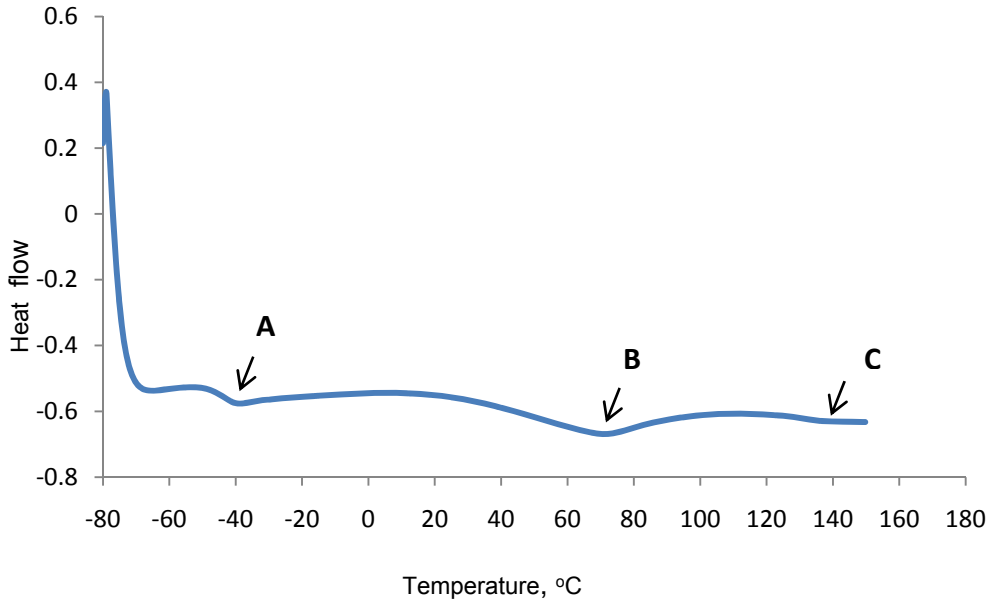


**Figure 4.3:** DSC spectrum of the core/shell particles (Arrows indicates the glass transition regions).

The functionalized crosslinked core/ shell particles were dispersed into the cycloaliphatic epoxy resin in the range between 5 and 15 wt%. Real-time FT-IR analysis were performed on photocurable formulations in order to evaluate the effect of the presence of core/shell particles on UV curing process. From the curves reported in figure 4.4, it is evident the high reactivity of the epoxy groups of the CE resin with a quite high initial rate of polymerization. The epoxy group conversion levels off, after 2 min of irradiation, to a value of about 95%. This is due to the formation of a glassy polymer network, which hindered the mobility of the reactive species so that epoxy group conversion is not complete and a number of unreacted epoxy groups remained trapped within the glassy polymer network.

The addition of core/shell particles to the photocurable formulations led to a decrease of the final epoxy group conversion as a function of loading fraction. When 15 wt% of the core/shell particles were added to the photocurable formulation the final epoxy group conversion reached ~85% after 2 min of irradiation. The observed slight lowering in epoxy group conversion could be attributed to an increase in the viscosity when CS-GMA

is added to the photocurable formulation and to an enhanced vitrification effect: the presence of epoxy groups on the surface of the core/shell particles make them behave as a multifunctional crosslinker. Fast vitrification during polymer network formation reduces the polymer chain mobility with a consequent decrease of epoxy group conversion.

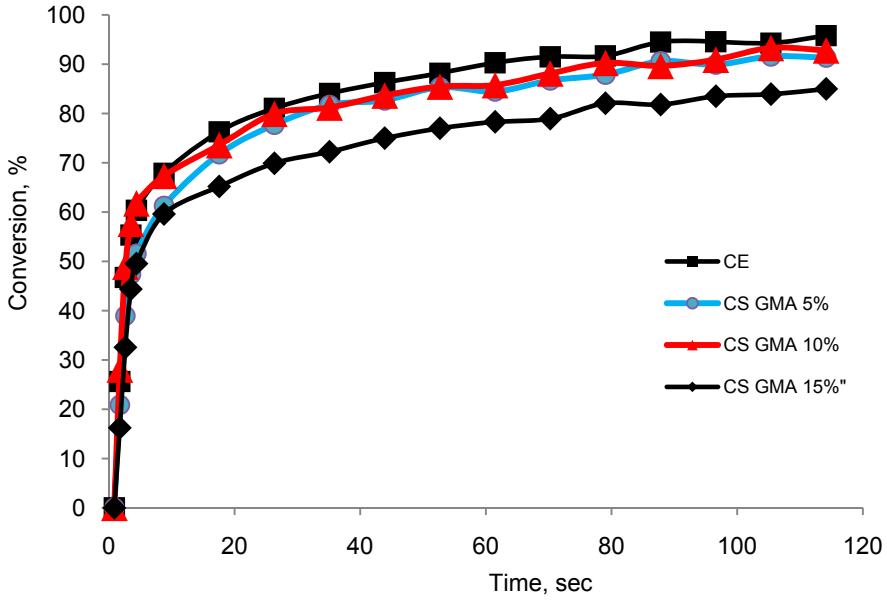


**Figure 4.4:** Epoxy conversion as a function of irradiation time for pure (CE) and reinforced epoxy resin (CS-GMA).

All the cured films modified with the core/shell particles showed high gel content values (>98.5%, see Table 4.1), indicating almost absence of extractable monomer or oligomers. This is a clear indication that core/shell particles (CS-GMA) can interact with the carbocationic growing chain through a copolymerization mechanism involving the epoxy groups present on the particle surface. Thus, they become chemically linked to the polymer network.

Dynamic-mechanical properties of UV-cured materials were investigated by DMTA analysis. The tan δ curves are reported in Figure 4.5, for the pristine epoxy cured system and for the cured films containing core/shell nanoparticles.

**Table 4.1:** properties of cured epoxy samples

| Sample | Gel content[a)] % | $T_g$[b)] °C | Impact resistance[c)] (J/cm$^2$) |
|---|---|---|---|
| CE | 98 | 189 | 0.415 ± 0.02 |
| CS-GMA 5% | 98.5 | 186 | 0.534 ± 0.03 |
| CS-GMA 10% | 99 | 181 | 0.521 ± 0.05 |
| CS-GMA 15% | 99.5 | 191 | 0.543 ± 0.02 |

[a)] Determined on UV-cured samples, ASTM D2765-01; [b)]Determined as the maximum of tan δ curve from DMTA analysis; [c)]Determined with Charpy test, ASTM D 6110-04.

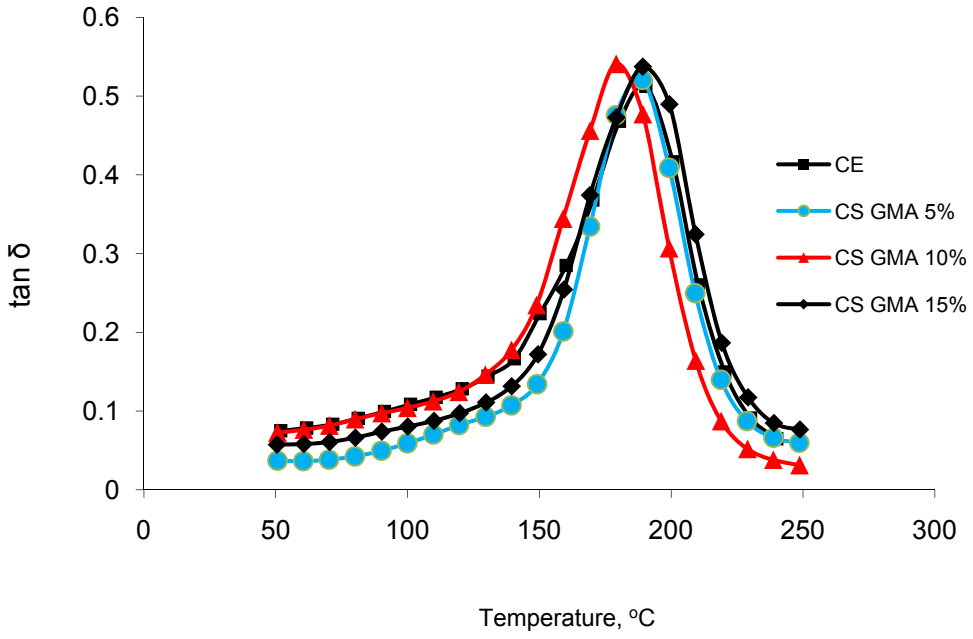


**Figure 4.5:** DMTA curves of the UV-cured pristine epoxy resin (CE) and for the cured materials containing core/shell nanoparticles (CS-GMA).

It is very interesting to observe that the addition of core/ shell nanoparticles did not significantly affected the $T_g$ values of the cured blends, which corresponds to the $T_g$ value of the pure epoxy cured system. This result suggests that a segregation of the CS-GMA particles occurred and therefore we can expect that their presence will not compromise the thermomechanical behavior of the crosslinked material. This could be promising results for enhancement of impact resistance of the UV-cured epoxides. The rubbery core

of the particles could increase the impact resistance of the cured material, while the functionalized shell will play an important role for the particle-matrix interaction.

Impact resistance measurements were performed on thick UV-cured samples by means of a Charpy pendulum. The impact resistance values for the investigated cured films are reported in Table 4.1. The impact resistance was found to increase in the presence of the core/shell particles, even though the effect is not dependent on the particles content.

Shear band yielding has previously been reported for epoxy systems toughened with rubber-core/rigid-shell particles, [3] and it is expected to occur. Hence, plastic void growth of the epoxy polymer and shear yielding could be the expected toughening mechanisms for these particle modified epoxies, responsible for the increase on impact resistance.

For core/shell particles, some authors have observed shear yielding and cavitation of the particles. Sue[4] used transmission electron microscopy to show extensive particle cavitation around a sub-critically loaded crack tip, with plastic void growth followed by the formation of shear bands. Pearson and Yee[5] reported particle cavitation and shear banding toughening mechanisms in epoxy with methacrylated butadiene-styrene core/shell rubber particles. Either particle cavitation or debonding will create voids, relieving the triaxial stress state ahead of the crack tip, and allowing plastic void growth.

The morphology of the cured samples containing CS-GMA particles was investigated by FESEM analysis performed on the Charpy fracture surfaces and compared with the fracture surface of the pristine epoxy. The fracture surfaces of cured samples are shown in figure 4.6. The fracture surface of the pristine epoxy (figure 4.6a) is relatively smooth and glassy, which is typical of a brittle thermosetting polymer. The feather markings, which are caused due to the excess of energy associated with the relatively fast crack growth, and the multi-planar nature of the surface, are ways of absorbing this excess energy in a very brittle material.[6]

The addition of reactive core/shell nanoparticles to epoxy matrix results in completely homogeneous morphology, as shown in figure 4.6b and c. The homogeneous distribution of the particles in the cured matrix could be due to a strong chemical interaction between the particles and the polymer network, due to the large number of epoxy groups present on the surface of the functionalized core/shell particles.

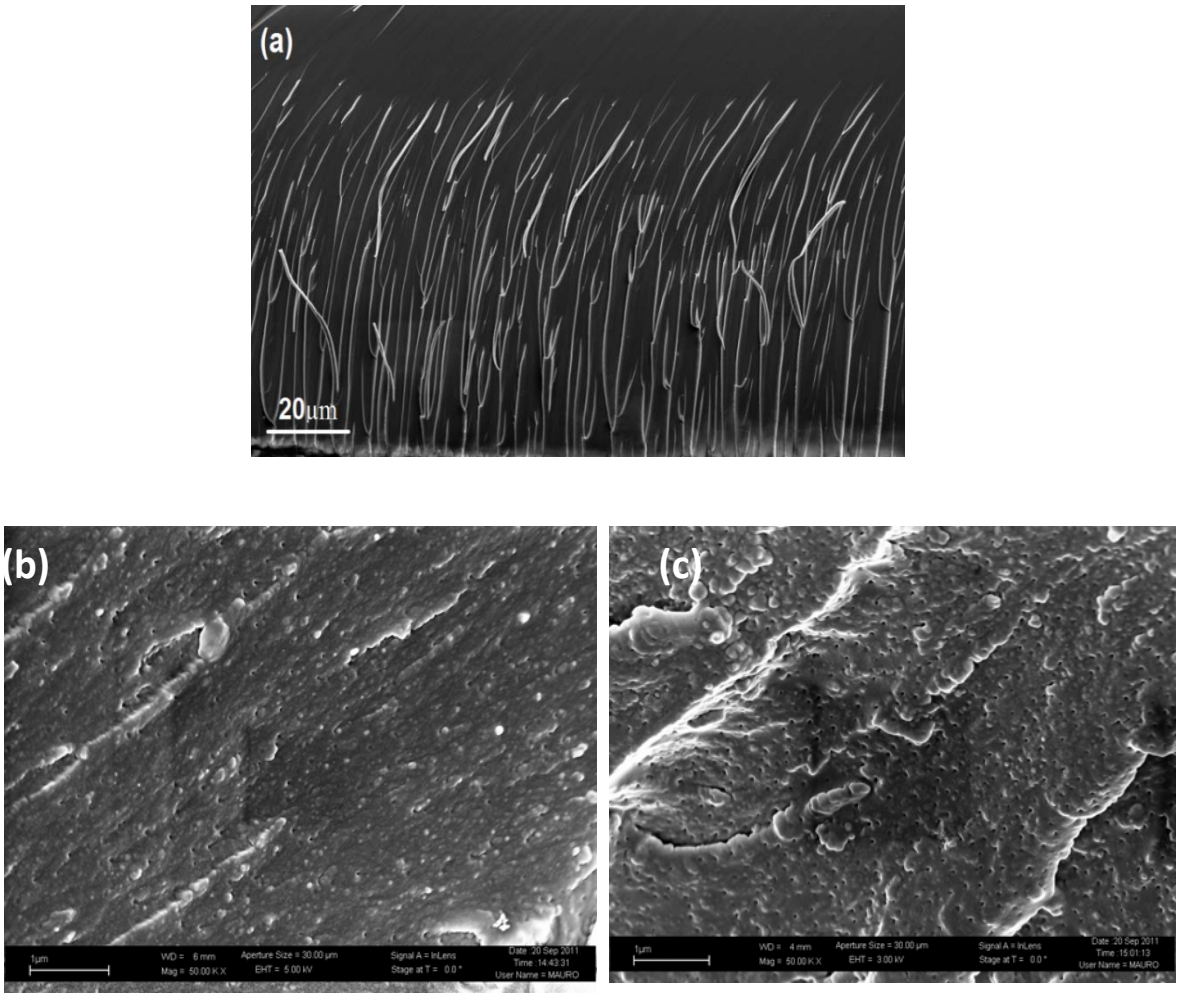


**Figure4.6:** FESEM micrographs of the fracture surfaces of (a) neat epoxy, (b) epoxy with 5% and (c) epoxy with 15% CS-GMA

The dimensions of the CS-GMA particles dispersed within the epoxy network are around 200–250 nm, in great accordance with the DLS measurements; this is an indication of absence of significant agglomeration of the core/shell particles during curing. The very rapid nature of the photopolymerization process may allow a polymer network formation much more rapidly than macroscopic aggregation.[7]

By carefully investigation of the facture surface of core/ shell particles containing epoxy samples figure 4.6b and c, we can observe rougher facture surface and hence, higher fracture energy. This is in accordance with the observed increase of impact resistance.

The particle cavitation is shown in the FESEM micrographs for epoxy filled with core/shell particles 5% (figure 4.6b) and become more clear by increase the core/shell content (figure 4.6c). The role of the particle cavitation, therefore, is to relieve the plane strain constraint from the surrounding matrix and allow plastic deformation, where the energy absorption due to the plastic deformation has a great influence on the fracture toughness enhancement.[8]

## 4.5. Conclusion

Crosslinked core-shell CS-GMA particles were prepared by seeded emulsion polymerization. After shell formation the average particles size was around 200 nm, as measured by DLS analysis and following confirmed by FESEM morphology investigations. The particles were dispersed into the cycloaliphatic epoxy resin in the range between 5 and 15 wt% and photocured in the presence of the suitable cationic photoinitiator. The presence of the particles did not significantly affect the UV-curing process: a slight decrease of final epoxy group conversion was attributed to an increase in the viscosity when CS-GMA is added to the photocurable formulation and to an enhanced vitrification effect. The presence of the particles did not modify the $T_g$ of the cured materials, while impact resistance enhancement was observed independently on the particle content. Morphology investigations on Charpy fractured surfaces showed a homogeneous distribution of the particles through the polymeric matrix with no agglomeration being observed. Particle cavitation was clearly shown in the FESEM micrographs for epoxy reinforced with core/shell particles, evidencing a plastic void growth of the epoxy polymer and shear yielding toughening mechanism.

## 4.6. References:


1. Z. Zeng, J. Yu, Z.-X. Guo, J. Polym. Sci. Part A: Polym. Chem. 2004; 42:2253.
2. K.-F. Lin, Y.-D. Shieh, J. Appl. Polym. Sci. 1998; 69:2069.
3. T. H. Hsieh, A. J. Kinloch, K. Masania, J. Sohn, A. C. Lee, S. Taylor, S. Sprenger, J. Mater. Sci. 2010; 45:1193.
4. H. J. Sue, Polym. Eng. Sci. 1991; 3:275.
5. R. A. Pearson, A. F. Yee, J. Mater. Sci. 1991; 26:3828.
6. E. H. Andrews, Fracture in Polymers, 1st edition, Oliver & Boyd, Edinburgh; 1968.
7. K.-F. Lin, Y.-D. Shieh, J. Appl. Polym. Sci. 1998; 70:2313.
8. R. Bagheri, R. A. Pearson, Polymer 2000; 41:269.

# 5

# Epoxy containing block copolymer

## 5.1. Abbreviations

ATRP: atom transfer radical polymerization

PMDETA: pentamethyldiethylenetriamine

EBrIB: Ethyl 2-bromoisobutyrate

PEG-OH: polyethylene glycol methyl ether

PEO-b-PGMA: polyethylene oxide-*block*- polyglycidyl methacrylate

PEO-b-PS: polyethylene oxide-*block*-polystyrene

PS: polystyrene

St: styrene

GMA: glycidyl methacrylate

## 5.2. Abstract

Reactive and non-reactive diblock copolymers based on polyethylene oxide (PEO) are prepared via ATRP. The block copolymer was incorporated into cycloaliphatic epoxy to obtained modified thermosets. $^{1}$H NMR and SEC measurements are carried out and used to estimate the molecular weight of the content and polydispersity of prepared block copolymers. The viscoelastic properties and morphology of the modified epoxy were carried out using DMTA and FESEM, respectively. The addition of reactive PEO-b-PGMA into epoxy resin has insignificant effect on the glass transition temperature, $T_g$, if compared homopolymer PGMA which has profound impact on glass transition temperature. The other non-reactive block copolymer causes a little decrease in $T_g$ values. The measurement of critical stress factor, $K_{IC}$, showed that the fracture toughness of the composite materials was enhanced by inclusion of non-reactive block copolymer. In contrary, the reactive block copolymer has negative effect on the fracture toughness especially in case of short PEO block. FESEM micrographs studied the fracture surfaces sustain the microphase separation or increase the surface roughness in the toughened samples, indicating more energy was dissipated.

## 5.3. Synthesis of the block copolymers

### 5.3.1. Homopolymerization of PGMA

GMA Polymerization was carried out in diphenyl ether via ATRP.[1] In a modified procedure, degassed monomer (6 mmole), PMDETA ligand (0.15 mmole) and diphenyl ether (12 mmole) through three freeze-pump-thaw cycles were added to dry flask with CuBr (0.15 mmole). Then, the initiator (EBrIB, 0.15 mmol) was introduced into the flask using degassed syringes in order to start the polymerization. The flask was immediately placed in oil bath at 30 $^{o}$C. After 60 min, the reaction mixture was diluted with methylene chloride and passed through neutral alumina to remove the catalyst, and then rotary evaporated to eliminate the eluent. The solution was precipitate in a large excess of hexane. Finally, the polymers were dried under a vacuum.

### 5.3.2. Syntheses of poly(ethylene oxide) macroinitiator (PEO-Br)

PEO-Br is synthesized according to Armes et al.[2] PEG-OH (5 mmol) was dried under vacuum at 60 °C for 60 min followed by adding anhydrous THF (80 ml), the reaction flask was cooled to room temperature followed by adding triethylamine (10 mmol) and flushing with nitrogen. 2-bromoisobutyryl bromide (10 mmol) diluted in anhydrous THF (10 ml), was finally added dropwise to the reaction solution over 20 min. After 48 h of stirring at ambient temperature, the mixture was filtered to remove salt and the filtrate was concentrated by evaporation most of solvent. PEO-Br was obtained as a white powder by precipitation in 100 ml hexane. Yield: 85 %. $^{1}$H NMR (500 MHz, $CDCl_3$): δ 1.93 (s, 6H), δ 3.38 (s, 3H), δ 3.64 (s, 180 H) (see supporting data).

### 5.3.3. Synthesis of PEO-b-PGMA block copolymer

ATRP procedure was carried out in solvent, where PEO-Br macroinitiator (0.15 mmole) and CuBr (0.15 mmole) were charged into a dry Schlenk flask and kept under vacuum at ambient temperature for 60 min. PMDETA ligand (0.15 mmole), GMA, and diphenyl ether were carefully degassed through several freeze-thaw cycles prior to introduce into the Schlenk flask. The flask was then immediately immersed in an oil bath at 30 $^{o}$C to start the polymerization for 120 min. the reaction mixture was diluted with methylene chloride and passed through neutral alumina to remove the catalyst, and then rotary evaporated to eliminate the eluent. Then the solution was poured into a large amount of

hexane. Finally, the block copolymers were dried under vacuum overnight. The yields were determined gravimetrically.

### 5.3.4. Synthesis of PEO-b-PS block copolymer

PEO-b-PS was prepared by bulk ATRP. where PEO-Br (0.5 mmol), and CuCl (0.5 mmole) were added to a Schlenk flask capped with a rubber plug and kept under vacuum at ambient temperature for 60 min. Degassed monomer, St, and PMDETA (0.5 mmol) Through three freeze-thaw cycles were introduced into the Schlenk flask. The mixture was heated at 100 $^{o}$C in an oil bath under stirring. The reaction was stopped after 4 h, and the mixture was then quickly cooled to room temperature with cool water. The flask was opened and exposed to the air. The sample was further diluted with THF and the copper salts were removed by passing the solution through neutral aluminum oxide. Finally the sample was precipitated into a large volume of cold methanol, filtered off, and dried in a vacuum oven overnight at 50 $^{o}$C.

## 5.4. Preparation of UV-cured epoxy containing block copolymer

Typically, the block copolymers were dispersed into the epoxy resin in the range between 4 and 8 phr. The formulation was ultrasonicated for 4 h and subsequently Ultra Turrax was used for 5 min at 25,000 rpm. The triphenylsulfonium hexafluoroantimonate as cationic photoinitiator was added to all the formulations at 2 wt% with respect to the CE content. The formulations were cured with a medium vapour pressure mercury static UV lamp with intensity on the sample surface of 35 mW/cm$^2$ (measured with EIT instrument). The thickness of the photocured films was in the range of 100 ±10 μm for all the series of samples.

## 5.5. Results and discussion

### 5.5.1. Synthesis of reactive and nonreactive block copolymer

PGMA homopolymer, PEO-b-PGMA, and PEO-b-PS with different block length have been prepared using ATRP. The epoxy group in PGMA can be involved in the UV-induced epoxy-curing process and covalently link to the polymeric matrix. PGMA homopolymer is prepared in diphenyl ether in the presence of EBrIB as initiator, as described in the experimental part. The synthetic route is summarized in scheme 5.1.

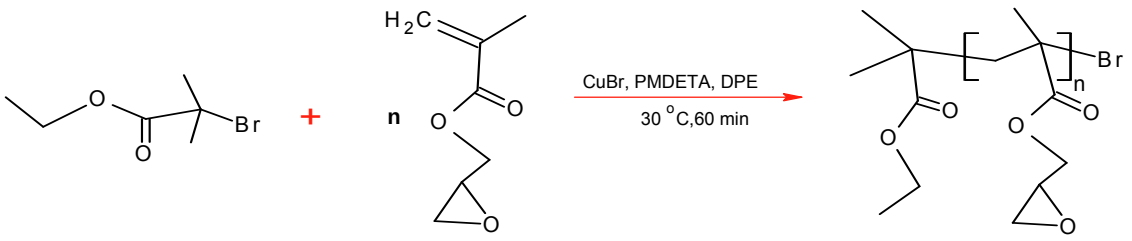


**Scheme 5.1:** synthesis of PGMA-Br homopolymer

$^1$H NMR of PGMA is shown in figure 5.1 which indicates the resonance characteristics of PGMA and ATRP initiator. The molecular weight of PGMA was calculated using (–$CH_2$–) of initiator as reference peak and found to be $M_n$ = 5750. GPC curves indicate that the obtained PGMA has relatively narrow distributions with $M_w/M_n$= 1.4.

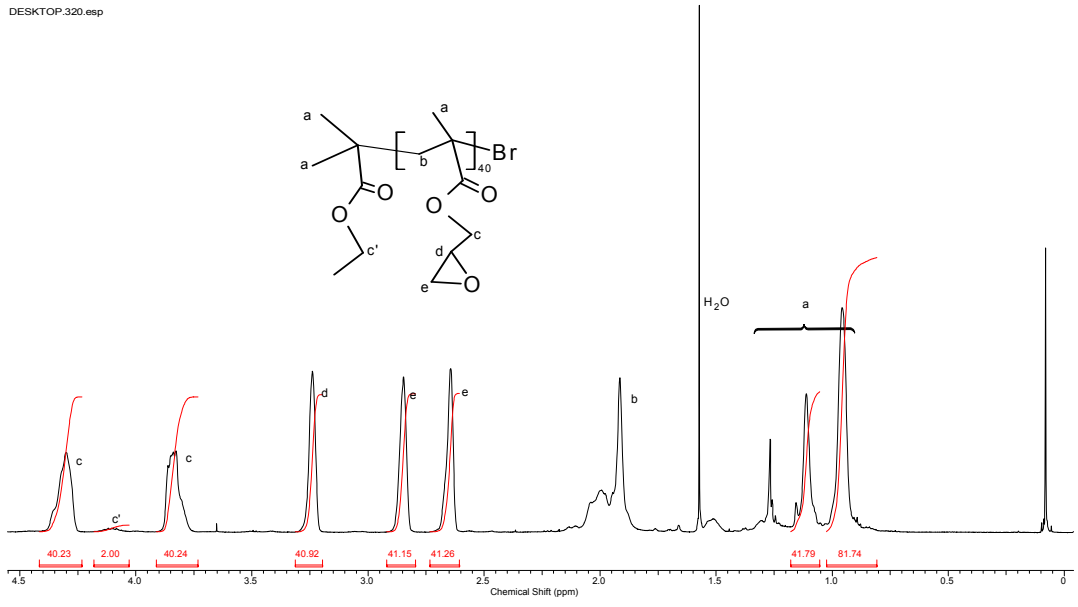


**Figure 5.1**: $^1$H NMR spectrum of PGMA homopolymer

PEO-*b*-PGMA reactive block copolymers with different block length are synthesized via ATRP (see table 5.1). Figure 5.2 shows the $^1$H NMR of PEO-*b*-PGMA. The resonance signals of methyl group in PGMA split into three peaks at 0.96, 1.12, and 1.17 ppm which were assigned to syndiotactic, heterotactic, and isotactic configurations, respectively.[1]

**Table 5.1:** Molecular weight and polydispersity of PEO-b-PGMA block copolymer

| Sample | $M_n$, $^1$H NMR | PDI |
|---|---|---|
| PGMA-Br | 5750 | 1.40 |
| $PEO_{45}$-b-$PGMA_{65}$ | 11400 | 1.31 |
| $PEO_{113}$-b-$PGMA_{70}$ | 15100 | -- |
| $PEO_{45}$-b-$PS_{60}$ | 8400 | -- |
| $PEO_{113}$-b-$PS_{115}$ | 17100 | -- |

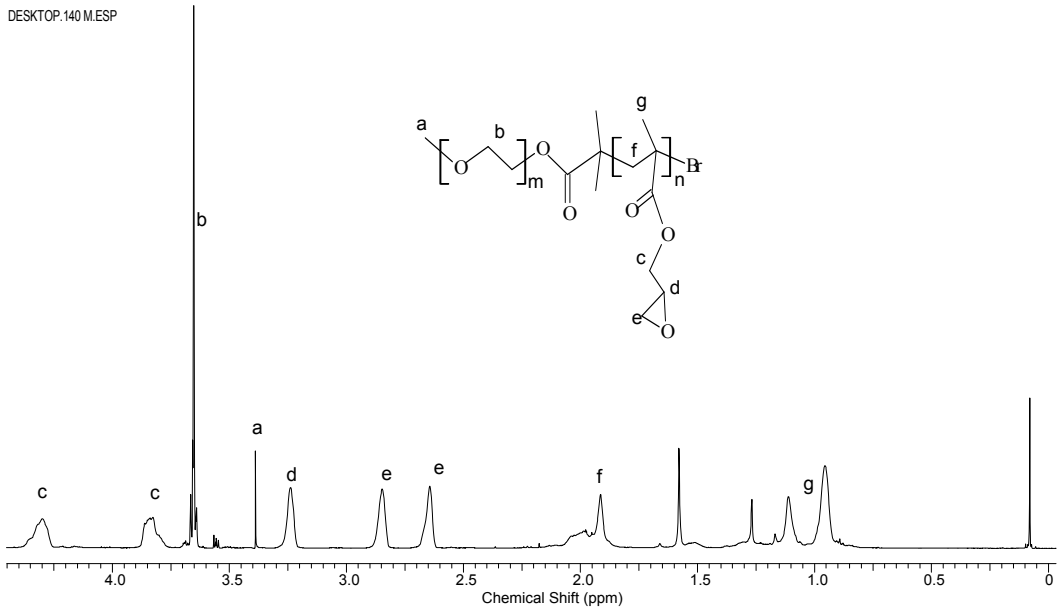


**Figure 5.2:** $^1$H NMR spectrum of PEO-b-PGMA block copolymer

Additionally, PEO-b-PS as nonreactive block copolymer with different block length (see table 1) were prepared in bulk. The result of $^1$H NMR indicates the successful synthesis of the block copolymer as shown in figure 5.3.

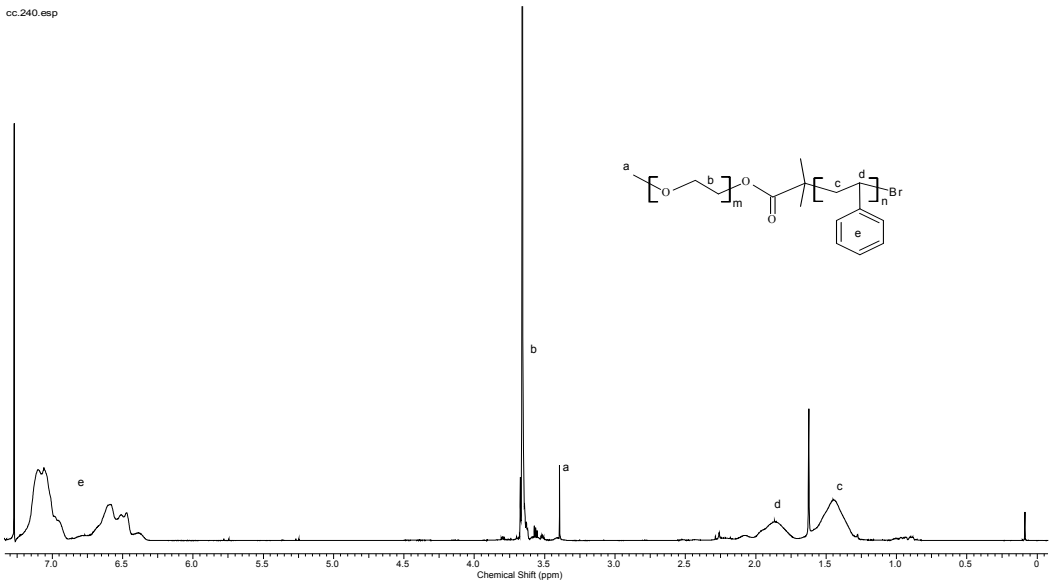


**Figure 5.3:** $^{1}$HNMR spectrum of PEO-b-PS block copolymer

### 5.5.2. Dynamic mechanical analysis of reactive BCP modified epoxy

DMA is usually used to study the viscoelastic properties of polymers under stress and elevated temperature. The DMA of UV-cured epoxy thermosets containing PGMA and PEO-b-PGMA diblock copolymer were performed on samples of diameter about 100μm.The contents of homopolymer or block copolymer in epoxy are 4 and 8 phr. The glass transition temperature, $T_g$, values are summarized the table 5.2.

The neat epoxy exhibits two relaxation processes; one is low-temperature relaxation (around -65 $^{o}$C) which corresponds to β-relaxation mode and the other one at 160 $^{o}$C which corresponds to α-relaxation mode and associated with glass transition temperature (figure 5.4).

**Table 5.2:** Viscoelastic properties of reactive block copolymer

| Sample | code | $T_g$, °C | Storage modulus E' (GPa) | | Gel content, % |
|---|---|---|---|---|---|
| | | | @ RT | @rubbery plateau | |
| Neat epoxy | Neat CE | 160 | 1.36 | 0.032 | 100 |
| Epoxy/PGMA 4% | PGMA 4% | 171 | 2.75 | 0.042 | 99.5 |
| Epoxy/PGMA 8% | PGMA 8% | 176 | 3.11 | 0.061 | 99.9 |
| Epoxy/ ($PEO_{45}$-b-$PGMA_{65}$) 4% | B4G 4% | 157 | 2.41 | 0.051 | 99 |
| Epoxy/ ($PEO_{45}$-b-$PGMA_{65}$) 8% | B4G 8% | 159 | 2.87 | 0.061 | 98.5 |
| Epoxy/ ($PEO_{113}$-b-$PGMA_{70}$) 4% | B5G 4% | 156 | 2.78 | 0.049 | 99.5 |
| Epoxy/ ($PEO_{113}$-b-$PGMA_{70}$) 8% | B5G 8% | 160 | 2.77 | 0.061 | 98.5 |

For the epoxy system containing PGMA homopolymer there is a noticeable increase in the $T_g$ values and this could be attributed to the involving the epoxy groups of PGMA in the curing process. Thus, they become chemically linked to the epoxy network and hence increase the crosslinking density.[3-5] Obviously, this increase in the crosslinking density has negative influence on the fracture toughness as appeared in the $K_{IC}$ values (see table 5.3).

It is very interesting to observe that the addition of the reactive block copolymer, PEO-*b*-PGMA, did not significantly affect the $T_g$ values of the cured blends (figure 5.5). Despite the presence of soft block, PEO, the glass transition temperature still not far from that of neat epoxy. This could be explained by the existence of reactive block, PGMA, which can interact with the carbocationic growing chain through a copolymerization mechanism and compensate the softening effect of other block in addition to the restriction in the mobility of PEO chains in the copolymer as described by other authors.[6]

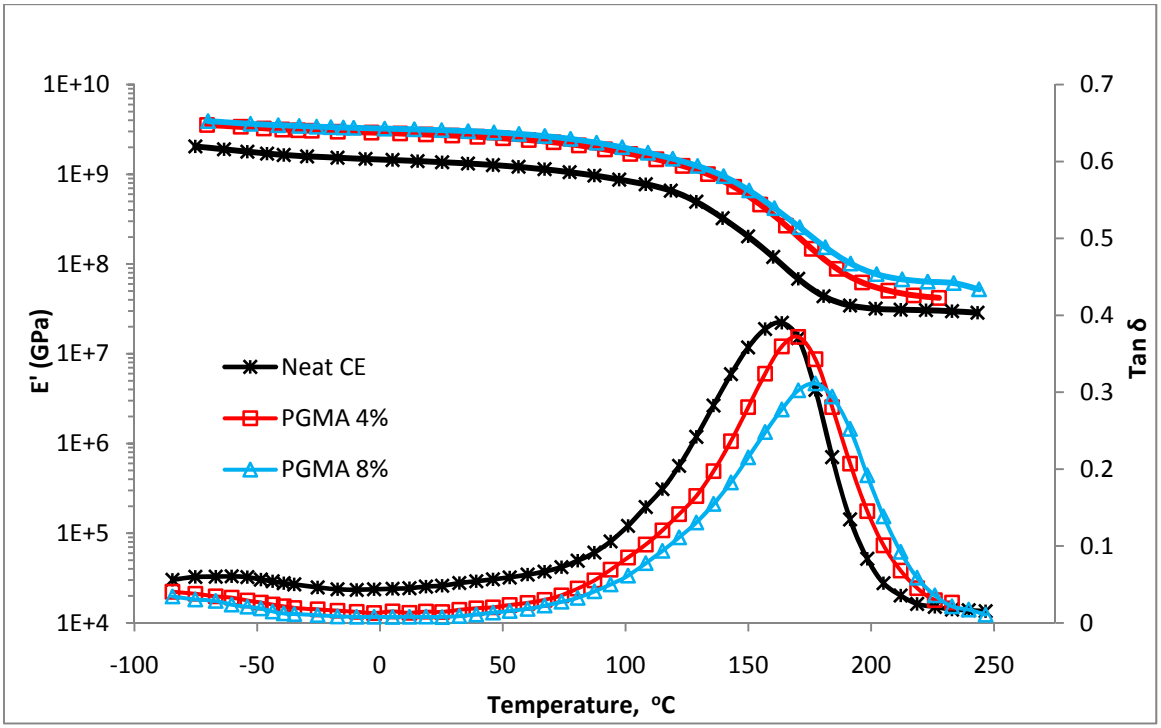


**Figure 5.4**: DMA plots of neat epoxy and PGMA modified epoxy

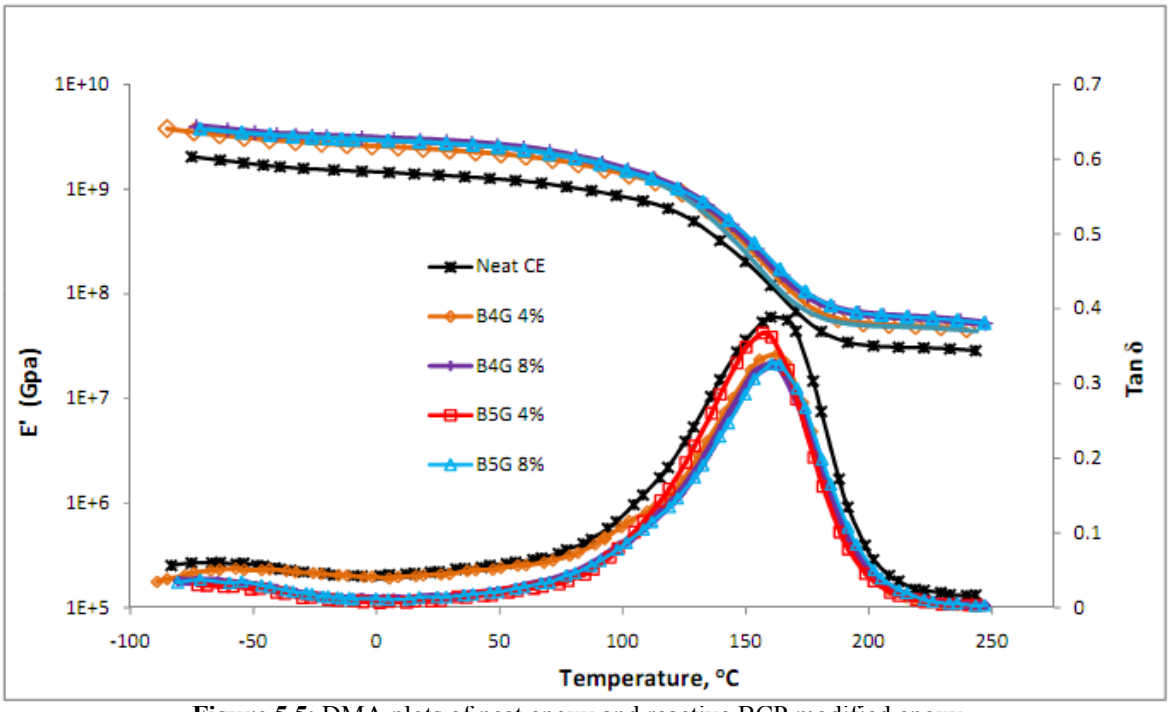


**Figure 5.5**: DMA plots of neat epoxy and reactive BCP modified epoxy

The storage modulus results of the epoxy containing PGMA homopolymer are shown in Figure 5.4 and Table 5.2. The storage moduli of the resulting composites were dramatically increased due to incorporating of reactive PGMA and hence higher crosslink

density. At room temperature epoxy/PGMA 4% and 8% showed about 100 and 125% higher storage modulus than pristine epoxy. As the temperature increased, both neat epoxy and epoxy containing PGMA showed a gradual drop at the glass transition temperature ($T_g$). At rubbery plateau region the epoxy containing PGMA also has higher storage modulus than neat epoxy.

In systems containing reactive block copolymer, PEO-b-PGMA, as modifier the storage modulus has noticeably improved as shown in figure 5.5. Where E recorded ≥ 100% higher than that of neat epoxy as indicated in table 5.2. Thus, epoxy/PEO-b-PGMA systems have much higher dimensional thermal stability than the neat epoxy. The higher storage modulus at low (T≤ Tg) and high temperatures (T≥ Tg) could be attributed to the enhancement of crosslinking density caused by PGMA block. The increase in storage modulus gives an evidence of stiffness improvement of epoxy containing reactive block copolymer.

### 5.5.3. Morphological characterization of reactive BCP modified epoxy

FESEM was used to study the morphology of fracture surfaces of UV-cured epoxy containing reactive homopolymer and block copolymer. At low and high magnification the fracture surface of epoxy/PGMA is nearby even and smooth as shown in figure 5.6. Clearly this was expected due to the incorporation of reactive PGMA in the epoxy matrix that prevent the chance of micro or nanophase separation.

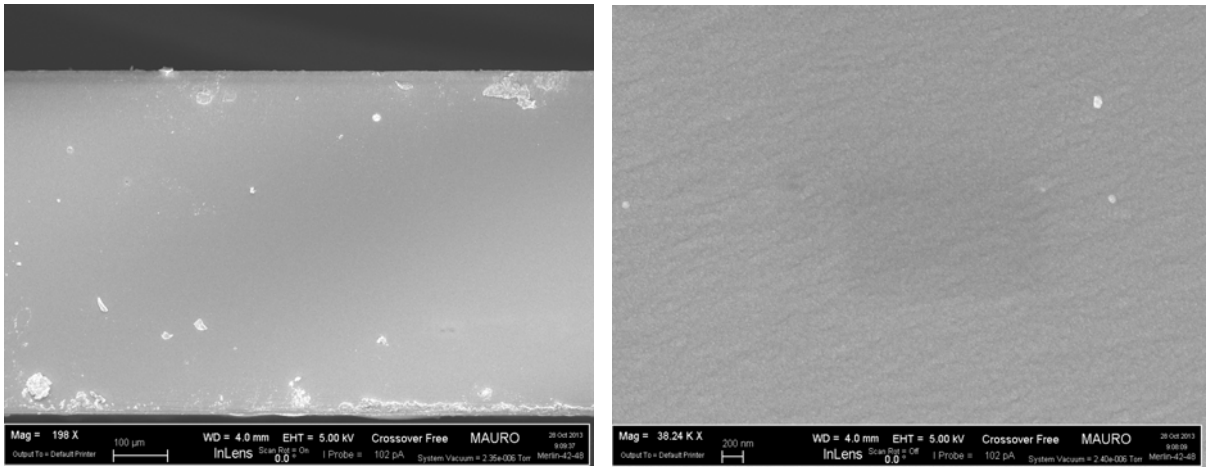


**Figure 5.6:** low and high magnification micrographs of fracture surface of epoxy containing PGMA homopolymer

The fracture surfaces of epoxy containing reactive BCP are more interesting. In case of B4G 8% (epoxy/$PEO_{45}$-b-$PGMA_{65}$) the micrographs also reveal smooth and homogenous fracture surfaces although the presence of PEO block as presented in figure 5.7. It is reported that the gelation of the epoxy resin forces an expulsion of the PEO from the matrix and also impedes the mobility of the block copolymer in the matrix, and thus macrophase separation of the block copolymer is kinetically hindered.[7,8] In case of $PEO_{45}$-b-$PGMA_{65,}$ because of the existence of relatively short PEO chains compared to reactive PGMA chains the opportunity of macro or microphase separation of the copolymer is limited and therefore the toughening effect could be very low.

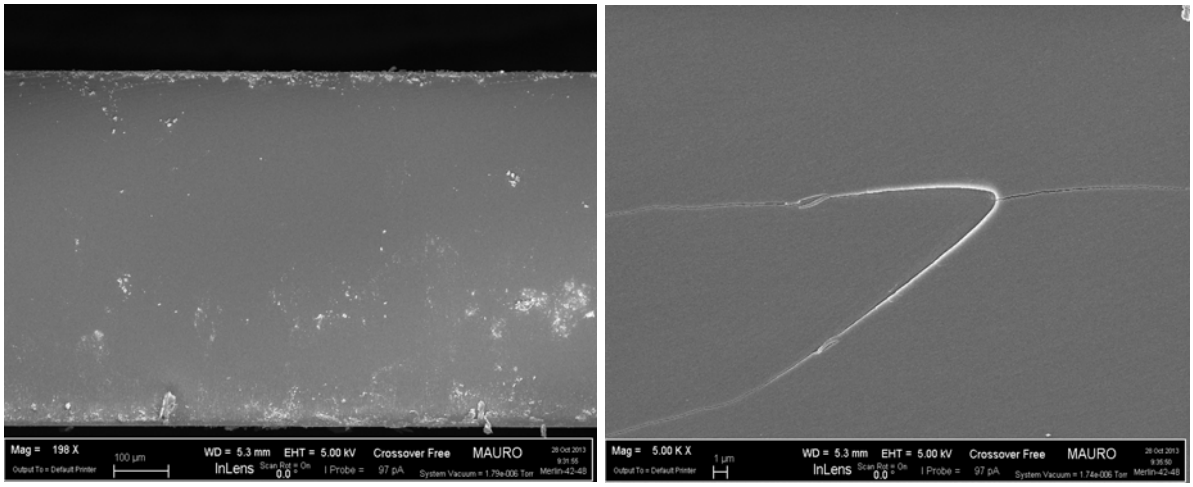


**Figure 5.7:** low and high magnification micrographs of fracture surface of epoxy containing 8% of $PEO_{45}$-b-$PGMA_{65}$

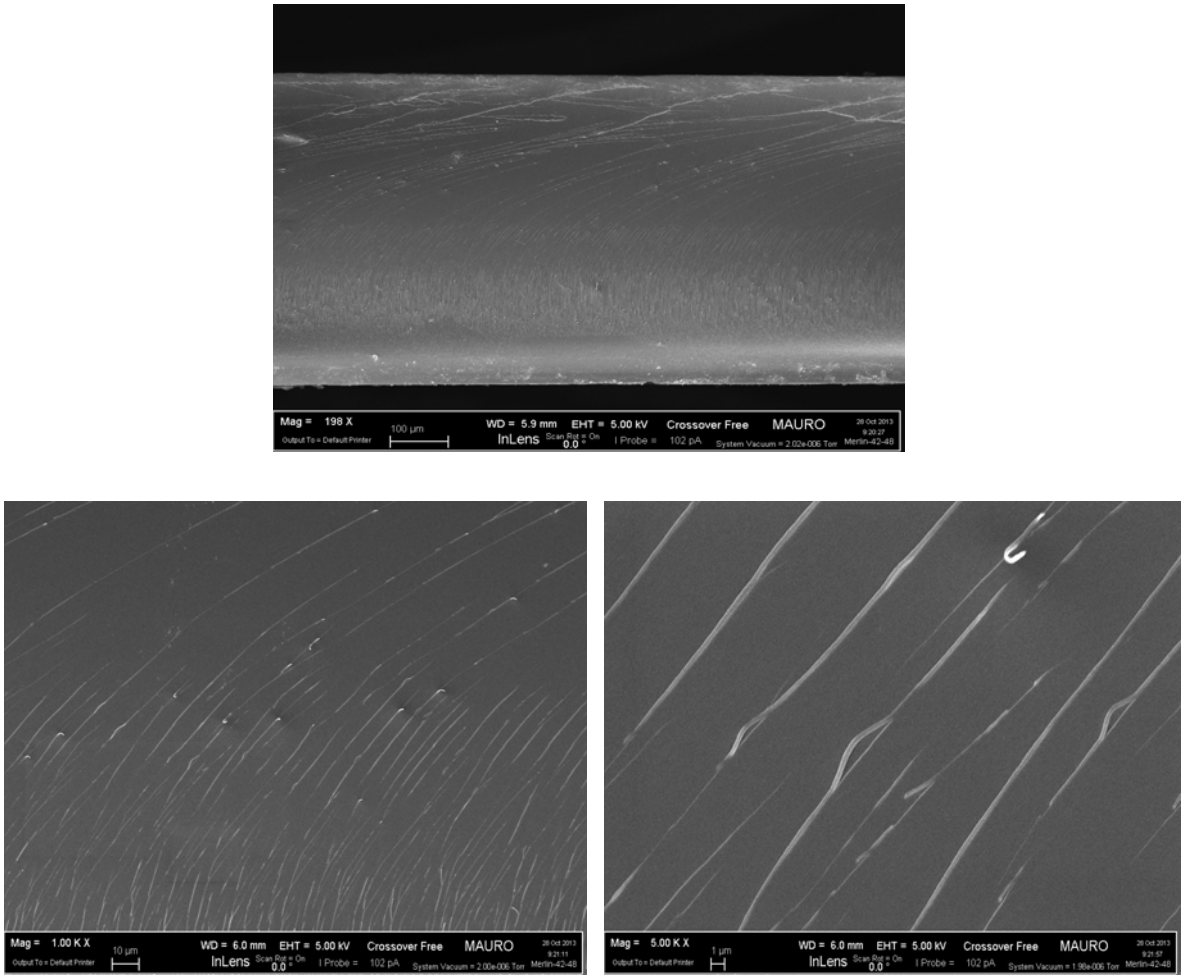


**Figure 5.8:** low and high magnification micrographs of fracture surface of epoxy containing 8% of $PEO_{113}$-b-$PGMA_{70}$

By increasing the PEO block length as in B5G (epoxy/$PEO_{113}$-b-$PGMA_{70}$) the surface roughness becomes clearly noticeable as shown in figure 5.8. The fracture surface of the B5G is much rougher than the neat epoxy due to the ejection of PEO chains from epoxy matrix upon curing.

### 5.5.4. Fracture toughness measurements of reactive BCP modified epoxy

Fracture toughness measurements of the prepared epoxy specimens were performed on the basis of the linear elastic fracture mechanics (LEFM) approach. A single-edge-notch three-point-bending (SENB) test was used to obtain the mode I critical stress intensity ($K_{IC}$) and fracture energy ($G_{Ic}$) of the neat epoxy and BCP modified epoxy in accordance with the ISO 13586-2000 method.

The critical stress intensity, $K_{IC}$, and fracture energy, $G_{Ic}$, values of neat epoxy and modified epoxy are summarized in table 5.3.

**Table 5.3:** fracture toughness measurements of UV-cured epoxy systems

| Sample | $K_{IC}$ [MPa.m$^{0.5}$] | $G_{IC}$ [kJ/m$^2$] |
|---|---|---|
| Neat CE | 1.31±0.09 | 0.442±0.06 |
| PGMA 8% | 0.95±0.08 | 0.203±0.05 |
| B2G 4% | 1.2±0.05 | 0.363±0.01 |
| B2G 8% | 1.08±0.01 | 0.322±0.01 |
| B5G 4% | 1.31±0.04 | 0.427±0.09 |
| B5G 8% | 1.29±0.05 | 0.40±0.04 |

By carefully studying the $K_{IC}$ values we could observe that the presence of GMA groups has negative effect on the crack propagation resistance and hence the fracture toughness. The $K_{IC}$ of epoxy/PGMA dropped 27% as compared to neat epoxy. This decrease in fracture toughness is expected as the reactive PGMA involved in the network curing causing higher crosslink density. Apparently, high $T_g$ values and smooth fracture surface as revealed by DMA and FESEM strongly support this interpretation.

In case of samples containing PEO-b-PGMA as modifier the $K_{IC}$ values is higher than that of epoxy/PGMA but do not exceed that of neat epoxy. This could be demonstrated by the contribution of PEO block in the system. It is interesting to find that the length of PEO has influence on the $K_{IC}$ values. For example, incorporation of block copolymer with high molecular weight of PEO, $M_n$=5000, (B5G) reduce the effect of PGMA block on the fracture toughness. This could be verified by looking at $K_{IC}$ values that nearly equal to neat epoxy values. In contrary, systems containing block copolymer with low molecular weight of PEO, $M_n$=2000, (B2G) has less $K_{IC}$ values if compared to that containing higher molecular weight of PEO (B5G). The previously discussed FESEM micrographs confirm these findings where a rougher surface is observed in B5G 8% while missing in B2G 8%.

### 5.5.5. Dynamic mechanical analysis of non-reactive BCP modified epoxy

The DMA of UV-cured epoxy resins containing non-reactive PEO-b-PS block copolymer were preformed on photo cured samples after additional thermal post-curing for 24 h at 75 $^{o}$C. The content of block copolymer in epoxy are 4 and 8 phr. Table 5.4 concludes the glass transition temperature, $T_g$, and storage modulus, E', results.

**Table 5.4:** viscoelastic properties of UV-cured modified epoxy

| Sample | code | $T_g$, $^{o}$C | Storage modulus E' (GPa) | | Gel content, % |
|---|---|---|---|---|---|
| | | | @ RT | @Rubbery plateau | |
| Neat epoxy | Neat CE | 160 | 1.36 | 0.032 | 100 |
| Epoxy/ ($PEO_{45}$-b-$PS_{60}$) 4% | S1G 4% | 158 | 1.38 | 0.034 | 99.5 |
| Epoxy/ ($PEO_{45}$-b-$PS_{60}$) 8% | S1G 8% | 159 | 2.35 | 0.035 | 99 |
| Epoxy/ ($PEO_{113}$-b-$PS_{115}$) 4% | S5G 4% | 157 | 1.94 | 0.036 | 99.5 |
| Epoxy/ ($PEO_{113}$-b- $PS_{115}$) 8% | S5G 8% | 152 | 2.5 | 0.026 | 98.5 |

It has been seen that addition of nonreactive block copolymer affect slightly on the glass transition temperature, $T_g$, of modified epoxy systems. However in case of S5G samples, where the block copolymer has higher molecular weight, the $T_g$ values are much affected. Further investigation on tan δ curves of BCP modified epoxy indicates the presence of small shoulder at 90 $^{o}$C (figure 5.9 & 5.10) which denotes to a partial microphase separation of PS from the epoxy matrix.[9]

Relative to neat epoxy, adding BCP shows a significant increase in storage modulus below room temperature and a slight increase at the rubbery plateau region as shown in figure 5.9 and figure 5.10. Interestingly, S5G 8% sample has obvious low storage modulus at the rubbery plateau region which might be a result of low $T_g$ value.

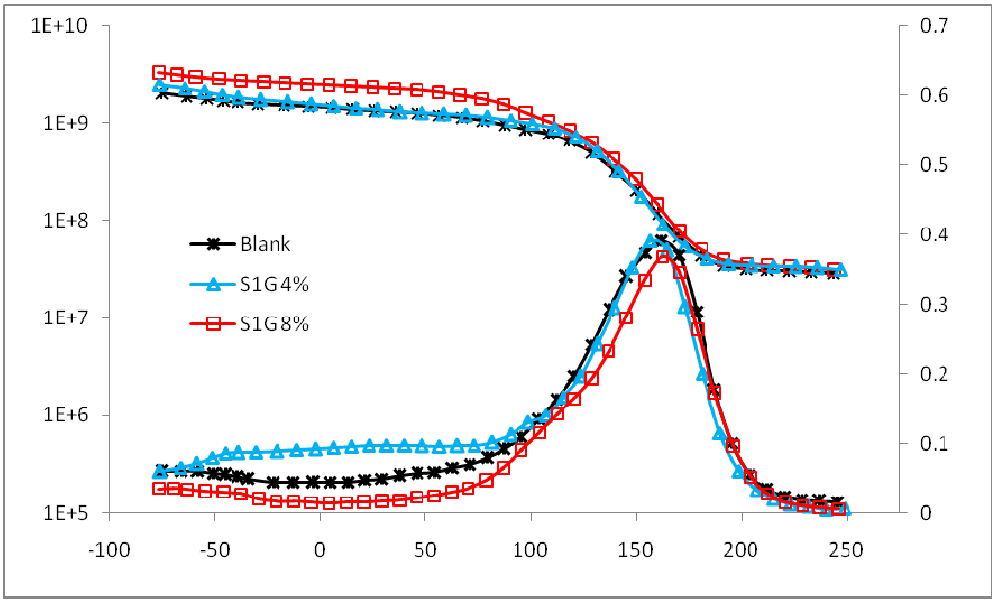


**Figure 5.9:** DMA plots of neat epoxy and $PEO_{45}$-b-$PS_{60}$ modified epoxy

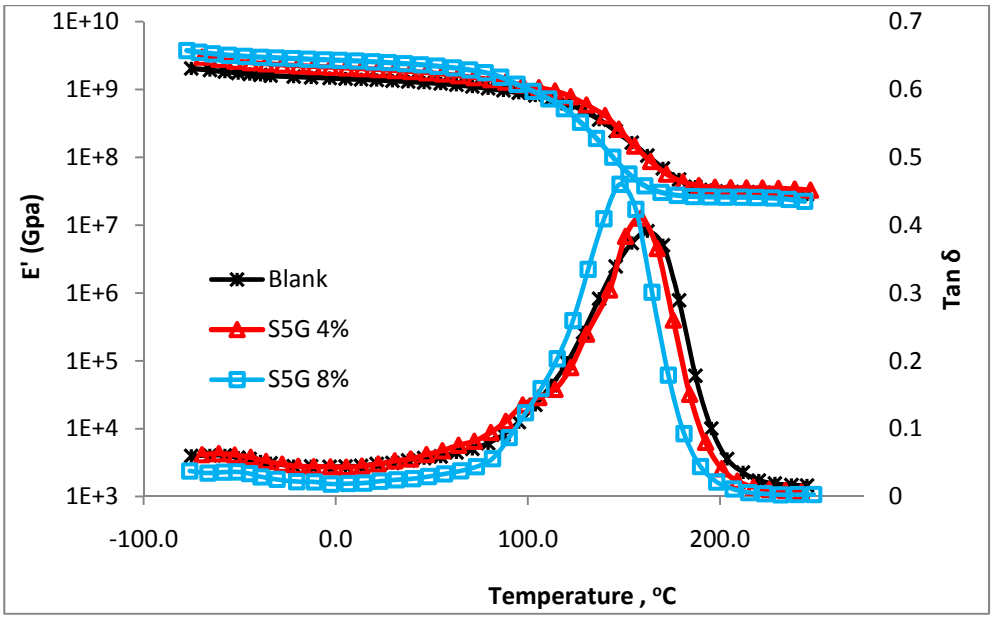


**Figure 5.10:** DMA plots of neat epoxy and $PEO_{113}$-b-$PS_{115}$ modified epoxy

### 5.5.6. Morphological characterization of non-reactive BCP modified epoxy

Subsequently, the morphology of the cured materials was investigated by screening the fracture surfaces of the test specimens with FESEM. The fracture surfaces of epoxy containing nonreactive block copolymer, PEO-b-PS, are exciting. It is seen that the fracture surfaces of PEO-b-PS modified epoxy have a heterogeneous morphology. At low magnification, several and clear river marks are shown indicating crack propagation on slightly different planes (figure 5.11). At high magnification, the fracture surfaces indicate increasing surface roughness of modified epoxy compared to smooth pristine epoxy. The new dimples observed in fracture surfaces might be accompanied by dissipation of much fracture energy and hence enhancing in fracture toughness. The heterogeneous surface may be ascribed to microphase separation of PS units from the epoxy-rich phase. Furthermore, partial microphase separation of some PEO units, as discussed in PEO-b-PGMA part, cannot be ignored. By increasing molecular weight of PEO-b-PS block copolymer in the modified epoxy as in S5G samples the heterogeneity and microphase separation become more noticeable as shown in figure 5.11.

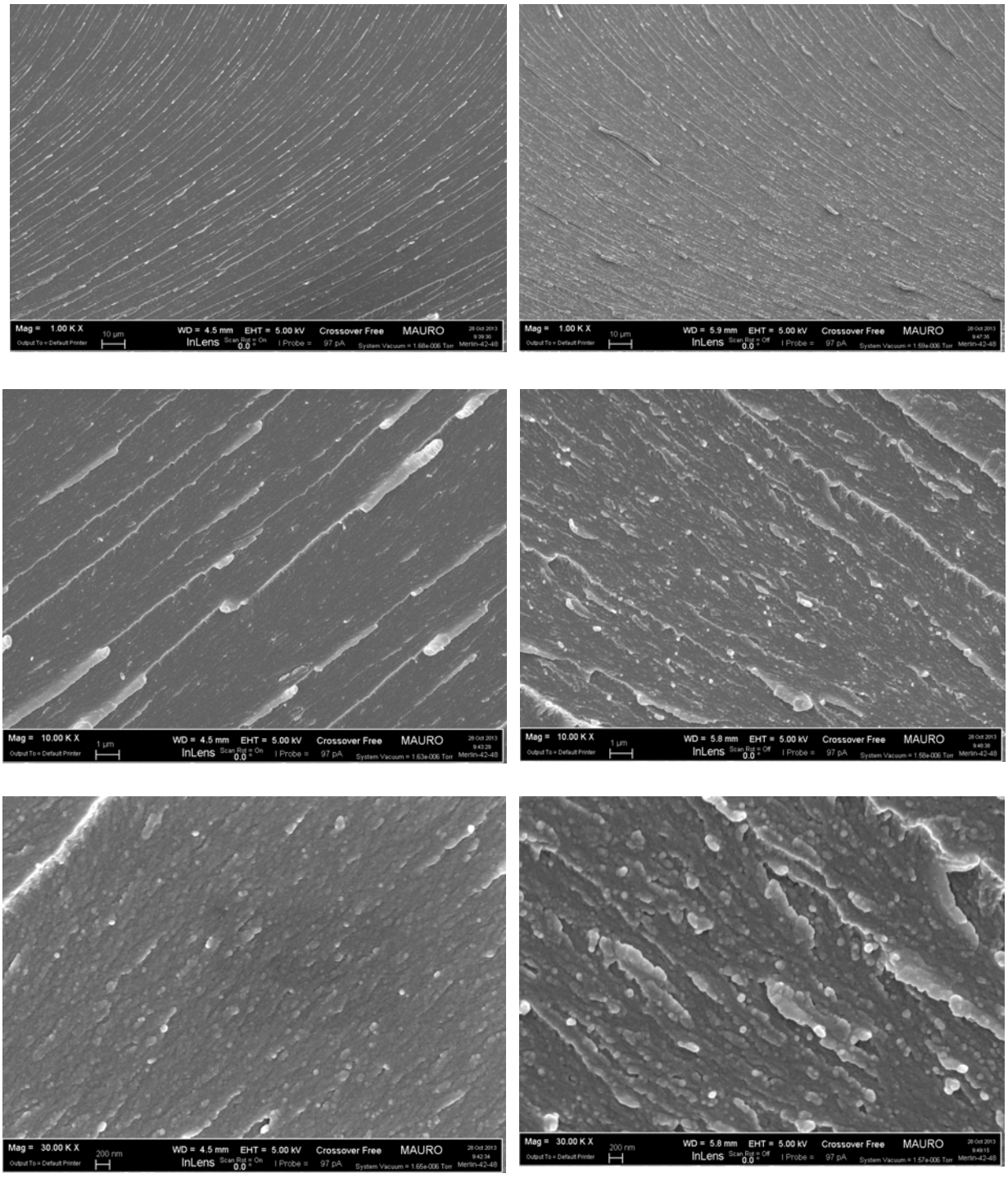


**Figure 5.11:** FESEM micrographs of fracture surface of UV-cured epoxy modified with $PEO_{45}$-b-$PS_{60}$ (left) and $PEO_{113}$-b-$PS_{115}$ (right)

### 5.5.7. Fracture toughness measurements non-reactive BCP modified epoxy

The fracture toughness was evaluated in terms of three-point bending test (SENB). Practically the critical stress intensity ($K_{IC}$) and fracture energy ($G_{Ic}$) of the control epoxy and PEO-b-PS modified epoxy were calculated. The plots of $K_{IC}$ value as a function of block copolymer content are presented in figure 5.12. The $K_{IC}$ values of all BCP modified epoxy are higher than that of neat epoxy, indicating that the cycloaliphatic epoxy resins were significantly toughened with inclusion of PEO-b-PS.

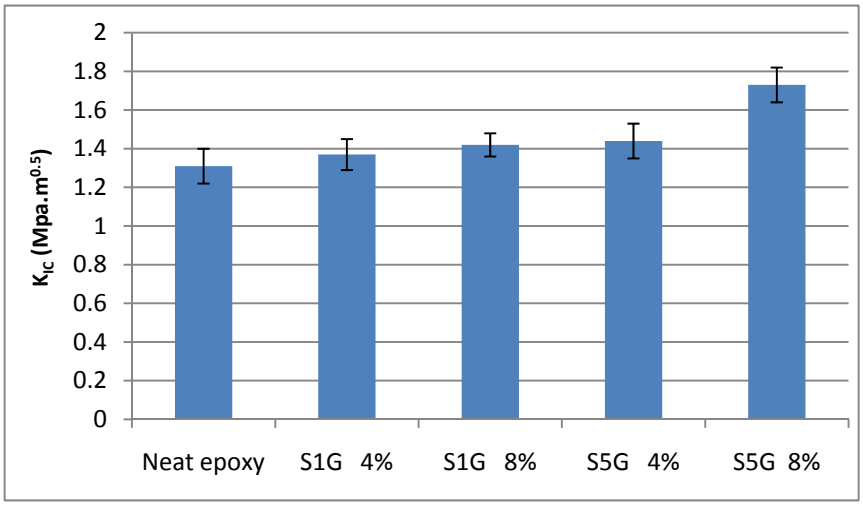


**Figure 5.12:** fracture toughness measurements of UV-cured epoxy modified with BCP

By carefully studying the $K_{IC}$ results we could observe that the molecular weight and blocks length of BCP are important parameters. For instance, the $K_{IC}$ of S1G 8% that contains low molecular weight ($PEO_{45}$-b-$PS_{60}$) is 1.42 MPa.$m^{0.5}$ while that of S5G 8% sample that composed of higher molecular weight ($PEO_{113}$-b-$PS_{115}$) is 1.73 MPa.$m^{0.5}$. Micrographs of fracture surface taken by FESEM support this observation as previously discussed. The enhancement in fracture toughness could be mainly attributed to the microphase separation generated by block copolymer as well as the decrease in crosslinking density.

## 5.6. Conclusion

Reactive PEO-b-PGMA and nonreactive PEO-b-PS block copolymers were prepared through ATRP technique. Subsequently, incorporation of these block copolymers into the cycloaliphatic epoxy and curing the entire system via UV light had been carried out. The reactive block has slight effect on the glass transition temperature, $T_g$, as compared by pristine epoxy. This could be demonstrated by the involving of epoxy group of PGMA in the polymerization reaction resulting in increase the crosslink density and mobility restriction of soft PEO chains. An improvement in storage modulus is observed which gives an evidence of stiffness enhancement. The fracture surface morphology revealed smooth and homogenous surfaces. However, by increasing the PEO block length the surface roughness becomes clearly noticeable. The $K_{IC}$ values support the results explained in terms of FESEM and DMTA. Where the incorporation of reactive block copolymer has negative effect on the fracture toughness. Clearly, the PEO block length has a crucial effect on the $K_{IC}$ values.

On the other side, the incorporation of nonreactive block copolymer into epoxy resins successfully enhances the fracture toughness without scarifying other thermal and mechanical properties. A heterogeneous morphology could be observed by studying the fracture surfaces. The fracture toughness measurements indicate an increase in $K_{IC}$ values by 33% if compared to neat epoxy. additionally, the molecular weight and blocks length of block copolymer are important parameters.

## 5.7. References


1. P. F. Canamero, J. L. de la Fuente, E. L. Madruga, M. Fernandez-Garcıa, Macromol. Chem. Phys. 2004; 205:2221
2. J. Z. Du, S. P. Armes, J. Am. Chem. Soc. 2005; 127:12800.
3. J. P. Pascault, R. J. J. Williams, J Polym Sci Part: B Polym Phys, 1990; 28:85.
4. A. Hale, , C. W. Macosko, H. E. Bair, Macromolecules 1991; 24:2610.
5. F. Yi, R. Yu, S. Zheng, X. Li, Polymer, 2011; 52:5669.
6. C. Ocando, E. Serrano, A. Tercjak, C. Pen a, G. Kortaberria, C. Calberg , B. Grignard, R.Jerome, P. M. Carrasco, D. Mecerreyes, I. Mondragon, Macromolecules 2007; 40:4068.
7. P. Lipic, F. Bates, M. Hillmyer, J. Am. Chem.Soc. 1998; 120:8963.
8. M. Hillmyer, P. Lipic, D. Hajduk, K. Almdal, F. Bates, J. Am. Chem. Soc. 1997; 119:2749.
9. S. Ritzenthaler, F. Court, L. David, E. Girard-Reydet, L. Leibler, J. P. Pascault, Macromolecules, 2002; 35:6245.

## 5.8. Supporting data

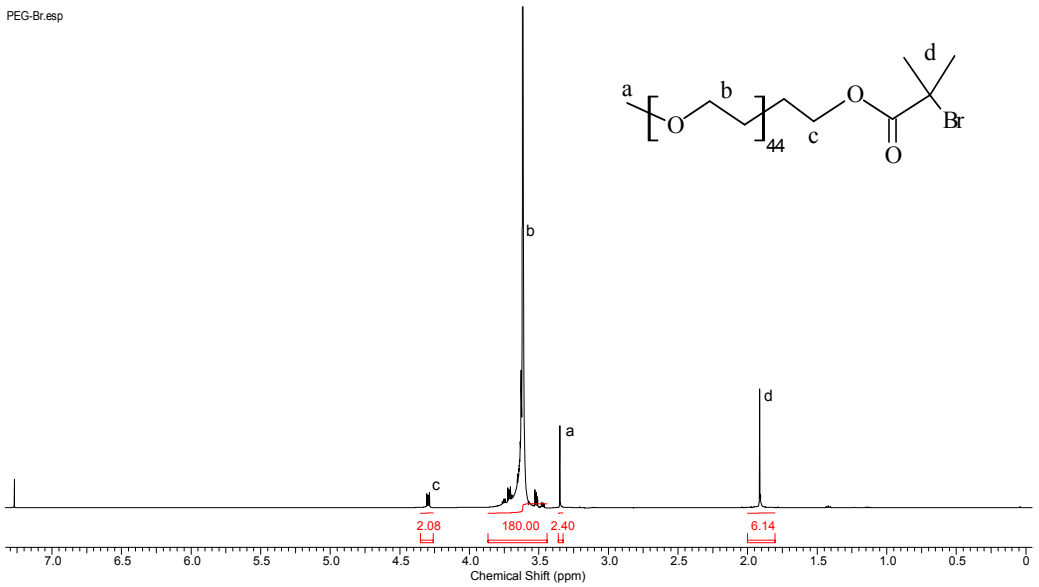


**Figure 5.13:** $^{1}$H NMR spectrum of $PEO_{45}$-Br

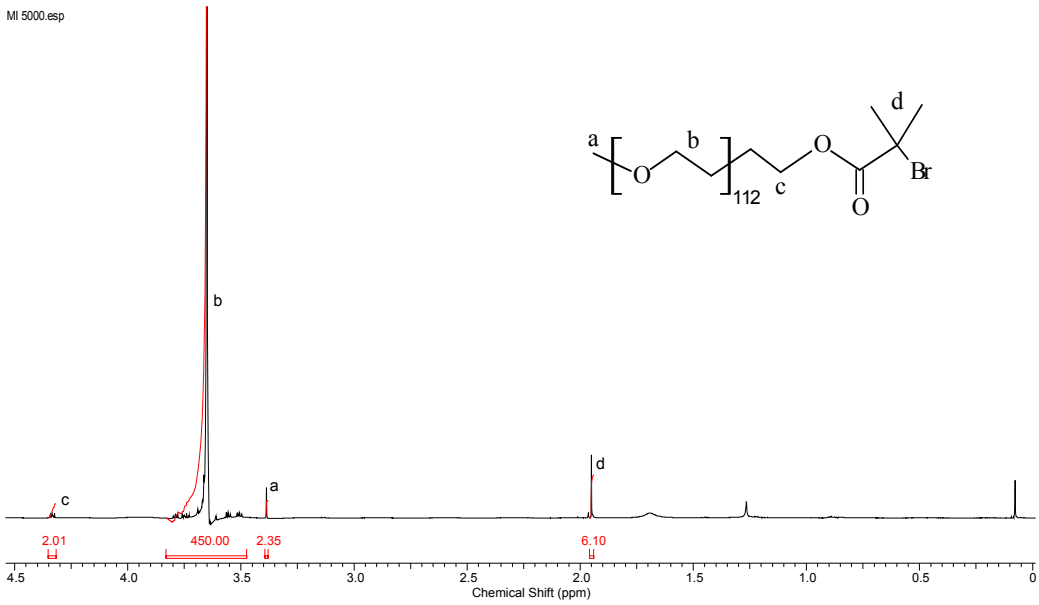


**Figure 5.14:** $^{1}$H NMR spectrum of $PEO_{113}$-Br

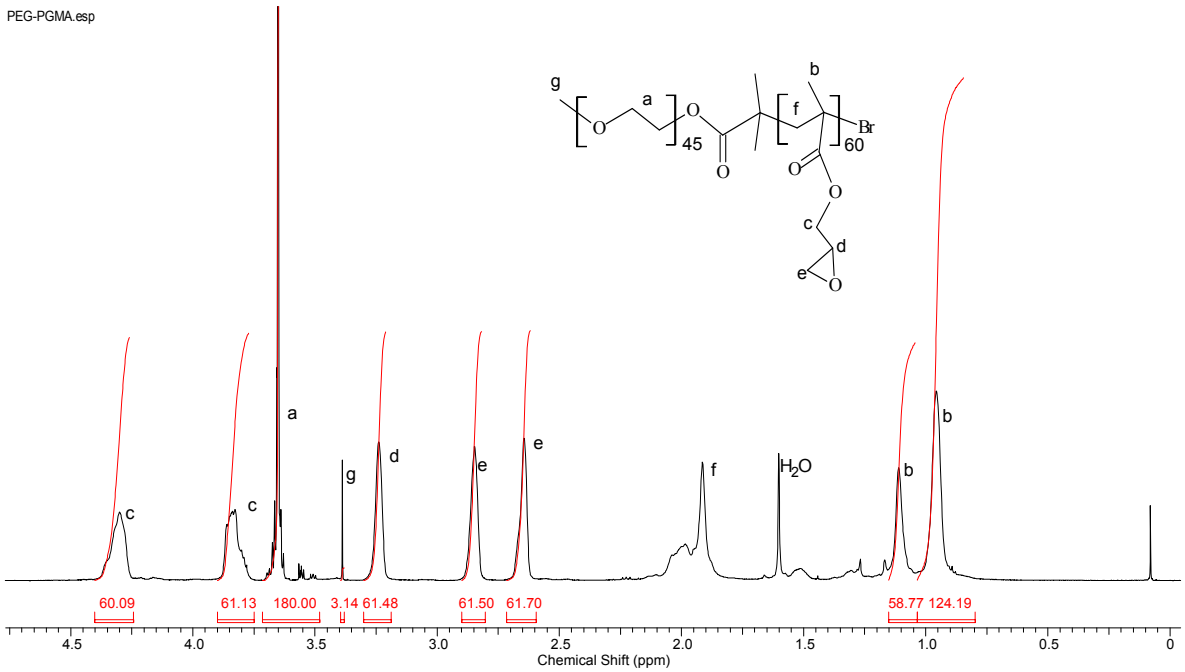


**Figure 5.15:** $^{1}$H NMR spectrum of $PEO_{45}$-b-$PGMA_{60}$ block copolymer

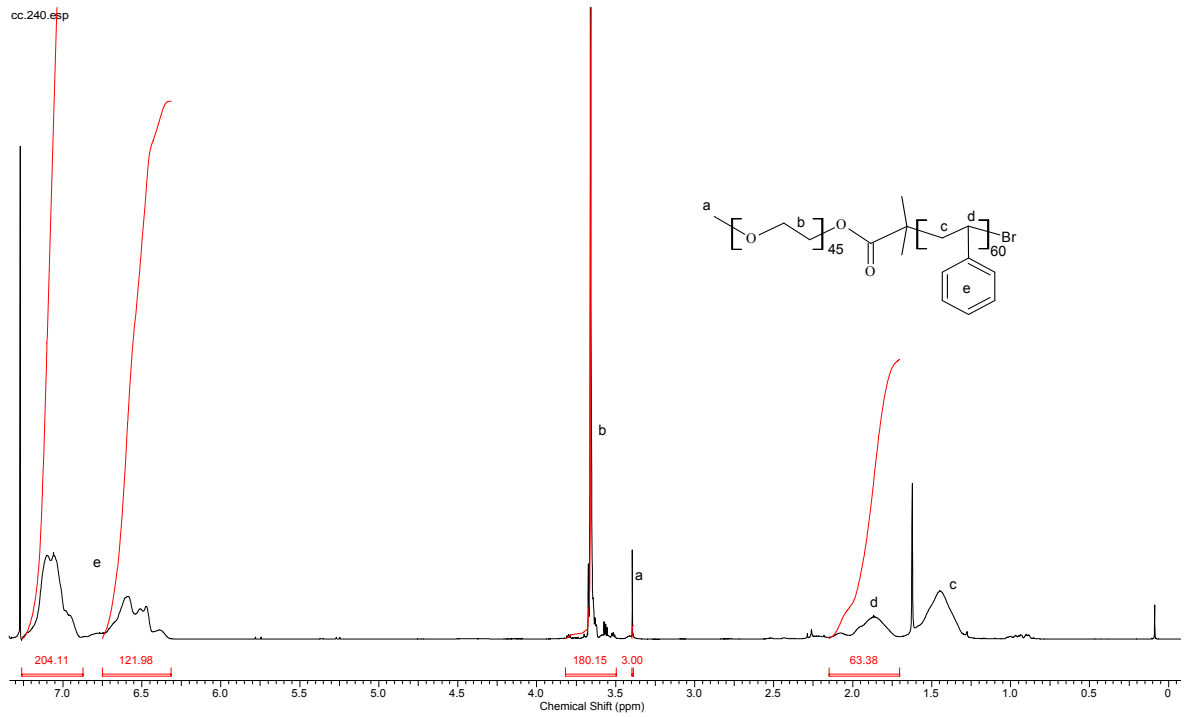


**Figure 5.16:** $^{1}$H NMR spectrum of $PEO_{45}$-b-$PS_{60}$ block copolymer

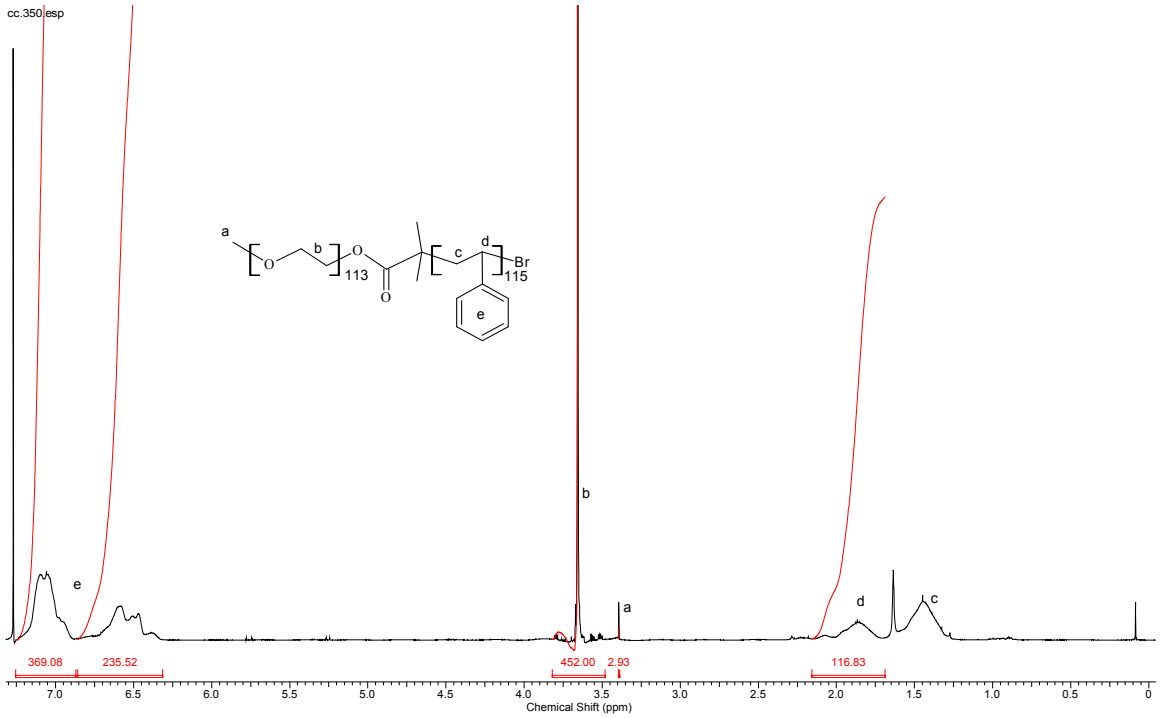


**Figure 5.17:** $^{1}$H NMR spectrum of $PEO_{113}$-b-$PS_{115}$ block copolymer

# 6

# Epoxy containing $Al_2O_3$ nanoparticles

## 6.1. Abstract

Commercially available alumina (α-$Al_2O_3$) powder of 150 nm is added up to 4 vol. % into the cycloaliphatic epoxy resins, CE, and cured via UV light. Chemical and physical investigations of these UV-cured reinforced epoxy resin are carried out. The real-time FTIR analysis indicates a decrease of the curing rate by increasing the ceramic powder. The FESEM study for the fracture surface of reinforced epoxy resins revealed increase in the surface roughness that might be signal for toughness enhancement. Generally, rigid fillers with good adhesion to the matrix interfere with crack propagation via various toughening mechanisms such as pining, bridging and/or deflection leading to a higher toughness and rougher fracture surface.[1] Conversely, weakly bonded rigid particles debond easily to activate the plastic void growth, thus dissipating more energy.[2,3] Also, an improvement in the scratch resistance was noticed for samples containing alumina filler.

## 6.2. Formulation of alumina modified epoxy systems

Different amounts of alumina nanoparticles in the range between 0.5 to 4 vol.% were dispersed into the cycloaliphatic epoxy resin, CE, using ultrasonic bath for 2 hrs and subsequently Ultra Turrax for 5 min at 25000 rpm. This high shear process helps the dispersion of nanoparticles agglomerates. All the formulations were then added with 2 wt% of cationic photoinitiator and cured under static UV lamp with intensity on the surface of the samples of 55 $mWcm^{-2}$ (measured with EIT instrument).

## 6.3. Results and discussion

### 6.3.1. RT-FTIR analyses

The α-$Al_2O_3$ filler was homogeneously dispersed in the UV-curable epoxy resin and the curing conditions evaluated by real-time FTIR analysis. Despite alumina particles have hydroxyl groups which could accelerate the photopolymerization rate through a chain transfer mechanism, as previously observed for silica nanoparticles[4], the real time FTIR analysis has revealed a decrease in the curing rate in the presence of $Al_2O_3$ (figure 6.1). This gradual decrease in the curing rate by increasing alumina content might be due to two distinct factors: first, by increasing the inorganic particle content we induced an important increase of viscosity which could decrease the mobility of the reactive species with a reduction on curing rate and epoxy group conversion. Second, UV-shielding caused by Alumina particles which has a strong UV- absorption in the same spectral range of photoinitiator, will strongly decrease the production of the reactive species, with a consequent decrease of reactivity.

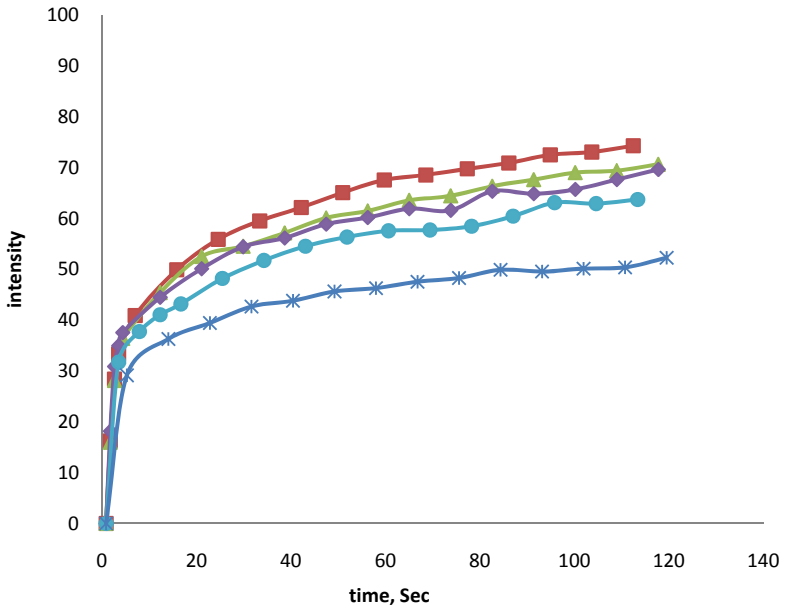


**Figure 6.1:** Conversion curves as a function of irradiation time for the pristine epoxy resin (■) and for the epoxy resin containing 0.5 vol.% ( ▲), 1 vol.% ( ◆), 2 vol.% ( ●) and 4 vol.% (✱) $Al_2O_3$ nanofiller

### 6.3.2. Gel content

Fully cured films were obtained notwithstanding the lowering of epoxy group conversion induced by the presence of the alumina filler. All the UV-cured films showed always high gel content values (above 98%, see Table 6.1), indicating almost absence of extractable monomer or oligomers.

**Table 6.1:** Gel content and $T_g$ of the UV-cured epoxy films

| Sample | Gel content[a)] % | $T_g$ [b)] °C |
|---|---|---|
| CE | 100 | 211 |
| $Al_2O_3$ 0.5 vol% | 99 | 205 |
| $Al_2O_3$ 1 vol% | 98 | 201 |
| $Al_2O_3$ 2vol% | 99 | 206 |
| $Al_2O_3$ 4vol% | 100 | 208 |

[a)]Determined on UV-cured samples, ASTM D2765-01; [b)]Determined as the maximum of tan δ curve from DMTA analyses.

### 6.3.3. Dynamic mechanical thermal anaylsis-DMTA

Viscoelastic characterization was performed on UV-cured films by means of DMTA analysis, tan δ curves are reported in figure 6.2. The maximum of tan δ peak can be taken as the $T_g$ of the cured films. It is interesting to observe that the presence of the alumina particles did not strongly influenced the $T_g$ values of the cured films which remained unmodified with respect to the pristine UV-cured film. We can explain this behavior taking into account that two contrasting effect can be expect. The presence of the ceramic filler induced a decrease of epoxy group conversion with a consequent decrease of crosslinking density and therefore a flexibilization of the cured film. This flexibilization effect is contrasted by the mobility hindering effect of the ceramic fillers which should increase the stiffness of the crosslinked filled film.

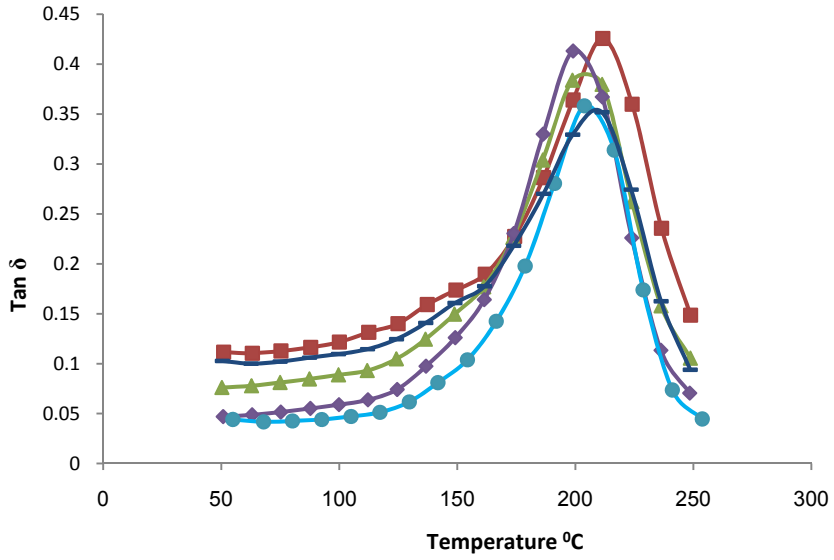


**Figure 6.2:** DMTA of UV-cured pristine epoxy resin (■) and for the epoxy resin containing 0.5 vol.% ( ▲), 1 vol.% ( ◆), 2 vol.% ( ●) and 4 vol.% (-)$Al_2O_3$

### 6.3.4. Morphological analysis

The topography morphology of the fracture surfaces for pristine UV-cured epoxy and epoxy composites was studied by FESEM. At low magnification the fracture surface of neat epoxy is relatively smooth (Figure 6.3a) however, several river marks are shown for epoxy composites indicating cracks propagation on slightly different planes (Figure 6.3b,c).

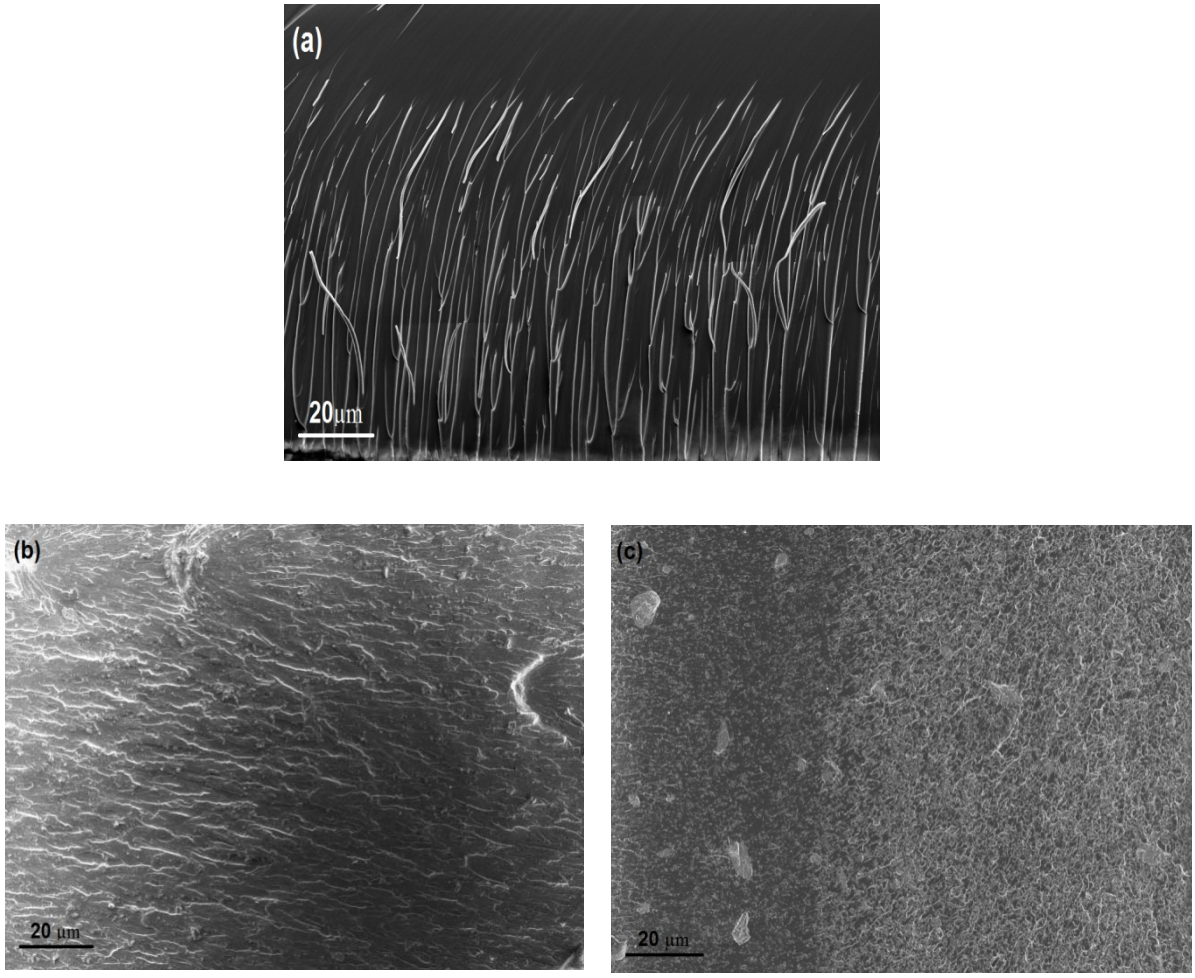


**Figure 6.3:** low magnification FESEM of fracture surface of the neat UV-cured epoxy matrix (a) and the UV-cured nanocomposites containing 0.5 vol.% (b) and 4 vol.% (c) of ceramic filler.

Clearly, the high magnification FESEM of the facture surface (Figure 6.4) elucidates increasing surface roughness of the alumina epoxy composites compared to pristine epoxy. The formation of the dimples in epoxy composites is accompanied by the creation of new fracture surfaces, and therefore much fracture energy can be dissipated. The dimples are increasing as the percent of alumina increase. Several fracture mechanisms for dissipating energy are known for epoxy resins and their composites. For particles-modified epoxy, crack deflection is most common mechanism and has been proposed to play a crucial role in the toughening. The theory was documented by Faber and Evans.[5] It is assumed that a crack can be deflected at an obstacle and be forced to move out of the initial crack propagation plane by tilting and twisting. Therefore, higher energy absorption is noticed and hence an increase in the total fracture toughness of the nanocomposites can be expected.

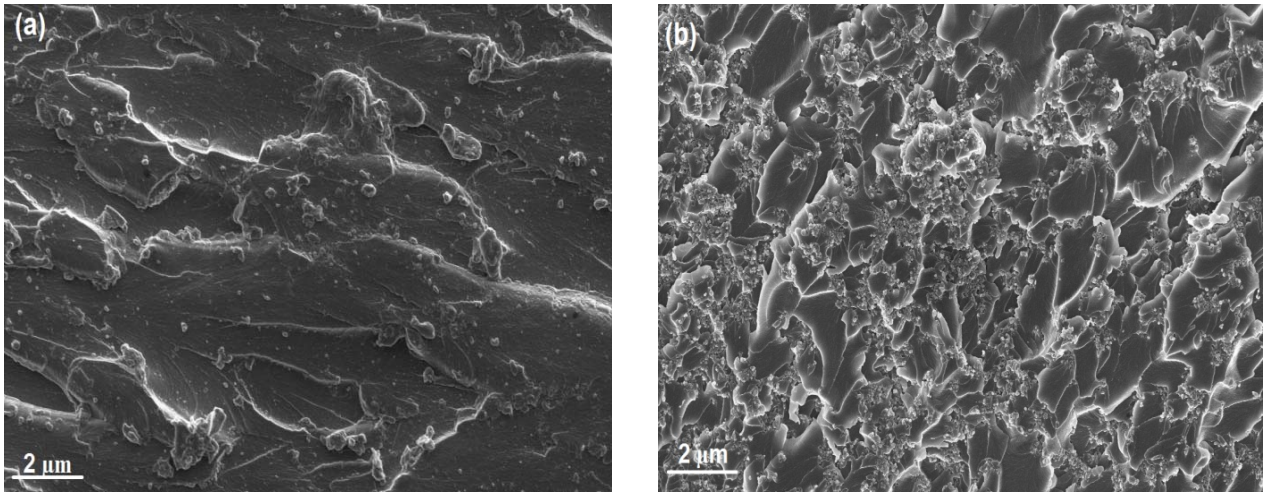


**Figure 6.4:** high magnification FESEM of fracture surface of the CE/$Al_2O_3$ nanocomposites: 0.5 vol.%, (a) 4 vol.% (b)

### 6.3.5. Impact resistance

Impact resistance measurements were performed on 0.25 cm thick UV-cured samples by means of Charpy Pendulum. The impact resistance values for the investigated cured films are reported in Table 6.2. The impact resistance was found to increase in the presence of the ceramic fillers, in accordance with the expected toughening effect evidenced by morphology investigation of the fracture surface of the UV-cured films.

### 6.3.6. Scratch resistance

Scratch test was performed on 100 µm thick UV-cured films. Excellent scratch resistance is evident when high critical load, small cracks and high recovery are recorded. The cured samples containing zero to 4 vol.% of dispersed alumina particles are subjected to the scratch test. The critical load (N) is reported as the detachment of the coated film observed. As reported in Table 6.2 the scratch failure and detachment for the pristine CE occur at 10 N. A noticeable increase in the scratch failure value was observed as the amount of alumina filler increase which indicates an enhancement in scratch resistance. The highest critical load value is reported for sample containing 1 vol.% Alumina (22.9 N). Introducing much amount of alumina reduces the critical load value but still higher than that of pristine epoxy cured material.

**Table 6.2:** The scratch and impact resistance analysis

| Sample | Critical load[a] (N) | Impact resistance[b] J/cm$^2$ |
|---|---|---|
| Pristine CE | 10 ±1.2 | 0.122 ±.027 |
| $Al_2O_3$ 0.5 vol% | 13.2 ±2.5 | 0.145 ±.048 |
| $Al_2O_3$ 1 vol% | 22.9 ±1.8 | --- |
| $Al_2O_3$ 2vol% | 17.8 ±2.1 | --- |
| $Al_2O_3$ 4vol% | 18.1 ±1.6 | --- |

[a]Determined by scratch-resistance test on 100 μm thick UV-cured films;
[b]Determined with Charpy test according to ASTM D 6110-04.

## 6.4. Conclusion

Alumina particles with 150 nm were introduced into cycloaliphatic epoxy resins in the range between 0.5 and 4 vol% and photocured in the presence of cationic photoinitiator. The presence of the nanofillers significantly affects the UV-curing process: where the conversion of epoxy group reduced from 75% for pristine CE to 53% for epoxy resin with 4 vol.% alumina particles. This reduction in the conversion might be attributed to the increase in formulation viscosity as well as to the UV absorption of alumina particles which could compete with photoinitiator absorption.

The presence of these nanoparticles did not notably change the $T_g$ of the cured materials, while impact resistance enhancement was observed. FESEM morphology investigations on Charpy fractured surfaces elucidates increasing surface roughness of the alumina epoxy nanocomposites compared to pristine epoxy matrix. Clearly, the increase in roughness could be explained by crack deflection mechanism which plays a crucial role in the toughening of nanoparticles modified epoxy. Scratch resistance of the coated films has been enhanced by introducing alumina particles.

In conclusion, by dispersing $Al_2O_3$ filler into UV-curable epoxy resin it is possible to achieve a multifunctional epoxy coatings characterized by high scratch resistance properties, good thermomechanical behavior and enhanced toughness.

## 6.5. References


1. A. Dorigato, A. Pegoretti, *J. Nanopart. Res*. 2011; 13:2429.
2. J. Lee, A. F. Yee, *Polymer* 2000; 41:8363.
3. A.J. Kinloch, A.C. Taylor, *J. Mater. Sci.* 2002; 37:433.
4. M. Sangermano, G. Malucelli, E. Amerio, A. Priola, E. Billi, G. Rizza, *Prog. Org. Coat*, 2005; 54:134.
5. A. A. Collyer, *Rubber toughened Engineering Plastics*, Chapman & Hall, London; 1994.

# Summary & Conclusion

Different strategies have been applied for toughening the UV-cured cycloaliphatic epoxy resins. These strategies based on incorporation of polymeric materials or inorganic $Al_2O_3$ into the 3,4-epoxy-cyclohexylmethyl- 3,4-epoxycyclohexyl carboxylate (CE). The effect of these modifiers on the rate of the curing process, thermo-mechanical properties, morphology, as well as the fracture toughness has been investigated.

The first strategy depends on incorporation of new hyperstar polymers (HSP) based on a hyperbranched polyester core (HBP-OH) and PMMA or P(MMA-b-HEMA) block copolymer arms in an epoxy matrix, investigating their effect on UV-curing and evaluating the final properties of the cured materials in terms of thermal and viscoelastic properties. These HSPs were prepared with or without reactive OH groups at the end of the arms and can be considered as polymeric soft nanoparticles. The morphology of the cured materials was investigated in order to understand the phase separation behavior of the hyperstar polymers as a function of their functionality and the curing process.

In general, through addition of hyperstar into epoxy samples a flexibilization documented in $T_g$ decrease could be observed. This was mainly attributed to the decrease of epoxy group conversion together with the insertion of the HEMA-arm containing hyperstar polymers through a chain transfer reaction. According to FESEM morphological investigations, the addition of HBP-PMMA/0%HEMA results in phase separation during UV-curing of the epoxy formulations, while the hyperstar polymers HBP-PMMA/12%HEMA and HBP-PMMA/26%HEMA were tightly incorporated into the network structure through transfer reaction by the OH groups and thus, phase separation during curing was avoided. It offers higher chances to fully exploit the positive effects of our hyperstar polymers as organic soft particles and reactive toughening agents in epoxy resins.

The second strategy depends on incorporation of crosslinked core-shell CS-GMA particles into the cycloaliphatic epoxy. The reactive CS-GMA based on PBA as core and PMMA/PGMA as shell and it was prepared by seeded emulsion polymerization. After shell formation the average particles size was around 200 nm. The particles were dispersed into the cycloaliphatic epoxy resin in the range between 5 and 15 wt% and photocured in the presence of the suitable cationic photoinitiator. The presence of the

particles did not significantly affect the UV-curing process: a slight decrease of final epoxy group conversion was attributed to an increase in the viscosity when CS-GMA is added to the photocurable formulation and to an enhanced vitrification effect. The presence of the particles did not modify the $T_g$ of the cured materials, while impact resistance enhancement was observed independently on the particle content. Morphology investigations on Charpy fractured surfaces showed a homogeneous distribution of the particles through the polymeric matrix with no agglomeration being observed. Particle cavitation was clearly shown in the FESEM micrographs for epoxy reinforced with core/shell particles, evidencing a plastic void growth of the epoxy polymer and shear yielding toughening mechanism.

The third one was introducing block copolymer into the cycloaliphatic epoxy and curing the entire system via UV light. Where reactive PEO-b-PGMA and nonreactive PEO-b-PS block copolymer were prepared through ATRP technique. The reactive block has slight effect on the glass transition temperature, $T_g$, as compared by pristine epoxy. This could be demonstrated by the involving of epoxy group of PGMA in the polymerization reaction resulting in increase the crosslink density and mobility restriction of soft PEO chains. An improvement in storage modulus is observed which gives an evidence of stiffness enhancement. The fracture surface morphology revealed smooth and homogenous surfaces. However, by increasing the PEO block length the surface roughness becomes clearly noticeable. The $K_{IC}$ values support the results explained in terms of FESEM and DMTA. Where the incorporation of reactive block copolymer has negative effect on the fracture toughness. Clearly, the PEO block length has a crucial effect on the $K_{IC}$ values.

On the other side, the incorporation of nonreactive block copolymer into epoxy resins successfully enhances the fracture toughness without scarifying other thermal and mechanical properties. A heterogeneous morphology could be observed by studying the fracture surfaces. The fracture toughness measurements indicate an increase in $K_{IC}$ values by 33% if compared to neat epoxy. additionally, the molecular weight and blocks length of block copolymer are important parameters.

Finally, the fourth strategy based on introducing of alumina nanoparticles with 150 nm into cycloaliphatic epoxy resins in the range between 0.5 and 4 vol% and photocuring in the presence of cationic photoinitiator. The presence of the nanofillers significantly

affects the UV-curing process: where the conversion of epoxy group reduced from 75% for pristine CE to 53% for epoxy resin with 4 vol.% alumina particles. This reduction in the conversion might be attributed to the increase in formulation viscosity as well as to the UV absorption of alumina particles which could compete with photoinitiator absorption.

The presence of these nanoparticles did not notably change the $T_g$ of the cured materials, while impact resistance enhancement was observed. The fracture surfaces investigation using FESEM elucidates increasing in the surface roughness of the alumina epoxy nanocomposites compared to pristine epoxy matrix. Clearly, the increase in roughness could be explained by crack deflection mechanism which plays a crucial role in the toughening of nanoparticles modified epoxy. Scratch resistance of the coated films has been enhanced by introducing alumina particles.

# List of publications

## *Articles:*

1. Marco Sangermano, Mohamed Naguib, Massimo Messori "Fracture Toughness Enhancement of UV-Cured Epoxy Coatings Containing Al2O3 Nanoparticles" Macromol. Mater. Eng., 298, 1184-1189, 2013.
2. Mohamed Naguib, Sabrina Grassini, Marco Sangermano "Core-Shell PBA/PMMAPGMA nanoparticles to enhance the impact resistance of UV-cured epoxy systems" *Macromol. Mater. Eng*., 298, 106–112, 2013.
3. Frank Däbritz, Brigitte Voit, Mohamed Naguib, Marco Sangermano "Hyperstar poly(ester-methacrylate)s as additives in thermally and photocured epoxy resins" polymer, 52(25), 5723- 5731, 2011.
4. M. Naguib, M. Sangermano, D. Pospeich, B. Voit, "Influence of reactive and non-reactive block copolymer on fracture toughness of UV-cured cycloaliphatic epoxy resins" ***in process.***

## *conferences:*

1. Mohamed Naguib et al., Polymeric core-shell nanoparticles to enhance the impact resistance of UV-cured epoxy systems, 7th International Conference on Nanostructured Polymers and Nanocomposites, April 24 - 27, 2012, Prague, Czech Republic.
2. Mohamed Naguib et al., Reactive block copolymer for toughening of UV-cured epoxy resins, 12th International Conference on polymers for advanced technologies, Berlin, Germany, 29/9–2/10/13.